UCRL-11757

University of California

Ernest O. Lawrence Radiation Laboratory

TWO-WEEK LOAN COPY

This is a Library Circulating Copy which may be borrowed for two weeks. For a personal retention copy, call Tech. Info. Division, Ext. 5545

COMPUTATIONAL STUDIES OF TRANSIENTS IN PACKED TUBULAR CHEMICAL REACTORS

Berkeley, California

DISCLAIMER

This document was prepared as an account of work sponsored by the United States Government. While this document is believed to contain correct information, neither the United States Government nor any agency thereof, nor the Regents of the University of California, nor any of their employees, makes any warranty, express or implied, or assumes any legal responsibility for the accuracy, completeness, or usefulness of any information, apparatus, product, or process disclosed, or represents that its use would not infringe privately owned rights. Reference herein to any specific commercial product, process, or service by its trade name, trademark, manufacturer, or otherwise, does not necessarily constitute or imply its endorsement, recommendation, or favoring by the United States Government or any agency thereof, or the Regents of the University of California. The views and opinions of authors expressed herein do not necessarily state or reflect those of the United States Government or any agency thereof or the Regents of the University of California.

UCRL-11757

UNIVERSITY OF CALIFORNIA

Lawrence Radiation Laboratory
Berkeley, California

AEC Contract No. W-7405-eng-48

COMPUTATIONAL STUDIES OF TRANSIENTS IN PACKED TUBULAR CHEMICAL REACTORS

John Earl Crider and Alan S. Foss

M. S. Thesis

January 1965

COMPUTATIONAL STUDIES OF TRANSIENTS IN PACKED TUBULAR CHEMICAL REACTORS

John Earl Crider and Alan S. Foss

Lawrence Radiation Laboratory
University of California
Berkeley, California

January 1965

ABSTRACT

Concentration and temperature transients in a packed bed tubular chemical reactor are calculated for three different mathematical models of the reactor. Two of the models represent the reactor as an array of continuous perfectly mixed stages; one model is two-dimensional, the other is one-dimensional. The third model is a one-dimensional differential representation without axial fluid dispersion. The chemical reaction is an exothermic, homogeneous, liquid-phase, second order reaction.

Machine calculations of transients following step changes in feed temperature or concentration show that the effects of axial fluid dispersion are small compared with the dispersive effects of finite rates of heat transfer between fluid and packing. Cases were found in which the transient concentration initially moved in the direction leading away from the final steady state. Such behavior, which derives from the coupling of concentration and temperature in exothermic reactions, can make the control of reactors difficult. Radial concentration and temperature gradients, arising from incomplete radial mixing, are shown to be small, and their effect upon transients is imperceptible in the cases treated.

These studies show that mathematical models which adequately simulate chemical reactors in unsteady state must incorporate the following phenomena: the thermal capacity of the packing, finite (as distinguished from infinite) rates of heat transfer between fluid and packing, and coupling between concentration and temperature. Both of the one-dimensional models studied include these phenomena and yet are simple enough to be useful in further studies of reactor dynamics and in studies of reactor control.

CONTENTS

Chapter 1. Introduction 1
Chapter 2. The Reactor Models 13
Chapter 3. Finite Stage Wall Heat Transfer Coefficient Correlation 62
Chapter 4. General Features of the Computer Programs . . . 89
Chapter 5. Selection of Numerical Values of Parameters . . . 93
Chapter 6. Results of Program Calculations 98
Chapter 7. Conclusions 166
Acknowledgments 167
Appendix A. A Two Dimensional Runge-Kutta Method . . . 168
B. Derivation of the Two Dimensional Runge-Kutta Method 178
Table of Notation 186
References 190

CHAPTER 1

INTRODUCTION

Part A. General

This is a study of mathematical models of a packed-bed tubular chemical reactor in unsteady-state operation. The major objectives of this study are: to determine the major features of the reactor dynamics, to study the effect upon the reactor dynamics of various phenomena in the reactor, and to find a mathematical model suitable for further studies.

Phenomena considered in this study are those which are known to be present in the reactor and which are expected to have an appreciable effect upon the dynamics. The heat capacity of the packing causes temperature disturbances to travel through the reactor more slowly than concentration disturbances. The rate of heat transfer between the packing and the fluid appears to have a dispersive effect upon the reactor dynamics. Axial mixing should also affect the dynamics in a similar manner. And the effect of radial gradients, caused by the loss of heat through the reactor wall and incomplete radial mixing, is studied to determine whether one-dimensional models, which neglect these radial gradients, are satisfactory.

Several mathematical models which have been proposed in the literature are described by computer programs written for this study. These models differ in the manner in which they account for the effects of the phenomena listed above. The response of these models to a step change in feed concentration or in feed temperature are described by the results of calculations performed according to these programs by an automatic computer. The effects of these phenomena are determined by comparison of the behavior of the different models. It will be seen that two of these models adequately describe the major features of the dynamics of a packed tubular reactor and yet are simple enough to be very useful in studies of the proper design of a control system for the packed tubular reactor.

The chemical reactor considered here is a cylindrical tube or pipe filled with packing, or granular material. The reactants are carried through the reactor in a fluid which enters the reactor at one end of the tube, the entrance, or inlet, and leaves the reactor at the other end of the tube, the exit. Inside the reactor, the fluid, carrying reactant and products, flows through the voids between the packing particles, and through the pores of the particles, if the particles are porous.

In many cases, the packing particles are of a porous chemical catalyst, and the reaction occurs on the surfaces of the pores of the particles. In other cases, the packing may be chemically inert, having been added for heat transfer regulation or for other reasons; in such cases, the reaction occurs in the fluid, which is in the packing voids and in the pores of the packing particles. If the particles are porous, heat and material move from the pore surfaces and the fluid in the pores, through the pores, and through the voids. In addition, heat is conducted through the packing.

The heat generated in the chemical reaction is removed partially through the wall of the reactor. This loss of heat through the reactor wall and incomplete radial mixing cause radial differences in temperature and also in concentration, because of the coupling of temperature and concentration in the reaction terms.

In order to devise a mathematical model of the reactor just described, certain assumptions must be made. These present assumptions are made primarily to make the physical concept of the reactor more precise, to relate certain phenomena to their well-known mathematical formulations, and to eliminate certain phenomena which greatly complicate the study of reactor dynamics. These assumptions apply to the physical model of the reactor, and therefore to all of the mathematical models considered in this study. These assumptions are stated in the following paragraphs.

The reactor is axially symmetric. The flow of the fluid in the voids is turbulent (this is true if the Reynolds number, based upon the average diameter of the packing and the superficial velocity of the fluid, is greater[1] than 100). The average fluid velocity radial profile is flat, that is, there is no net flow of fluid in the radial direction (this is usually a valid assumption if the fluid is in turbulent flow and if the ratio of the reactor diameter to the average particle diameter is greater[2] than 10). The physical properties of the fluid and of the solid, for example, density and heat capacity, are independent of species concentrations, temperature, position in the reactor, or time (this is usually a valid assumption for a reactor with liquid reactants).

The geometry of the packing and of the packing particles is adequately represented by the packing porosity, the specific surface area of the packing, and an average particle diameter. The particles are nonporous, and the reaction occurs in the fluid in the voids between particles. The rate of reaction has the Arrhenius type of temperature dependency, and this rate is proportional to the concentration of the reactant if there is one reactant, and to the concentration of each reactant if there are two reactants. The rate of reaction is not otherwise dependent upon the stoichiometry of the reaction. The heat of reaction is constant.

The temperature within any packing particle is uniform throughout that particle. There is no heat transfer between any two particles, or between any particle and the reactor wall, except by convection through the fluid. The wall of the reactor is at a constant temperature. Newton's law of cooling applies to heat transfer between the fluid and the wall, and between the fluid and the packing particles.

As implied in these preceding assumptions, the reactor is a liquid reactor. Also, certain of these assumptions involve parameters which may be adjusted in these models to produce special cases: for example, in the expression for heat transfer between the fluid and the wall, the heat transfer coefficient is set to zero to simulate an adiabatic reactor.

Statements concerning axial and radial dispersion of heat and mass are omitted from the above listing of assumptions because these and the other phenomena enumerated above which are of interest in this study are treated differently in the different models. In fact, some of these phenomena are ignored in some of the models. The treatment of these phenomena in the various models are the chief differences in the models.

Because of the nonlinear temperature dependence of the Arrhenius form of the rate term in the heat and mass balance equations and the coupling of concentration and temperature through this term, these equations can in general be solved only by numerical techniques. Even with efficient numerical techniques and high-speed automatic computers, solution of the conservation equations for the most physically accurate conceivable model would be prohibitively time consuming. The use of the assumptions listed above greatly simplifies this most complex model. For example, assumption of a flat velocity profile eliminates the need for the solution of a fluid momentum balance equation. Thus, simpler models can be obtained from the more complex models by the neglecting of certain phenomena known, or expected, to have small effect upon the dynamics of the reactor. The differences in the behavior of a more complex model and of a simpler model can be attributed to the phenomenon neglected in the derivation of the simpler model.

The three models considered in this study are: a two-dimensional finite stage model, a one-dimensional finite stage model, and a first-order differential model called here the plug flow model. The two-dimensional finite stage model, proposed by Deans[3, 4, 5] is the most complex of these models. This model is a two-dimensional array of continuous flow stirred tank reactor stages, each stage being the size of an average packing particle. Each stage represents a void between packing particles in which turbulent mixing occurs, and the arrangement of the stages in the array simulates the turbulent axial and radial dispersion of heat and mass in the reactor.

The one-dimensional finite stage model is the one-dimensional form of the two-dimensional finite stage model; it is an arrangement of continuous flow stirred tank reactors in series. Being one dimensional, it has no radial gradients, but flat radial concentration and temperature profiles. However, the mixing stages simulate axial dispersion of heat and mass in the reactor. The only two differences between this model and the two-dimensional finite stage model are the differences in radial gradients and the differences in the driving force for heat transfer at the wall: in the one-dimensional finite stage model, the driving force is the difference between the wall temperature and the stage temperature at the axial position of interest; in the two-dimensional finite stage model, it is the difference between the wall temperature and the temperature in the wall stage at the axial position of interest. The temperatures in the one-dimensional model correspond to radially averaged temperatures in the two-dimensional model.

The plug flow model is the simplest of the continuous, or partial differential equation, models. It is a one-dimensional model, and its heat and mass balances are expressed as first-order partial differential equations. Thus it has no compensation for axial dispersion of heat or mass, which is the major difference between this model and the one-dimensional finite stage model.

A modification of the plug flow model is that model in which the temperature of the fluid and the temperature of the particles are assumed to be equal at all points in the model. This assumption is equivalent to the assumption that the heat transfer coefficient between the fluid and the particles is infinite. This assumption removes the effect of a finite rate of heat transfer between the particles and the fluid while retaining the effect of the heat capacity of the packing. It will be seen that this simplified plug flow model is conceptually important in this study. The partial differential equations which describe either of these two plug flow models are hyperbolic in nature, and may be treated by the method of characteristics.

All of these models are described in detail in Chapter 2. Numerical techniques for the solution of the heat and mass balance equations of these models are also presented here.

In the two-dimensional finite stage model, the resistance to radial heat flow through the bed to the wall is inherent in the structure of the bed, and the resistance to heat flow through the wall from the stages at the wall is represented by the wall heat transfer coefficient. For the one-dimensional models, however, the overall heat tranfer coefficient must reflect both the resistance to heat flow through the bed and resistance to heat flow through the wall. In order for all models to represent the same rate of heat loss through the wall, a correlation must be obtained between the overall heat transfer coefficient of the one-dimensional models and the wall heat transfer coefficient and other parameters of the two-dimensional model. This problem of correlation is essentially a steady state heat transfer problem, which can be treated analytically because of its linear nature. In Chapter 3, this correlation is derived. First, an empirical correlation is obtained by approximating the finite stage models with partial differential equation models. This treatment illustrates some differences between discrete (i. e., finite stage) models and continuous (i. e., partial differential equation) models. Then the two-dimensional finite stage model equations are treated by matrix algebra to obtain an exact correlation. This treatment allows a greater understanding of the finite stage model through a matrix expression of its equations.

The computer programs which describe these models are described in Chapter 4. With these programs, the dynamic behavior of the models when subjected to a step change in either feed concentration, or in feed temperature, or both, is calculated. These programs also allow the machine plotting of this dynamic behavior.

In Chapter 5, the numerical values for the parameters of the reactor simulated in the computer runs is presented. These values describe, primarily, the experimental reactor studied by Sinai,[6] in which the reaction was the homogeneous liquid phase reaction of sodium thiosulfate and hydrogen peroxide.

In Chapter 6, the results of the thirteen computer runs made with these programs is presented, including the plotted output of all runs. These results are compared to determine the dynamic effects of the various phenomena under study, and the significance of these effects is discussed. The plug flow model and the one-dimensional finite stage model are recommended for use in other studies, on the basis of accuracy and simplicity. Various models are suggested for use in frequency response studies.

In Chapter 7, the conclusions of this work are presented.

Part B. Parameters and Dimensionless Numbers

The behavior of the chemical reactor being modeled and the behavior of the models being studied can be conveniently expressed in terms of dimensionless parameters and dimensionless variables. A set of values for these dimensionless numbers may actually characterize several similar reactors. Many of these dimensionless parameters are measures of the relative effects of various phenomena in the system.

A convenient characteristic length in the reactors is the average particle diameter, d_p. This is the length of each stage in the finite stage models. The total dimensionless length of the reactor, which is the total number of stages along the axis of the finite stage models, is L:

$$N \equiv \frac{N^*}{d_p} \tag{1.1}$$

The dimensionless diameter of the reactor is M:

$$M \equiv \frac{M^*}{d_p} \tag{1.2}$$

For the continuous models, the dimensionless distance from the inlet is x:

$$x = \frac{x^*}{d_p} \tag{1.3}$$

A convenient characteristic velocity is the average fluid velocity v. Then the characteristic time is d_p/v, named here the "particle residence time." Dimensionless time is

$$t = \frac{t^* v}{d_p} \tag{1.4}$$

The reactor may have either one reactant or two. In the first case, the reaction is

$$A \longrightarrow \text{products}, \tag{1.5}$$

and the volumetric rate of reaction, or the rate of disappearance of moles of A per unit volume of fluid, is

$$R^* = k^* \exp\left[-E/R_g T^*\right] c_A^* \ . \tag{1.6}$$

In the second case, the reaction is

$$A + \gamma B \longrightarrow \text{products}, \tag{1.7}$$

and the volumetric rate of reaction is

$$R^* = k^* \exp\left[-E/R_g T^*\right] c_A^* c_B^* \tag{1.8}$$

The rate of disappearance of moles of B per volume is γR^*.

Any convenient concentration may be chosen as a reference concentration c_r, usually the initial or the final feed concentration of A, the primary reactant. Any convenient temperature may be chosen as the reference temperature, T_r, usually the initial or the final feed temperature or the wall temperature; this temperature and the total adiabatic temperature rise (based upon the reference concentration) is used to convert all temperatures to convenient dimensionless temperatures in the neighborhood of 0 to 1. The dimensionless concentrations are

$$c_A = \frac{c_A^*}{c_r} , \tag{1.9}$$

$$c_B = \frac{c_B^*}{c_r} . \tag{1.10}$$

The total adiabatic temperature rise (based upon the reference concentration) is

$$\Delta T_a = \frac{(-\Delta H)c_r}{\rho_f c_f} . \tag{1.11}$$

The dimensionless temperatures are

$$T = \frac{T^* - T_r}{\Delta T_a} , \tag{1.12}$$

$$T_p = \frac{T_p^* - T_r}{\Delta T_a} , \tag{1.13}$$

$$T_w = \frac{T_w^* - T_r}{\Delta T_a} , \tag{1.14}$$

and

$$T_0 = \frac{T_r}{\Delta T_a} . \tag{1.15}$$

The dimensionless rate of reaction for the case of one reactant is

$$K = k \exp[AT/(T_0 + T)]\, c_A , \tag{1.16}$$

where

$$k = \frac{k^* d_p}{v} e^{-A} ; \tag{1.17}$$

for the case of two reactants, it is

$$K = k \exp\left[AT/(T_0 + T)\right] c_A c_B \tag{1.18}$$

where

$$k = \frac{k^* c_r d_p}{v} e^{-A} . \tag{1.19}$$

In both cases,

$$A \equiv \frac{d_p R^*}{R_g T_r} \tag{1.20}$$

and

$$R = \frac{d_p R^*}{v c_r} . \tag{1.21}$$

The dimensionless heat capacity and heat transfer parameters are:

heat capacity parameter: $$\beta \equiv 1 + \frac{\rho_p c_p (1-\epsilon)}{\rho_f c_f \epsilon} ; \tag{1.22}$$

particle-fluid heat transfer coefficient: $$Hp \equiv \frac{h_p a_p (1-\epsilon) d_p}{\rho_f c_f \epsilon v} ; \tag{1.23}$$

wall heat transfer coefficient: $$Hw \equiv \frac{h_w}{\rho_f c_f v} \tag{1.24}$$

The wall heat transfer coefficient is a type of Stanton number. For two-dimensional models, h_w is analogous to a wall film heat transfer coefficient, and for one-dimensional models, h_w is analogous to an overall heat transfer coefficient. The relationship between the wall heat transfer coefficients of the models is discussed in Chapter 3.

Peclet numbers, which indicate the ratio of bulk transport of heat or mass to the dispersive transport of heat or mass, are not fundamental parameters of the finite stage models, in which dispersion

is accounted for in the geometrical arrangements of the models, or of the plug flow model, which excludes axial dispersion and which includes radial transport in the wall heat transfer coefficient. However, Peclet numbers are used in the heat transfer coefficient correlation of Chapter 3. In the physical model, molecular diffusion is assumed to be negligible compared with turbulent dispersion. Then the turbulent mass diffusivity is equal to the turbulent thermal diffusivity in both the axial and the radial directions, because the mechanism of mixing is the same for both mass and heat transport:

$$D_x = \frac{k_x}{\rho_f c_f} \tag{1.25}$$

$$D_r = \frac{k_r}{\rho_f c_f} \quad . \tag{1.26}$$

The axial and radial Peclet numbers, for both mass transfer and heat transfer, are defined as:

$$Pe_x \equiv \frac{d_p v}{D_x} = \frac{d_p v \rho_f c_f}{k_x} \tag{1.27}$$

$$Pe_r \equiv \frac{d_p v}{D_r} = \frac{d_p v \rho_f c_f}{k_r} \tag{1.28}$$

In the numerical studies, the unsteady state of the reactor is caused by a step change in either feed concentration, or feed temperature, or both. The step change occurs at $t = 0$.

The inlet conditions for all the models are:

$$\left.\begin{array}{lll} \text{at } x = 0, & & \\ \quad \text{for } t < 0, & c_A = c_{A_{if}} & \\ & T = T_{if} & \\ \quad \text{for } t > 0, & c_A = c_{A_{ff}} & \\ & T = T_{ff} & \\ \text{if there is a second reactant, at } x = 0, & c_B = c_{B_f} \text{ for all } t & \end{array}\right\} . \quad (1.29)$$

Before the step change, for $t < 0$, the reactor is at steady state. The initial conditions for the unsteady state of the models are obtained from the steady state model equations; that is, from the model equations in which all time derivatives are set to zero. The reactor parameters are chosen so that the models have only one steady state; that is, that the steady state model equations have only one solution.

For the case of two reactants, a useful variable which is used in place of the second reactant is the stoichiometric concentration difference, defined as

$$\delta \equiv c_A - \frac{c_B}{\gamma} . \qquad (1.30)$$

It will be seen in Chapter 2 that the use of this variable simplifies the system equations, because the variable has no radial gradients in two-dimensional models, is a step function in the plug flow model, and in general is described by a linear equation. With this variable used to eliminate c_B, the rate of reaction is

$$R = k \exp [AT/(T_0+T)] \quad c_A \gamma (c_A - \delta) . \qquad (1.31)$$

CHAPTER 2

THE REACTOR MODELS

Part A. The Two-Dimensional Finite Stage Model

The two-dimensional finite stage model was proposed by Deans.[3, 4, 5] The model is made up of concentric rings of square cross section, arranged in longitudinal layers, called rows. Each ring, or stage, is a continuous-flow stirred-tank reactor. The length and the width of the cross section of each stage are equal to the average particle diameter. Physically, each stage represents a void space between particles in which turbulent mixing occurs. The model, its cross section, and the physical model upon which it is based, are shown in Figure 1. The mixing characteristics of the model are derived from geometrical considerations only. Each stage is fed by the two adjacent stages on the preceding row, and in turn feeds the two adjacent stages on the following row.

Each stage is identified by an axial position i and a radial position j. A stage (i, j) includes the portions of the particles and the voids of the reactor which are bounded axially by two planes at distances $(i-1)d_p$ and id_p from the inlet of the bed, and radially by two concentric cylinders of diameters $(j-2)d_p$ and jd_p. The exceptions to this description are the half-stages at the center and at the wall of the reactor. At every odd axial position (i.e., when i is odd), the stage at the axis is a half-stage, named thus because its cross-sectional width is half that of the other stages. It is bounded radially by a cylinder of diameter d_p. And at every other axial position, the stage at the wall is a half-stage, bounded radially by cylinders of diameters $(M-1)d_p$ and Md_p. This half-stage, at axial position i, is characterized by $(i, M+1)$.

On an odd row (i.e., when i is odd), the radial positions j take on all odd numbers from 1 (the half-stage at the axis) to M or $M+1$, whichever is odd; and on an even row, the radial positions j take on all even numbers from 2 (the whole stage at the axis) to M or $M+1$, whichever is even. The half stages at the wall, $(i, M+1)$, occur at odd rows

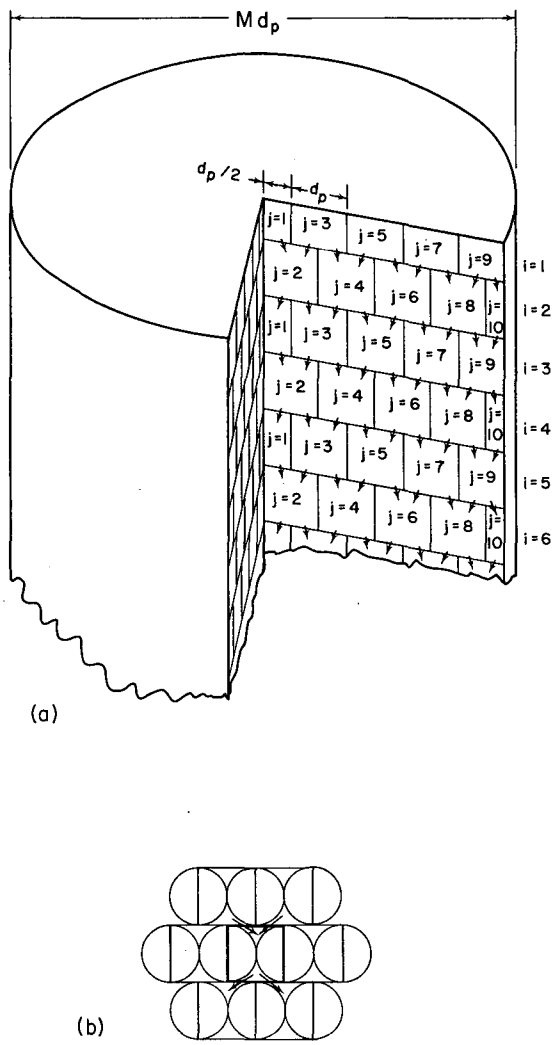

Fig. 1. Arrangement of stages in the two-dimensional finite stage model.
(a) Details of stage arrangement
(b) Arrangement of particles upon which this model is based; here, M = 9.

if $M+1$ is odd, and on even rows if $M+1$ is even. There are a total of $M+1$ stages in any two successive rows.

Heat and mass transport in all stages except the wall stages is by turbulent convection only. The flow of heat through the wall from a wall stage is proportional to the difference between the wall temperature and the temperature of the fluid in the wall stage. There is no flow between two adjacent stages on the same row. The flow between any stage and another stage at the next row is proportional to the geometrical area shared by the two stages.

The area of a stage, A_j, is defined as the area of the cross section of the stage which is perpendicular to the axis of the reactor. This area is a function of the radial position j only; it is independent of the axial position i. The volume of voids in a stage (i, j) is

$$V_j = \epsilon A_j d_p ; \qquad (2.1)$$

this volume is also independent of i. Similarly, the volumetric flow rate to and from this stage is

$$Q_j = \epsilon A_j v , \qquad (2.2)$$

also independent of i.

The area shared by stage (i, j) and stage $(i+1, j+1)$ is $A_{j,j+1}$, which is independent of i and is identical to the area shared by stage (i, j) and stage $(i-1, j+1)$; i.e.,

$$A_{j,j+1} = A_{j+1,j} . \qquad (2.3)$$

Similarly, $A_{j,j-1}$ is the area shared by stages (i, j) and $(i+1, j-1)$ or by stages (i, j) and $(i-1, j-1)$:

$$A_{j,j-1} = A_{j-1,j} . \qquad (2.3)$$

The flow rate from stage (i-1, j+1) to stage (i, j), or from stage (i, j) to stage (i+1, j+1), is

$$Q_{j,j+1} = Q_{j+1,j} = \epsilon\, A_{j,j+1}\, v, \qquad (2.5)$$

also independent of i. Similarly,

$$Q_{j,j-1} = Q_{j-1,j} = \epsilon\, A_{j,j-1}\, v\,. \qquad (2.6)$$

The material flowing from stage (i, j) flows into stages (i+1, j-1) and (i+1, j+1); i.e.,

$$Q_j = Q_{j,j-1} + Q_{j,j+1}\,, \qquad (2.7)$$

or

$$A_j = A_{j,j-1} + A_{j,j+1}\,. \qquad (2.8)$$

From the geometry, for a whole stage (i, j),

$$A_{j,j+1} = \tfrac{1}{4}\pi d_p^{\,2}\,[j^2 - (j-1)^2] = \tfrac{1}{4}\pi d_p^{\,2}\,(2j-1), \qquad (2.9)$$

$$A_{j,j-1} = \tfrac{1}{4}\pi d_p^{\,2}\,[(j-1)^2 - (j-2)^2] = \tfrac{1}{4}\pi d_p^{\,2}(2j-3). \qquad (2.10)$$

and

$$A_j = \tfrac{1}{4}\pi d_p^{\,2}[j^2 - (j-2)^2] = \tfrac{1}{4}\pi d_p^{\,2}\,(4j-4)\,. \qquad (2.11)$$

For the half-stage at the axis, j = 1;

$$A_{1,0} = 0 \qquad (2.12)$$

$$A_1 = A_{1,2} = A_{2,1} = \tfrac{1}{4}\pi d_p^{\,2} \qquad (2.13)$$

Similarly, for the half-stage at the wall, j = M+1;

$$A_{M+1,\,M+2} = 0,$$

$$A_{M+1} = A_{M,\,M+1} = A_{M+1,\,M} = \tfrac{1}{4}\pi d_p^{\,2}(2M-1). \qquad (2.14)$$

A component mass balance at stage (i, j) gives

$$V_j \frac{dC^*_{A_{i,j}}}{dt^*} = Q_{j,j-1} C^*_{A_{1-1,j-1}} + Q_{j,j+1} C^*_{A_{i-1,j+1}} - Q_j C^*_{A_{i,j}} - V_j R^*_{i,j} . \tag{2.15}$$

In dimensionless form, this equation becomes

$$\frac{dC_{A_{i,j}}}{dt} = \left(\frac{A_{j,j-1}}{A_j}\right) C_{A_{i-1,j-1}} + \left(\frac{A_{j,j+1}}{A_j}\right) C_{A_{i-1,j+1}} - C_{A_{i,j}} - R_{i,j} . \tag{2.16}$$

For a whole stage (i, j), this equation is

$$\frac{dC_{A_{i,j}}}{dt} = \left(\frac{2j-3}{4j-4}\right) C_{A_{i-1,j-1}} + \left(\frac{2j-1}{4j-4}\right) C_{A_{i-1,j+1}} - C_{A_{i,j}} - R_{i,j} . \tag{2.17}$$

For the half-stage at the axis, equation (2.16) reduces to

$$\frac{dC_{A_{i,1}}}{dt} = C_{A_{i-1,2}} - C_{A_{i,1}} - R_{i,1}, \tag{2.18}$$

and for the half stage at the wall, equation (2.16) reduces to

$$\frac{dC_{A_{i,M+1}}}{dt} = C_{A_{i-1,M}} - C_{A_{i,M+1}} - R_{i,M+1} . \tag{2.19}$$

The corresponding temperature equations are found from a heat balance on a stage:

$$V_j \rho_f c_f \frac{dT^*_{i,j}}{dt^*} = Q_{j,j-1}\, \rho_f c_f\, T^*_{i-1,j-1} + Q_{j,j+1}\, \rho_f c_f\, T^*_{i-1,j+1} - Q_j\, \rho_f c_f\, T^*_{i,j}$$

$$+ (-\Delta H) V_j R^*_{i,j} + h_p a_p (1-\epsilon) A_j d_p (T^*_{p_{i,j}} - T^*_{ij}) + h_w A_{w_j} \epsilon\, (T^*_w - T^*_{i,j}), \tag{2.20}$$

$$\left(\frac{1-\epsilon}{\epsilon}\right) V_j\, \rho_p\, c_p \frac{dT^*_{p_{i,j}}}{dt} = h_p\, a_p\, (1-\epsilon)\, A_j\, d_p\, (T^*_{i,j} - T^*_{p_{i,j}}) . \tag{2.21}$$

In dimensionless form, these equations are

$$\frac{dT_{i,j}}{dt} = \left(\frac{A_{j,j-1}}{A_j}\right) T_{i-1,j-1} + \left(\frac{A_{j,j+1}}{A_j}\right) T_{i-1,j+1} - T_{i,j} + R_{i,j} + Hp(T_{p_{i,j}} - T_{i,j})$$

$$+ \frac{A_{w_j}}{A_j} Hw\, (T_w - T_{i,j}) , \tag{2.22}$$

and

$$\frac{dT_{p_{i,j}}}{dt} = \frac{Hp}{\beta - 1} (T_{i,j} - T_{p_{i,j}}) . \tag{2.23}$$

A_{w_j} is the geometrical area shared by a stage and the wall of the reactor.

For a stage not a wall stage,

$$A_{w_j} = 0 \qquad j < M . \tag{2.24}$$

For a wall stage,

$$A_{w_j} = \pi M d_p^2 , \quad j = M \text{ or } M + 1. \tag{2.25}$$

For a whole stage not a wall stage, equation (2.22) becomes

$$\frac{dT_{i,j}}{dt} = \left(\frac{2j-3}{4j-4}\right) T_{i-1,j-1} + \left(\frac{2j-1}{4j-4}\right) T_{i-1,j+1} - T_{i,j} + R_{i,j} + Hp(T_{p_{i,j}} - T_{i,j}) \tag{2.26}$$

For a half stage on the axis, equation (2.22) reduces to

$$\frac{dT_{i,j}}{dt} = T_{i-1,2} - T_{i,1} + R_{i,1} + Hp(T_{p_{i,1}} - T_{i,1}) . \tag{2.27}$$

For the whole stage at the wall and for the half stage at the wall, equation (2.22) becomes

$$\frac{dT_{i,M}}{dt} = \left(\frac{2M-3}{4M-4}\right) T_{i-1,M-1} + \left(\frac{2M-1}{4M-4}\right) T_{i-1,M+1} - T_{i,M} + R_{i,M} + Hp(T_{p_{i,M}} - T_{i,M}) + \left(\frac{4M}{4M-4}\right) Hw(T_w - T_{i,M}) , \tag{2.28}$$

and

$$\frac{dT_{i,M+1}}{dt} = T_{i-1,M} - T_{i,M+1} + R_{i,M+1} + Hp\,(T_{p_{i,M+1}} - T_{i,M+1}) + \left(\frac{4M}{2M-1}\right) Hw(T_w - T_{i,M+1}) \tag{2.29}$$

If there is a second reactant, its concentration is described by an equation similar to that which describes the concentration of the first reactant:

$$\frac{dC_{B_{i,j}}}{dt} = \left(\frac{A_{j,j-1}}{A_j}\right) C_{B_{i-1,j-1}} + \left(\frac{A_{j,j+1}}{A_j}\right) C_{B_{i-1,j+1}} - C_{B_{i,j}} - \gamma R_{i,j} \tag{2.30}$$

From this can be obtained an equation which describes the stoichiometric concentration difference δ:

$$\frac{d\delta_{i,j}}{dt} = \left(\frac{A_{j,j-1}}{A_j}\right) \delta_{i-1,j-1} + \left(\frac{A_{j,j+1}}{A_j}\right) \delta_{i-1,j+1} - \delta_{i,j} \qquad (2.31)$$

Because this model is two dimensional, it has several initial stages, at axial position 1. The concentrations and the temperatures of the feed streams to these stages are not necessarily the same. For instance, the steady-state concentration of a reactionless species could be non-zero in the feed to the center inlet stage, (1, 1), and zero in the feed to the other inlet stages, (1, j), $j \neq 1$. With this input Deans found that the effective radial Peclet number for the finite stage model was 8.2.

If the feed concentrations of the reactants are the same for every inlet stage, then $\delta_{i,j}$ will never exhibit radial gradients, because it is independent of temperature. In this case, $\delta_{i,j}$ is independent of j:

$$\delta_i = \delta_{i,j} \qquad \text{for all } j \text{ at row } i, \qquad (2.32)$$

and

$$\frac{d\delta_i}{dt} = \delta_{i-1} - \delta_i \ . \qquad (2.33)$$

For a step change in the feed concentration of the primary reactant, this equation can be easily integrated analytically or numerically. For no step change in the feed concentration, or at steady state,

$$\delta_i = \delta_{i-1} = \delta_0 \ , \qquad (2.34)$$

where δ_0 is the stoichiometric difference of the feed concentrations. This stoichiometric difference is therefore constant even in an unsteady state period, if the stoichiometric difference of the feed concentrations is constant with time.

At the steady state, all time derivatives are zero, and the above equations reduce to algebraic equations, from which steady state profiles are obtained. Because of the temperature coupling in the Arrhenius term, these equations are generally nonlinear.

At the steady state, $T_{i,j} = T_{p_{i,j}}$, so the value of Hp does not affect the steady-state profiles.

Part B. Techniques for the Numerical Solution of the Two-Dimensional Finite Stage Equations

The steady-state values of concentration and temperature for the stages of the finite stage model are the initial values needed for the integration of the unsteady-state equations (2.16), (2.20), (2.22), (2.23), and (2.33). These steady-state values are roots of the algebraic equations which result from setting the time derivatives of the unsteady-state equations equal to zero. These steady-state values can be found numerically by any methods suitable for finding roots of nonlinear simultaneous algebraic equations. Newton-Raphson methods[7] are used here.

For the solution for these roots, two cases can be considered: the case in which there is only one reactant, and the case in which there are two reactants. If there is only one reactant, the concentration equation is linear in concentration, and can be used to eliminate the unknown concentration from the temperature equation:

$$p_{C_{i,j}} - C_{A_{i,j}} - k \exp\left[AT_{i,j}/(T_0+T_{i,j})\right] C_{A_{i,j}} = 0 \qquad (2.35)$$

where

$$p_{c_{i,j}} = \left(\frac{2j-3}{4j-4}\right) C_{A_{i-1,j+1}} + \left(\frac{2j-1}{4j-4}\right) C_{A_{i-1,j+1}}$$

for a whole stage (i, j) ; (2.36)

$$p_{c_{i,1}} = C_{A_{i-1,2}}, \qquad (2.37)$$

and

$$p_{c_{i,M+1}} = C_{A_{i-1,M}}. \qquad (2.38)$$

Then

$$C_{A_{i,j}} = \frac{p_{A_{i,j}}}{1+k \exp\left[AT_{i,j}/(T_0+T_{i,j})\right]} \quad . \tag{2.39}$$

and

$$p_{T_{i,j}} - T_{i,j} + k \exp\left[AT_{i,j}/(T_0+T_{i,j})\right] C_{A_{i,j}} + \theta_j(T_w - T_{i,j}) = 0 \tag{2.40}$$

where

$$p_{T_{i,j}} = \left(\frac{2j-3}{4j-4}\right) T_{i-1,j-1} + \left(\frac{2j-1}{4j-4}\right) T_{i-1,j+1} \quad , \tag{2.41}$$

$$p_{T_{i,1}} = T_{i-1,2} \; , \tag{2.42}$$

$$p_{T_{i,M+1}} = T_{i-1,M} \; , \tag{2.43}$$

$$\theta_M = \left(\frac{4M}{4M-4}\right) Hw \; , \tag{2.44}$$

$$\theta_{M+1} = \left(\frac{4M}{2M-1}\right) Hw \; , \tag{2.45}$$

$$\theta_j = 0, \quad j < M \; . \tag{2.46}$$

Then

$$p_{T_{i,j}} - T_{i,j} + \frac{p_{C_{i,j}} k \exp\left[AT_{i,j}/(T_0+T_{i,j})\right]}{1+k \exp\left[AT_{i,j}/(T_0+T_{i,j})\right]} + \theta_j(T_w - T_{i,j})$$

$$\equiv g(T_{i,j}) = 0 \; . \tag{2.47}$$

$T_{i,j}$ is the only unknown in $g(T_{i,j})$ so the desired value of $T_{i,j}$ is that for which $g(T_{i,j}) = 0$.

The Newton-Raphson method used in this case is a third-order method, also known as the third-order Richmond method,[8] which in this case is the iteration

$$T_{i,j}^{(m+1)} = T_{i,j}^{(m)} - \frac{g(T_{i,j}^{(m)})/g'(T_{i,j}^{(m)})}{1-\frac{1}{2}[g(T_{i,j}^{(m)})/g'(T_{i,j}^{(m)})][g''(T_{i,j}^{(m)})/g'(T_{i,j}^{(m)})]} \tag{2.48}$$

where the superscript primes denote first or second derivatives of g with respect to $T_{i,j}$. For notational and computational convenience, g and its derivatives can be expressed in terms of auxiliary functions a_1, a_2, a_3, which are defined as

$$a_1 = a_1(T_{i,j}) \equiv k \exp[AT_{i,j}/(T_0 + T_{i,j})] , \tag{2.49}$$

$$a_2 = a_2(T_{i,j}) \equiv a_1 p_{c_{i,j}}/(1 + a_1) , \tag{2.50}$$

$$a_3 = a_3(T_{i,j}) \equiv AT_0/(1 + a_1)(T_0 + T_{i,j})^2 ; \tag{2.51}$$

then

$$a_1' = a_1 AT_0/(T_0 + T_{i,j})^2 , \tag{2.52}$$

$$a_2' = a_2 a_3 , \tag{2.53}$$

$$a_3' = - a_3[a_1 a_3 + 2/(T_0 + T_{i,j})] . \tag{2.54}$$

Then

$$g = p_{T_{i,j}} - (1 + \theta_j) T_{i,j} + a_2 \tag{2.55}$$

$$g' = - (1 + \theta_j) + a_2 a_3 \tag{2.56}$$

$$g'' = a_2' a_3 + a_2 a_3' = a_2 a_3[a_3(1-a_1) - 2/(T_0 + T_{i,j})] \tag{2.57}$$

The equation (2.48) is iterated until the difference between two successive values of $T_{i,j}$ is negligible. Then the concentration $c_{A_{i,j}}$ is found directly from the equation (2.39).

For the case of two reactants, a similar procedure could be used, because here the concentration equation is quadratic in concentration, so the concentration could be expressed explicitly in terms of the temperature. Because such a procedure would involve complicated algebra, the concentration equation and the temperature equation are instead iterated simultaneously by the Newton-Raphson method (7). The concentration and temperature functions are:

$$f(c_{A_{i,j}}, T_{i,j}) = p_{c_{i,j}} - c_{A_{i,j}} - k \exp\left[AT_{i,j}/(T_0 + T_{i,j})\right] c_{A_{i,j}} \gamma(c_{A_{i,j}} - \delta_0), \tag{2.58}$$

$$g(c_{A_{i,j}}, T_{i,j}) = p_{T_{i,j}} - T_{i,j} + k \exp\left[AT_{i,j}/(T_0 + T_{i,j})\right] c_{A_{i,j}} \gamma(c_{A_{i,j}} - \delta_0) + \theta_j(T_w - T_{i,j}) \quad . \tag{2.59}$$

The iterations are

$$c_{A_{i,j}}^{(m+1)} = c_{A_{i,j}}^{(m)} - \frac{1}{D}\left[f \frac{\partial g}{\partial T} - g \frac{\partial f}{\partial T}\right]^{(m)} \tag{2.60}$$

$$T_{i,j}^{(m+1)} = T_{i,j}^{(m)} - \frac{1}{D}\left[g \frac{\partial f}{\partial c} - f \frac{\partial g}{\partial c}\right]^{(m)} \tag{2.61}$$

where

$$D \equiv \left[\frac{\partial g}{\partial T} \frac{\partial f}{\partial c} - \frac{\partial f}{\partial T} \frac{\partial g}{\partial c}\right]^{(m)} \tag{2.62}$$

Then

$$D = (1+\theta_j) + k \exp\left[AT_{i,j}/(T_0 + T_{i,j})\right] c_{A_{i,j}} \gamma(c_{A_{i,j}} - \delta_0) \cdot$$
$$\left[(1+\theta_j)(2-\delta_0/c_{A_{i,j}})/(c_{A_{i,j}} - \delta_0) - AT_0/(T_0 + T_{i,j})^2\right] \tag{2.63}$$

$$f\frac{\partial g}{\partial T} - g\frac{\partial f}{\partial T} = (1+\theta_j)(c_{A_{i,j}} - p_{c_{i,j}}) + k\exp[AT_{i,j}/(T_0+T_{i,j})]c_{A_{i,j}}\gamma(c_{A_{i,j}}$$

$$- \delta_0)[(1+\theta_j) + (p_{T_{i,j}} - (1+\theta_j)T_{i,j} + p_{c_{i,j}} - c_{A_{i,j}})AT_0/(T_0$$

$$+ T_{i,j})^2] \qquad (2.64)$$

$$g\frac{\partial f}{\partial c} - f\frac{\partial g}{\partial c} = -p_{T_{i,j}} + (1+\theta_j)T_{i,j} - k\exp[AT_{i,j}/(T_0 + T_{i,j})] \cdot$$

$$c_{A_{i,j}}\gamma(c_{A_{i,j}} - \delta_0)[1 + (p_{T_{i,j}} - (1+\theta_j)T_{i,j} + p_{c_{i,j}}$$

$$-c_{A_{i,j}})(2 - \delta_0/c_{A_{i,j}})/(\delta_0 - c_{A_{i,j}})] \qquad (2.65)$$

The iterations are continued until the differences of two successive values of $c_{A_{i,j}}$ and $T_{i,j}$ are negligible.

The steady-state profiles are the initial conditions of the unsteady-state integration. With the final feed conditions, the final steady-state profiles can be obtained in the same manner.

The unsteady state differential equations are integrated by the Runge-Kutta-Gill method.[9] With this method, the errors are small and the machine storage is minimized. The Runge-Kutta-Gill method is a method of integrating numerically the first-order vector differential equation

$$\frac{dc}{dy} = f(c) \qquad (2.66)$$

(where c and f are vectors) with the scheme

$$
\left.
\begin{array}{ll}
 & c_0 = c(y) \\
i = 1: & k_1 = \frac{1}{2} h f(c_0) \\
 & c_1 = c_0 + k_1 \\
 & q_1 = 2k_1 \\
i = 2, 3: & k_i = \frac{1}{2} h f(c_{i-1}) \\
 & r_i = b_i(k_i - \frac{1}{2} q_{i-1}) \\
 & q_i = q_{i-1} + 3r_i - b_i k_i \\
 & c_i = c_{i-1} + r_i \\
i = 4: & k_4 = \frac{1}{2} h f(c_3) \\
 & c_4 = c_3 + \frac{1}{3}(k_4 - q_3) \\
\text{then} & c(y+h) \cong c_4 \quad . \\
\text{Here} & b_2 \equiv 2 - \sqrt{2} \\
\text{and} & b_3 \equiv 2 + \sqrt{2} .
\end{array}
\right\} \quad (2.67)
$$

This scheme is modified from that presented by Gill, to further minimize storage locations and computational steps, at the small expense of correction for round-off errors. Gill's scheme is a method for integrating a general system of ordinary first-order differential equations. In machine calculation with this method, storage is required for the three vectors c (the dependent variables), k (the derivatives of these variables),

and q (terms which include increments previously added to c and correction for round-off errors). In each of the four intermediate steps required for an advance by one increment in the independent variable, the newly calculated values of c, k, and q replace the previous values, which are no longer needed. Gill's scheme is an important improvement over previous fourth-order Runge-Kutta methods, which require storage for four vectors. In many systems, including the present one, these vectors are very large; for example, for a finite-stage model with 200 axial stages and with $M = 9$ (5 radial stages at each axial position), with heat transfer between particles and fluid, each vector c, k, and q has 3000 elements.

However, the concentration and fluid temperature in one stage of the finite-stage model is affected directly by the concentration and fluid temperature in only the two preceding stages, and the particle temperature in one stage is not directly affected by any other stage. Then if the concentrations and fluid temperatures of all the stages at a given axial position are stored elsewhere before being replaced with newly calculated values, they can be used in the calculations of the concentrations and temperatures in the stages at the next axial position. Then the vector k is not needed for storage between each of the four intermediate steps; all that is required in its place is a much smaller vector with elements of concentration and fluid temperature for each radial stage for any axial position. Thus, in the example above, the 3000-element vector k can be replaced with a 10-element vector.

Part C. The One-Dimensional Finite-Stage Model

The one-dimensional finite stage model is an array of continuous-flow stirred-tank chemical reactors in series. This model has no radial differences in concentration or temperature, but its axial characteristics are identical to those of the two-dimensional finite stage model. This model is shown in Figure 2.

Each reactor, or stage, is characterized by an axial position i. Each stage is a cylinder which includes portions of the particles and voids bounded by two planes at distances $(i - 1)\, d_p$ and $i d_p$ from the inlet of the bed; then each stage has a length d_p and a diameter equal to $M d_p$, the diameter of the tubular reactor being modeled.

Because of the similarity between the one-dimensional and the two-dimensional finite stage models, the equations describing the concentrations and temperatures of the one-dimensional model are easily obtained from those of the two-dimensional model. The area shared by stage i and stage i-1 is the cross-sectional area of the tubular reactor:

$$A = \tfrac{1}{4} \pi M^2 d_p^2 . \tag{2.68}$$

A mass balance on stage i gives

$$\frac{dc_{A_i}}{dt} = c_{A_{i-1}} - c_{A_i} - R_i . \tag{2.69}$$

A heat balance gives

$$\frac{dT_i}{dt} = T_{i-1} - T_i + R_i + Hp\,(T_{p_i} - T_i) + \frac{4Hw}{M}\,(T_w - T_i) , \tag{2.70}$$

and

$$\frac{dT_{p_i}}{dt} = \left(\frac{Hp}{\beta - 1}\right)(T_i - T_{p_i}) . \tag{2.71}$$

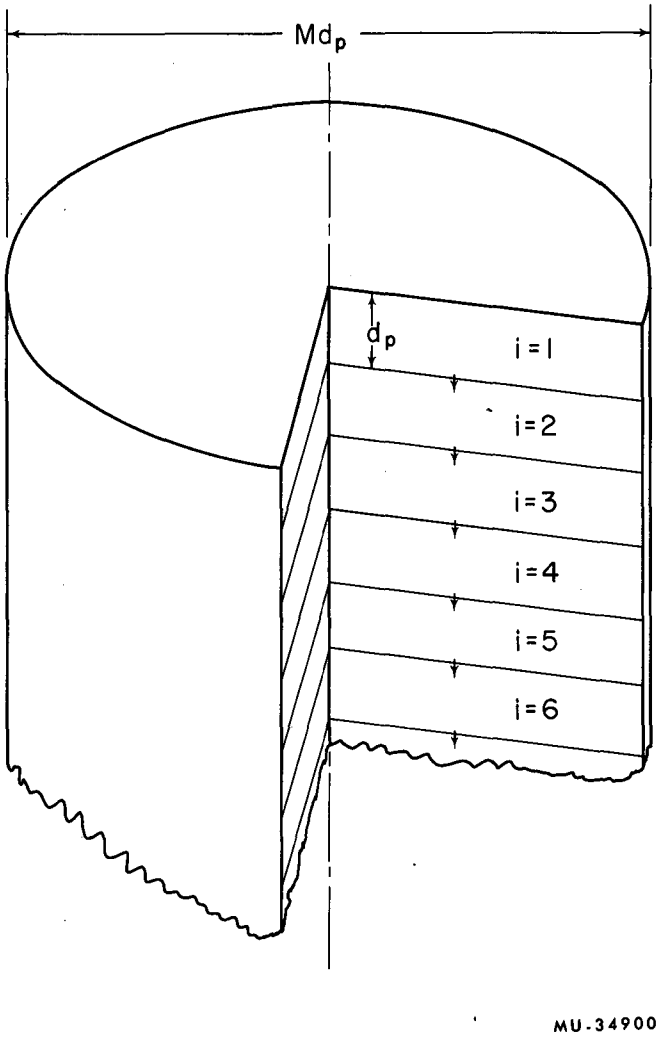

Fig. 2. Arrangement of stages in the one-dimensional finite stage model.

If there is a second reactant,

$$\frac{d\delta_i}{dt} = \delta_{i-1} - \delta_i \quad . \tag{2.72}$$

This last equation is identical to equation (2.33), obtained for the two-dimensional finite stage model for the case of equal feed concentrations in every inlet stage, and the same comments apply here.

The axial dispersion in this model results from the arrangement of the stirred-tank stages. The two-dimensional finite stage model exhibits the same axial dispersion.

The difference between this model and the two-dimensional finite stage model lies in the radial mixing feature of the latter. The one-dimensional model has no radial gradients. However, the two models are identical in every respect if they are adiabatic, in which case there are no radial gradients in the two-dimensional model. The differences between these two models is discussed in more detail in Chapter 3.

Part D. Techniques for Numerical Solution of the One-Dimensional Finite Stage Equations

Because the one-dimensional finite stage equations are just simplified forms of the two-dimensional finite stage equations, without dependence upon j, the numerical techniques for the solution of the one-dimensional finite stage equations are simplifications of the numerical techniques used in the solution of the two-dimensional finite stage equations.

The steady-state values of concentration and temperature are the roots of algebraic equations obtained by setting the time derivatives in equations (2.69), (2.70), and (2.71) to zero. For the solutions of these algebraic equations, equations (2.39) and (2.48) can be used for the case of one reactant, and equations (2.60) and (2.61) can be used for the case of two reactants, with the modification that the subscript j is ignored, and that

$$p_{c_i} = c_{A_{i-1}}, \tag{2.73}$$

$$p_{T_i} = T_{i-1}, \tag{2.74}$$

and

$$\theta = \frac{4Hw}{M} . \tag{2.75}$$

Similarly, the unsteady-state differential equations can be integrated numerically with the Runge-Kutta-Gill method discussed above.

Part E. The Plug Flow (Differential Equation) Model

The plug flow model is based upon these differential equations:

$$\frac{\partial c_A^*}{\partial t^*} + v \frac{\partial c_A^*}{\partial x^*} = - R^* , \tag{2.76}$$

$$\frac{\partial T^*}{\partial t^*} + v \frac{\partial T^*}{\partial x^*} = \left(\frac{-\Delta H}{\rho_f c_f}\right) R^* + \frac{h_p a_p (1-\epsilon)}{\rho_f c_f \epsilon} (T_p^* - T^*)$$

$$+ \left(\frac{4h_w}{\rho_f c_f M^*}\right) (T_w^* - T^*) , \tag{2.77}$$

and

$$\frac{\partial T_p^*}{\partial t^*} = \left(\frac{h_p a_p}{\rho_p c_p}\right) (T^* - T_p^*) . \tag{2.78}$$

These equations represent a component mass balance, a fluid heat balance, and a particle heat balance, respectively. In this model, axial dispersion is neglected and the concentration and temperatures in these equations represent radially averaged quantities.

In dimensionless form, these equations are

$$\frac{\partial c_A}{\partial t} + \frac{\partial c_A}{\partial x} = - R \tag{2.79}$$

$$\frac{\partial T}{\partial t} + \frac{\partial T}{\partial x} = R + Hp\,(T_p - T) + \frac{4Hw}{M}\,(T_w - T) \qquad (2.80)$$

$$\frac{\partial T_p}{\partial t} = \frac{Hp}{\beta - 1}\,(T - T_p)\ . \qquad (2.81)$$

These equations are the basic equations for the plug flow model.

It is sometimes assumed that the particle temperature is equal to the fluid temperature at any point in the reactor. Cowles[10] studied the effect of this assumption on the two-dimensional partial differential equation model of a catalytic gas reactor. The last equation shows that if T and T_p are equal, then $\partial T/\partial t$ and $\partial T_p/\partial t$ are equal and are generally finite and non-zero in the unsteady state, and thus Hp must be infinite. Only with an infinite Hp, i.e., no resistance at all to heat transfer between particles and fluid, are T and T_p equal at all times during unsteady state operation. Prior to the application of this assumption, the two heat balance equations can be combined into

$$\frac{\partial T}{\partial t} + \frac{\partial T}{\partial x} = R + \frac{4Hw}{M}\,(T_w - T) + (\beta - 1)\,\frac{\partial T_p}{\partial t}\ . \qquad (2.82)$$

With the assumption that T and T_p are equal, this equation becomes

$$\beta\frac{\partial T}{\partial t} + \frac{\partial T}{\partial x} = R + \frac{4Hw}{M}\,(T_w - T)\ . \qquad (2.83)$$

This equation is the only heat balance to be satisfied when the temperature of the particles is assumed to be indistinguishable from the temperature of the fluid at any point in the reactor. β incorporates the heat capacity of the packing as well as that of the fluid.

This special case will be referred to as the case of infinite Hp. The assumption of equal T and T_p is used to simplify the more general system by eliminating a parameter, Hp, and a dependent variable, T_p. For this case, the basic equations of the plug flow model are the component mass balance, equation (2.79), and the heat balance, equation (2.83).

For either case, the system equations are quasi-linear hyperbolic equations which can be treated by the method of characteristics.[11,12] This method relates the solution to the characteristics, which are curves in space-time along which discontinuities in the system propagate.

To obtain the velocities of propagation of the discontinuities, from which the characteristic curves are obtained, the system equations are written in a canonical form. For the case of infinite Hp, the equations become

$$\begin{vmatrix} \frac{\partial c_A}{\partial t} \\ \frac{\partial T}{\partial t} \end{vmatrix} + \begin{vmatrix} 1 & 0 \\ 0 & \frac{1}{\beta} \end{vmatrix} \begin{vmatrix} \frac{\partial c_A}{\partial x} \\ \frac{\partial T}{\partial x} \end{vmatrix} = \begin{vmatrix} -R \\ \frac{1}{\beta} R + \frac{1}{\beta} \frac{4Hw}{M} (T_w - T) \end{vmatrix} . \tag{2.84}$$

As shown by Jeffrey,[12] the velocities of propagation of the discontinuities are the characteristic roots of the matrix of coefficients:

$$\frac{dx}{dt} = 1, \ \frac{1}{\beta} .$$

The discontinuities in the reactor originate from the step change of the feed concentration or the feed temperature at $t = 0$. Then a discontinuity travelling with velocity 1 and another discontinuity travelling with a lower velocity $1/\beta$ is expected. These velocities suggest the introduction of new independent variables, which represent the (scaled) time from the appearance of either discontinuity at a given axial position x:

$$y = \frac{\beta x - t}{\beta - 1} , \qquad z = \frac{t - x}{\beta - 1} ; \tag{2.85}$$

and

$$t = y + \beta z , \qquad x = y + z . \tag{2.86}$$

The system equations can be expressed in this characteristic coordinate system through the partial derivative chain rules:

$$\left(\frac{\partial c_A}{\partial y}\right)_z = \left(\frac{\partial c_A}{\partial t}\right)_x \left(\frac{\partial t}{\partial y}\right)_z + \left(\frac{\partial c_A}{\partial x}\right)_t \left(\frac{\partial x}{\partial y}\right)_z = \frac{\partial c_A}{\partial t} + \frac{\partial c_A}{\partial x},$$

or

$$\frac{\partial c_A}{\partial y} = - R . \tag{2.88}$$

Similarly,

$$\left(\frac{\partial T}{\partial z}\right)_y = \left(\frac{\partial T}{\partial t}\right)_x \left(\frac{\partial t}{\partial z}\right)_y + \left(\frac{\partial T}{\partial x}\right)_t \left(\frac{\partial x}{\partial z}\right)_y = \beta \frac{\partial T}{\partial t} + \frac{\partial T}{\partial x} \tag{2.89}$$

or

$$\frac{\partial T}{\partial z} = R + \frac{4Hw}{M} (T_w - T) . \tag{2.90}$$

The line $z = 0$ represents the trajectory along which the discontinuity with velocity 1 travels; the line $y = 0$ represents the trajectory along which the discontinuity with velocity $1/\beta$ travels. These lines are shown in Figure 3, together with lines z = constant, which are parallel to the $z = 0$ line, and lines y = constant, which are parallel to the $y = 0$ line. The space-time region can be transformed to y-z region, as shown in Figure 4. The line $x = 0$ represents the inlet of the reactor, and the line $x = N$ represents the outlet of the reactor; these two lines bound the region of interest in the y-z plane. The line $t = 0$ represents the reactor at the instant that the step change occurs in the feed concentration or temperature; because the discontinuities travel at finite velocity, the reactor is at steady state everywhere along this line. The segment of the line $x = 0$ below the origin (for $t < 0$) is called here the initial feed line; the segment of the line $x = 0$ above the origin (for $t > 0$) is called the final feed line.

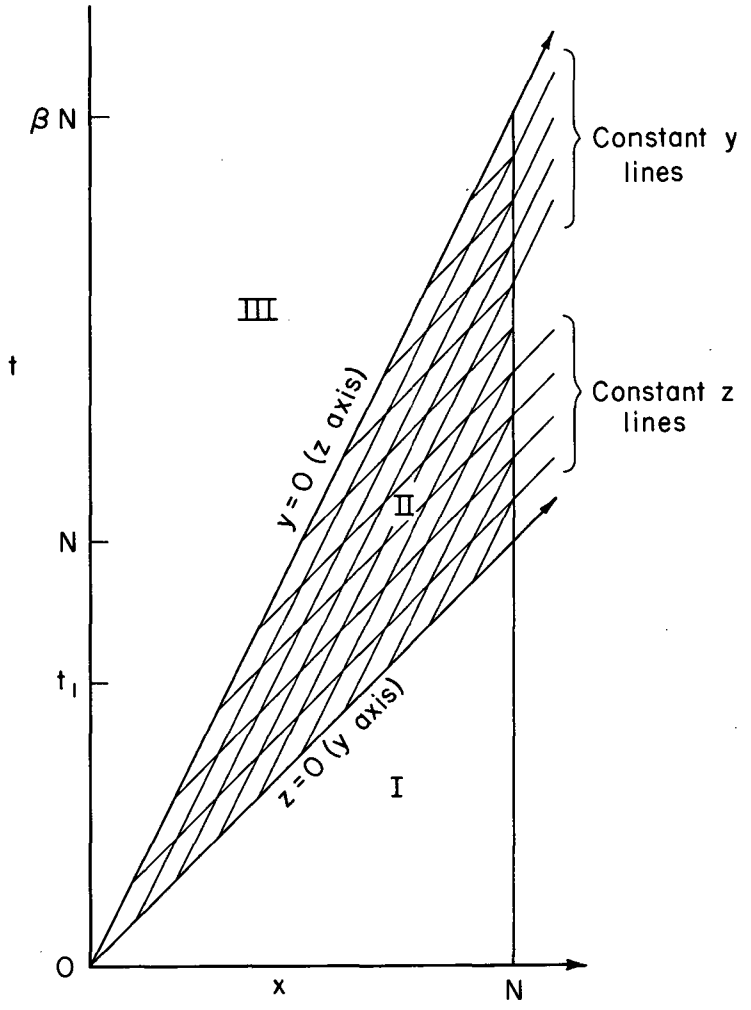

MU-34907

Fig. 3. Characteristics in space-time for the plug flow model (infinite Hp).

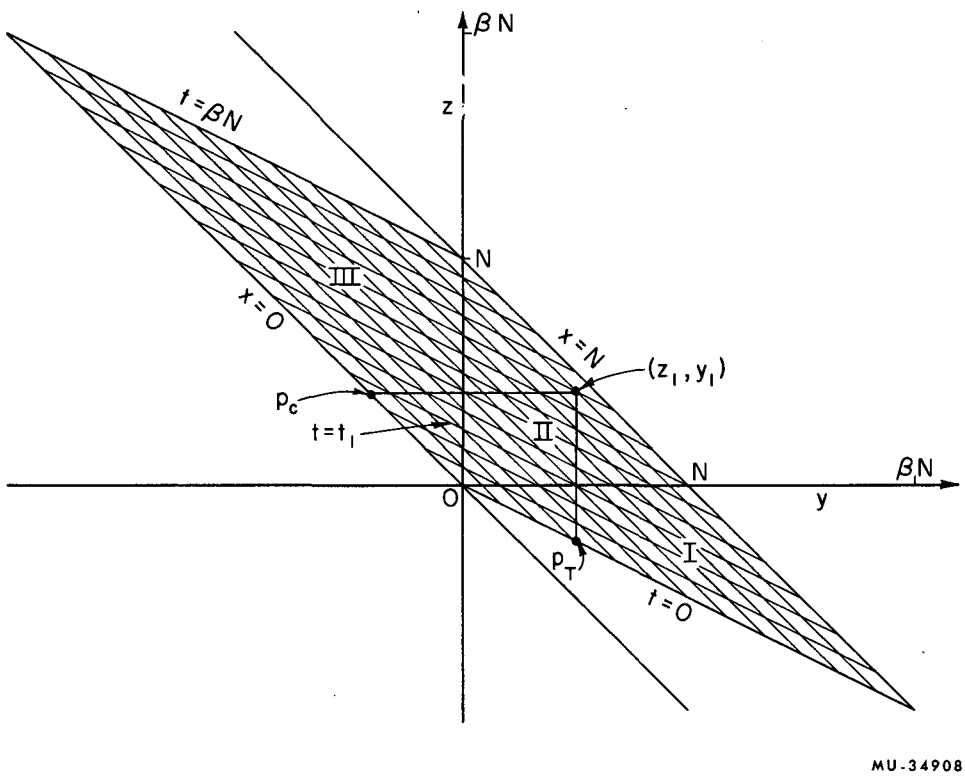

Fig. 4. Characteristic coordinates for the plug flow model (infinite Hp).

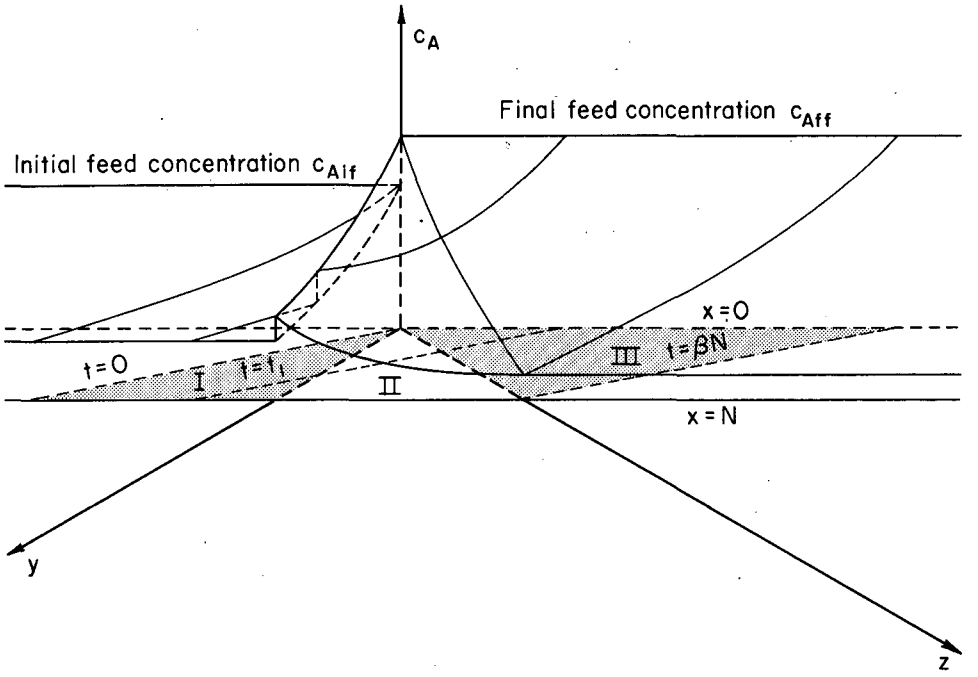

MU-34902

Fig. 5. Concentration, as a function of the characteristic coordinates, resulting from a concentration step. Plug flow model (infinite Hp).

A solution of these system equations is a representation of concentration and temperature as functions of x and t for a given set of system parameters and inlet conditions. The independent variables could instead be y and z, because transformation from one coordinate system to another is simple, by equations (2.85) and (2.86). Graphically, a solution may be represented as a surface in (c_A, y, z) space, and another surface in (T, y, z) space. Figure 5 shows how a concentration surface might appear for a step in feed concentration but constant in feed temperature; the corresponding temperature surface is not shown.

The concentration profile at the line $t = 0$ in Figure 5 represents the initial steady state profile. This same profile may be found at any constant time line, where time is less than zero. Similarly, for large time, a final steady state profile is found at any constant time, where time is sufficiently large; in the figure, the steady state profile is shown for the line $t = \beta N$. For any intermediate constant time line there is an unsteady state profile. For example, the unsteady state concentration profile for $t = t_1$ (where t_1, a constant, is less than N) is shown in Figures 5 and 6.

But for <u>any</u> line in the y-z plane which crosses the $x = 0$ and the $x = N$ lines there exist a concentration profile and a temperature profile. Only if such a line is a constant time line do the profiles exist in the reactor at an instant of time. If the line is not a constant time line, the points on these profiles exist at different instants of time at their respective axial positions, but it is useful to consider these profiles in the various regions of the y-z space.

Along the line $t = 0$, and along every constant time line where time is less than zero, lie the initial steady state profiles. These profiles can be found by setting the time derivatives in equations (2.79) and (2.83) equal to zero and integrating the resulting simultaneous ordinary differential equations with respect to x, with the initial feed concentration and temperature. But these profiles can also be found by integrating the equations (2.88) and (2.90) from the initial feed line.

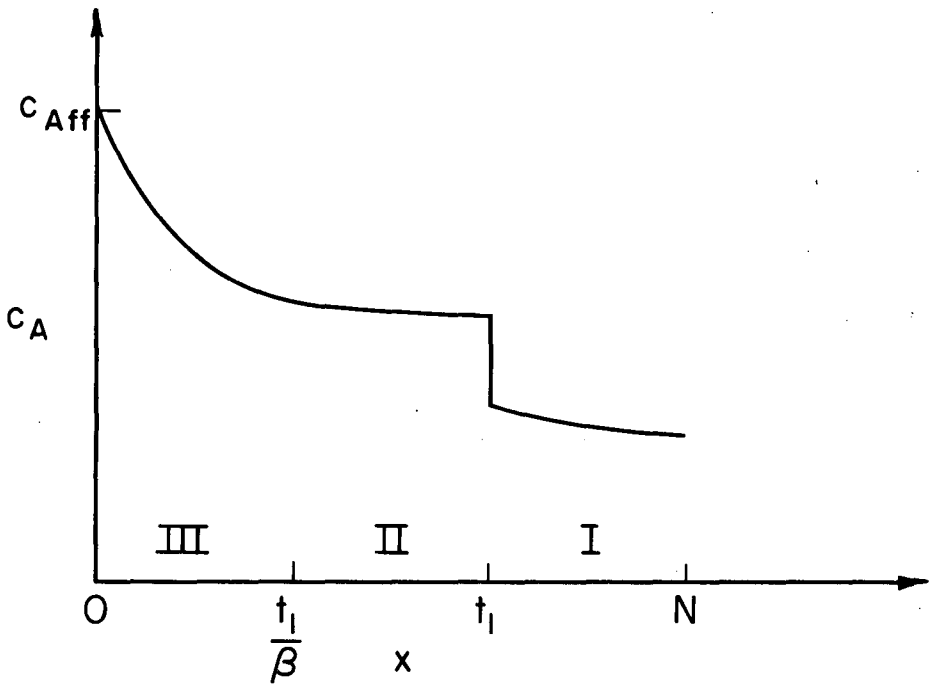

MU-34906

Fig. 6. An instantaneous concentration profile at time $t = t_1$ (constant). Plug flow model (infinite Hp).

The concentration equation, (2.88), is integrated along a line parallel to the y-axis; the temperature equation, (2.90), is integrated along a line parallel to the z-axis. Then, in this region, the steady state profiles lie along any constant z line (parallel to the y-axis) or any constant y line (parallel to the z-axis) or any other line which crosses the $x = 0$ and the $x = N$ lines.

The concentration and temperature at any point, (y_1, z_1), in the y-z plane can be found in the same manner: the concentration equation, (2.88), is integrated from the known feed concentration at point p_c to the point (y_1, z_1) along the constant z line, $z = z_1$ (assuming that the temperature profile along this line is known), and the temperature equation, (2.90), is integrated from the known feed temperature at the point p_T to the point (y_1, z_1) along the constant y line, $y = y_1$ (assuming that the concentration profile along this line is known). The temperature profile along the line $z = z_1$, needed for the determination of R in the concentration equation (2.88), is found by integrating the temperature equation in the z direction from the known feed temperatures at every point along the feed line from point p_c to point p_T; similarly, the concentration profile along the line $y = y_1$ is found by integrating the concentration equation in the y-direction from the known feed concentrations at every point along the feed line from point p_c to point p_T.

Thus, the primary effect of the feed concentration is in the y-direction through the concentration equation, and the primary effect of the feed temperature is in the z-direction through the temperature equation. This concept, that the feed concentration and feed concentration disturbances act in the y-direction and that the feed temperature and feed temperature disturbances act in the z-direction, is very useful in determining and describing the unsteady state behavior of the plug flow model.

For example, it is clear that the y-axis is the characteristic which represents the propagation of a step change in feed concentration through the reactor, and the z-axis is the characteristic which represents the propagation of a step change in feed temperature through the reactor.

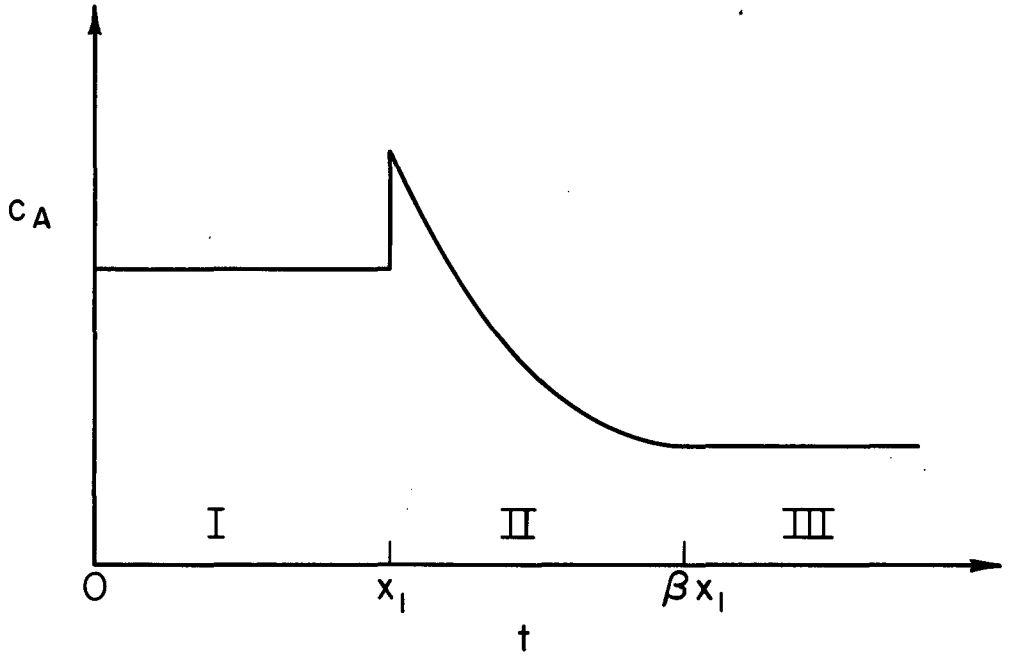

MU-34905

Fig. 7. Transient behavior of concentration at axial position x_1. Plug flow model (infinite Hp).

Also, the entire region in the y-z plane below the y-axis is affected only by the initial feed concentration and the initial feed temperature (on the initial feed line). This region is the initial steady state region. It is labeled I in Figures 5, 6, and 7. It includes the triangular region between the y-axis and the line $t = 0$ which represents that portion of the reactor which the concentration discontinuity, travelling with velocity 1, has not yet reached. Along any line in this region lie the initial steady state concentration and temperature profiles. Along any constant x line in this region, concentration and temperature are constant.

Similarly, the entire region in the y-z plane to the left of the z-axis is affected only by the final feed concentration and the final feed temperature (on the final feed line). This region is the final steady state region. It is labelled III in Figures 4, 5, 6, and 7. At $t = \beta N$, the temperature discontinuity has reached the end of the reactor. Then the region below the $t = \beta N$ line and left of the z-axis represents that portion of the reactor through which the temperature discontinuity has already passed. Thus the concentration and temperature at any axial position is at steady state immediately after the temperature discontinuity passes that axial position. Along any line in this region lie the final steady state concentration and temperature profiles. Along any constant x line in this region, concentration and temperature are constant.

Then the unsteady state region in the y-z plane is the triangle bounded by the z-axis, the y-axis, and the line $x = N$. The concentration and the temperature in this region are affected by the final feed concentration, on the final feed line, and the initial feed temperature, on the initial feed line. This region is labelled II in the figures.

Figure 5 shows concentration in a reactor as a function of y and z for a step change in feed concentration but not in feed temperature. The initial concentration profile in region I is shown, as is the final concentration profile in region III. The concentration discontinuity is seen lying along the y-axis. On the z-axis, the concentration and the concentration derivative, $(\partial c_A/\partial y)$, are continuous.

A discontinuity in either concentration or temperature causes a corresponding discontinuity in the temperature derivative, $(\partial T/\partial z)$, or the concentration derivative, $(\partial c_A/\partial y)$, through the coupling term R in equations (2.88) and (2.90). Thus, in the example shown in Figure 5, there is no temperature discontinuity; hence the concentration derivative is continuous across the z-axis. The concentration itself is always continuous across the z-axis, because concentration discontinuities travel in the y-direction. Similarly, the temperature is always continuous across the y-axis because temperature discontinuities travel in the z-direction. Also, the concentration discontinuity on the y-axis causes a discontinuity in the temperature derivative across the y-axis; so although the temperature is continuous across the y-axis, its derivative is not.

Although the primary effect of the feed concentration is in the y-direction, there are secondary effects through the coupling term, R, which propagate along the z-axis. These effects appear in the higher derivatives of concentration and temperature along the z-axis. Thus, in the example of Figure 5, although there is no temperature discontinuity, unsteady state behavior is found not only along the y-axis, but throughout the whole region II. Similarly, in the case of a temperature discontinuity but not a concentration discontinuity, changes begin along the y-axis, before the temperature discontinuity has passed through the reactor, even though concentration and temperature (and some derivatives) are continuous on the y-axis.

Figure 6 shows a concentration profile which lies along a constant time line which passes through all three regions of the y-z plane, for the example of Figure 5. This profile occurs in the reactor at the instant of time $t = t_1$, where t_1 is a constant less than N. The figure shows the intersection with the z-axis at this instant. Upstream from the z-axis (for $x \leq t_1/\beta$), the profile is that of the final steady state profile, as the temperature effects have already passed through this region. Downstream from the concentration discontinuity (for $x \geq t_1$), the profile is that of the initial steady state profile, because the

concentration discontinuity has not yet reached this region. In the middle is the unsteady state region.

That the whole of region II is an unsteady state region as a result of a step in feed concentration can be reasoned from a slightly different approach. The discontinuity in concentration along the y-axis causes disturbances in temperature along the y-axis (i.e., a discontinuity in the temperature derivative, $\partial T/\partial z$, along the y-axis). These disturbances affect region II through the temperature equation (2.90) from the y-axis. A temperature discontinuity similarly affects the unsteady state region, causing unsteady state behavior beginning along the y-axis.

Figure 7 shows the unsteady state behavior of concentration at a given axial position, x_1, for the example of Figure 5. Before the concentration discontinuity passes this point in the reactor, the concentration is at its initial value. The discontinuity passes this point at $t = x_1$; afterward, the concentration changes and approaches its final value, which it obtains when the temperature effect passes through, at $t = \beta x_1$.

These forms of presentation of unsteady state behavior, concentration and temperature profiles at given values of time and the unsteady state behavior of concentration and temperature at given axial position, are more understandable and more easily related to physical observations than are profiles along characteristics, which follow directly from solution with the method of characteristics, so the former forms are used in the presentation of numerical calculations. Figures 5, 6, and 7 are presented here only to illustrate the major features of such unsteady state behavior; they are not quantitative representations of a solution of the plug flow equations for a particular set of parameters.

Without study using the method of characteristics, the unsteady state region might reasonably be expected to be the space-time region between the inlet and the outlet of the reactor ($0 \leq x \leq L$) and between $t = 0$ and some indefinite time greater than $t = \beta N$. This analysis, with the method of characteristics, has shown that the unsteady state

region is actually the smaller region that is bounded by the two characteristics. The regions representing the portions of the reactor which the concentration characteristic has not yet reached or through which the temperature characteristic has already passed are steady state regions, and the concentration and temperature in these regions are known from the initial and final steady state profiles.

To obtain the concentration and the temperature in the unsteady state region, the concentration equation (2.88) and the temperature equation (2.90) are integrated in this region; to integrate these equations, the proper boundary conditions must be obtained. These boundary conditions, the concentration and temperature profiles along the y-axis and the z-axis, are easily obtained from these facts: Temperature is continuous across the y-axis, and concentration is continuous across the z-axis; the concentration equation (2.88) and the temperature equation (2.90) must be satisfied everywhere, including the y-axis and the z-axis; and the initial feed temperature and the final feed concentration primarily affect the unsteady state region.

Then, because temperature is continuous across the y-axis, the temperature profile along the y-axis is the initial steady state temperature profile. The concentration profile along the y-axis is obtained by integrating the concentration equation, using the final feed concentration as the inlet boundary condition and using the temperature profile along the y-axis in the evaluation of the coupling term R. The difference between this concentration profile and the initial steady state concentration profile is the concentration discontinuity which appears along the y-axis.

Similarly, because concentration is continuous across the z-axis the concentration profile along the z-axis is the final steady state concentration profile. The temperature profile along the z-axis is obtained by integrating the temperature equation, using the initial feed temperature as the inlet boundary condition and using the concentration profile along the z-axis in the evaluation of the coupling term R. The difference between this temperature profile and the final steady state temperature profile is the temperature discontinuity which appears along the z-axis.

Because of the concentration discontinuity along the y-axis, the temperature derivative, $(\partial T/\partial z)$, at every point along the y-axis also has a discontinuity, through the coupling term R. Most numerical integration methods require continuous derivatives, so the temperature equation could not generally be integrated numerically across the y-axis from initial conditions on the line $t = 0$, for example. However, by transforming to a characteristic coordinate system, and by finding the concentration and temperature profiles along the characteristic coordinate axes and using these profiles as boundary conditions, numerical integration across discontinuities has been avoided.

Although the concentration and the temperature affect each other in the unsteady state through the coupling term R, the characteristics along which the discontinuities travel are determined by the form of the derivatives, i.e., the left-hand side of the system equations, as equation (2.84) illustrates; the right-hand side does not affect the characteristics (except indirectly in cases where the characteristics, or velocities of propagation of discontinuities, are functions of the dependent variables). Then the characteristics for the case of finite Hp should be different from those for the case of infinite Hp, just discussed.

In fact, for the case of finite Hp, because the form of the derivatives in the concentration equation (2.79) is identical to the form of the derivatives in the temperature equation (2.80), discontinuities in concentration and in fluid temperature travel along the same characteristics for this case.

The velocities of propagation of the discontinuities for the case of finite Hp are found, as before, from the matrix of coefficients:

$$\begin{vmatrix} \dfrac{\partial c_A}{\partial t} \\ \dfrac{\partial T_p}{\partial t} \end{vmatrix} + \begin{vmatrix} 1 & 0 \\ 0 & 0 \end{vmatrix} \begin{vmatrix} \dfrac{\partial c_A}{\partial x} \\ \dfrac{\partial T_p}{\partial x} \end{vmatrix} = \begin{vmatrix} -R \\ \dfrac{Hp}{\beta - 1}(T - T_p) \end{vmatrix} . \qquad (2.91)$$

The fluid temperature equation could have been used in place of the concentration equation; the same matrix of coefficients would result. The velocities of propagation of the discontinuities are[12]:

$$\frac{dx}{dt} = 0,\ 1.$$

The absence of a $\partial T_p/\partial x$ term in the equations, resulting in a zero velocity of propagation of discontinuities, means that the particle temperature at any point in the reactor is not directly affected by the particle temperature at any other point in the reactor. This isolation of particle temperature is expected, because in this model conduction of heat through adjacent particles is excluded.

For this case, the characteristic coordinates are:

$$y = x, \qquad z = t - x\ ; \tag{2.92}$$

then

$$t = y + z, \qquad x = y\ . \tag{2.93}$$

Thus

$$\left(\frac{\partial c_A}{\partial y}\right)_z = \left(\frac{\partial c_A}{\partial t}\right)_x \left(\frac{\partial t}{\partial y}\right)_z + \left(\frac{\partial c_A}{\partial x}\right)_t \left(\frac{\partial x}{\partial y}\right)_z = \frac{\partial c_A}{\partial t} + \frac{\partial c_A}{\partial x} \tag{2.94}$$

or

$$\frac{\partial c_A}{\partial y} = -\ R; \tag{2.95}$$

and

$$\frac{\partial T}{\partial y} = R + \frac{4Hw}{M}\ (T_w - T) + Hp(T_p - T)\ . \tag{2.96}$$

Similarly,

$$\left(\frac{\partial T_p}{\partial z}\right)_y = \left(\frac{\partial T_p}{\partial t}\right)_x \left(\frac{\partial t}{\partial z}\right)_y + \left(\frac{\partial T_p}{\partial x}\right)_t \left(\frac{\partial x}{\partial z}\right)_y = \frac{\partial T_p}{\partial t} \tag{2.97}$$

or

$$\frac{\partial T_p}{\partial z} = \frac{Hp'}{\beta - 1}\ (T - T_p)\ . \tag{2.98}$$

Figure 8 shows the constant z lines and the constant y lines in the t-x plane, and Figure 9 shows the transformed constant t lines and constant x lines in the y-z plane. For this case, the constant y lines and the constant x lines are identical, from equation (2.92). Therefore the line $y = 0$, the z-axis, represents the inlet of the reactor, or the feed line. The step change in feed concentration or feed temperature, or both, occurs at the origin; so the z-axis below the y-axis is the initial feed line, and the z-axis above the y-axis is the final feed line.

As in the previous case, the region below the y-axis is the initial steady state region. This includes the region above the line $t = 0$, which represents that portion of the reactor which the concentration and temperature discontinuity has not yet reached. It is seen from equation (2.81) that at steady state, the fluid temperature and the particle temperature are identical; thus the fluid temperature profile and the particle temperature profile along a line in this initial steady state region are identical.

The concentration, fluid temperature, and particle temperature can be found at any point (y_1, z_1) in the y-z plane from the integration of the differential equations, as before: The concentration equation (2.95) and the fluid temperature equation (2.96) are integrated simultaneously in the y-direction along the line $z = z_1$ from the known values of concentration and fluid temperature at the feed line (the z-axis), and the particle temperature equation (2.98) is integrated in the z-direction along the line $y = y_1$ from the known value of particle temperature at any initial steady state profile in the region below the y-axis. The particle temperature profile along the line $z = z_1$, necessary for the evaluation of the right-hand side of the fluid temperature equation (2.96), is found from previous integrations; and similarly, the fluid temperature profile along the line $y = y_1$ is known from previous integrations.

Then the final feed concentration and the final feed temperature primarily affect the unsteady state region through the concentration

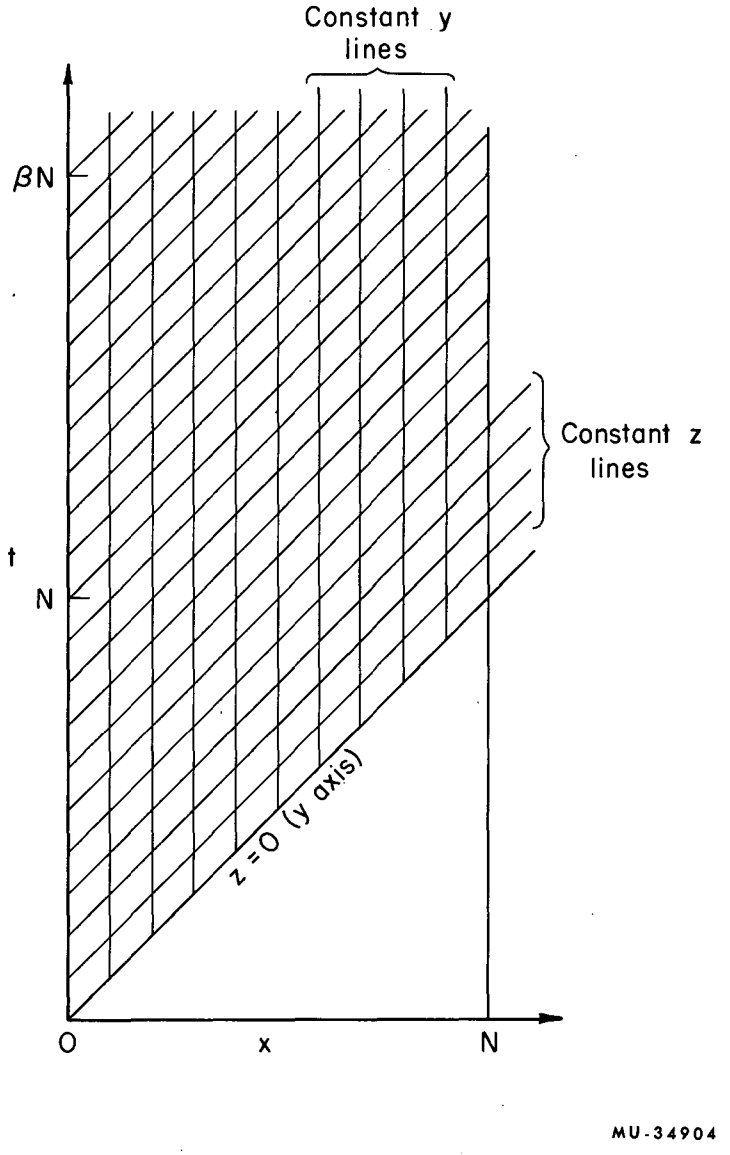

Fig. 8. Characteristics in space-time for the plug flow model (finite Hp).

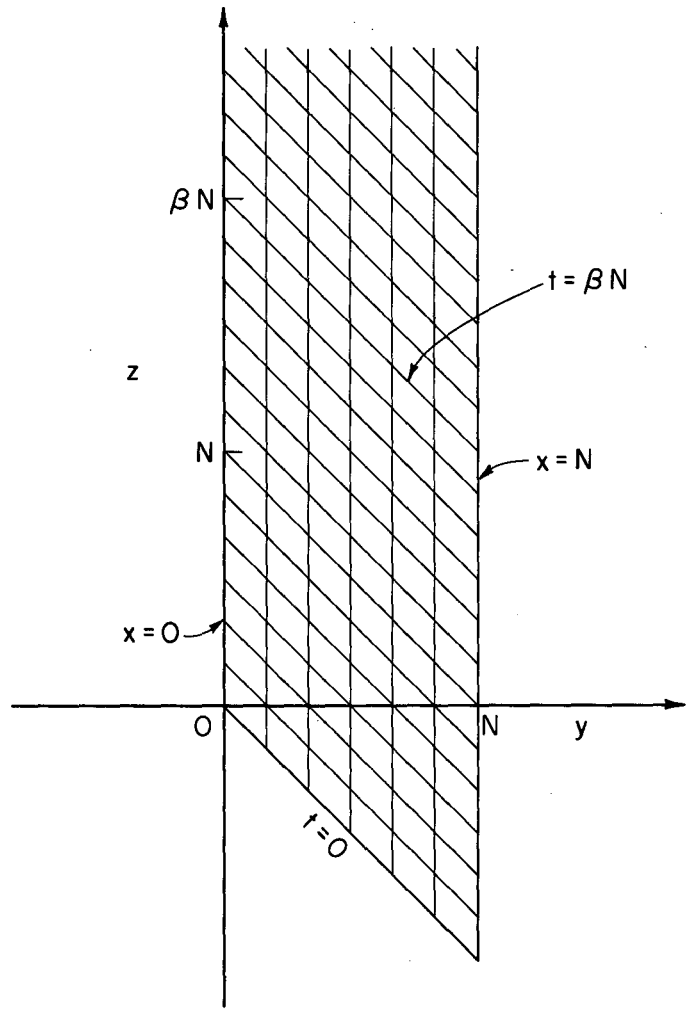

MU-34903

Fig. 9. Characteristic coordinates for the plug flow model (finite Hp).

equation (2.95) and the fluid temperature equation (2.96). With this fact, and the facts that the differential equations must be satisfied everywhere in the y-z space and the particle temperature is continuous acrossthe y-axis (particle temperature discontinuities, if present, lie along lines parallel to the z-axis), the profiles along the y-axis can be found. The particle temperature profile acrossthe y-axis is identical to the initial steady state particle (and fluid) temperature profile, and the concentration and fluid temperature profiles along the y-axis are found by integrating simultaneously the concentration equation (2.95) and the fluid temperature equation (2.96) along the y-axis, using the final feed concentration and final feed temperature as inlet boundary conditions and using the particle temperature profile along the y-axis in the evaluation of the right-hand side of the fluid temperature equation (2.96).

The differences between these concentration and fluid temperature profiles and the initial steady state profiles represent the discontinuities along the y-axis. Because the equations are integrated simultaneously, there are discontinuities in both concentration and fluid temperature, even though the step change in the feed may have been in only one of these variables. If there is a step change in feed concentration, for example, the fluid temperature cannot be expected to be continuous across the y-axis, because the initial steady state temperature profile does not satisfy the fluid temperature equation, which is affected by the concentration profile along the y-axis which is different from the initial steady state concentration profile.

The particle temperature at the feed line (the z-axis), necessary for the evaluation of the concentration and fluid temperature derivatives along the z-axis, is found in a similar manner, from the integration of the particle temperature equation along the z-axis:

$$\left.\begin{aligned} T_p &= T_{ff} - (T_{ff} - T_{if})\, e^{-\frac{Hpz}{\beta - 1}} \quad \text{at } y = 0,\ z \geqslant 0\ , \\ T_p &= T_{ff} - (T_{ff} - T_{if})\, e^{-\frac{Hpt}{\beta - 1}} \quad \text{at } x = 0,\ t \geqslant 0\ . \end{aligned}\right\} \qquad (2.99)$$

T_{if} and T_{ff} are the initial and final feed temperatures.

This equation shows that there is no final steady state region for this case, unlike the case of infinite Hp. Here, the unsteady state region is the entire region above the y-axis. The concentration, fluid temperature, and particle temperature in the unsteady state region are found by integrating the system equations, with the boundary conditions along the y-axis and the z-axis obtained as discussed above.

The final steady state profiles, which the unsteady state profiles approach as time (or z) increases, can be obtained by integrating the concentration and fluid temperature equations, with the final feed conditions and the fact that the fluid temperature and the particle temperature are equal at steady state. It is seen that the initial and final steady state profiles of the finite Hp case are the same as those of the infinite Hp case, because the effect of heat transfer between particles and fluid is a dynamic effect only.

Although there are fundamental differences in the characteristics of the two cases considered here, both cases are useful. For example, if continuous feed disturbances are considered, such as a sinusoidal feed disturbance for a frequency response determination, then the case of finite Hp is appropriate if the dominant period of disturbance is less than the time constant of the particle-fluid heat transfer ($\frac{\beta - 1}{Hp}$ in dimensionless form), but the case of infinite Hp is adequate if the dominant period of the disturbance is greater than the time constant of the particle-fluid heat transfer.

Further, it will be seen that for some systems the behaviors of the two cases agree better than might be expected from the

differences in characteristic form because the discontinuities on the characteristics are insignificant compared with large, continuous changes which occur in the unsteady state regions. And in actual reactors, discontinuities are attenuated and smoothed by axial dispersion, which is ignored in the plug flow model. Therefore the major dynamic effects in a system do not necessarily occur along the characteristics, but treatment by the method of characteristics reduces the system equations and unsteady state region to simple forms which allow an uncomplicated numerical solution.

Another similarity of the two cases is the treatment of the second reactant, if there are two reactants. The differential equation which describes the second reactant with respect to the characteristic coordinates, regardless of whether Hp is finite or infinite, is

$$\frac{\partial c_B}{\partial y} = - \gamma R \, . \tag{2.100}$$

Then

$$\frac{\partial \delta}{\partial y} = \frac{\partial c_A}{\partial y} - \frac{1}{\gamma} \frac{\partial c_B}{\partial y} = 0 \, . \tag{2.101}$$

Thus δ is constant along any constant z-line; but δ may have another constant value on another constant z-line. The value of δ along any constant z-line is the value of δ at the intersection of this line and the feed line, where δ is determined from the known feed concentrations of the two reactants. Because the feed concentrations are constant on the initial feed line (below the y-axis), everywhere below the y-axis δ has the constant value

$$\delta = c_{A_{if}} - c_{B_f}/\gamma \, , \tag{2.102}$$

and because the feed concentrations are constant on the final feed line, everywhere above the y-axis δ has the constant value

$$\delta = c_{A_{ff}} - c_{B_f}/\gamma \, . \tag{2.103}$$

Therefore, in the unsteady state region, the concentration of the second reactant is easily determined from the concentration of the primary reactant by

$$c_B = \gamma (c_A - \delta) \tag{2.104}$$

where δ has the constant value determined in equation (2.103).

Part F. Numerical Techniques for the Solution of the Plug Flow Equations

The two cases of the plug flow model, that of finite Hp and that of infinite Hp, can be treated by the same numerical techniques, because the system differential equations have the same general form, and boundary conditions lie along the y-axis and the z-axis in both cases. These boundary conditions are known or can be obtained by well-known numerical integration techniques which are independent of the techniques used in the unsteady state region. The boundary conditions will be discussed later.

In both cases, the system equations have the same general form, which can be expressed in vector notation as

$$\frac{\partial c}{\partial y} = f(c, u) \tag{2.105}$$

and

$$\frac{\partial u}{\partial z} = g(c, u) \tag{2.106}$$

where y and z are the scalar characteristic coordinates, as before, and c, u, f, and g are vectors, the components of which are the appropriate dependent and independent variables. For example, for the case of finite Hp, with two reactants, the vectors may be written elaborately as

$$c = \begin{bmatrix} c_A \\ T \\ \delta \\ y \\ x \\ t \end{bmatrix}, \quad f = \begin{bmatrix} -ke^{\frac{AT}{T+T_0}} c_A \gamma (c_A - \delta) \\ ke^{\frac{AT}{T+T_0}} c_A \gamma (c_A - \delta) + \frac{4Hw}{M}(T_w - T) + Hp(T_p - T) \\ 0 \\ 1 \\ 1 \\ 1 \end{bmatrix}$$

$$u = \begin{bmatrix} T_p \\ z \\ x \\ t \end{bmatrix}, \quad g = \begin{bmatrix} \frac{Hp}{\beta - 1}(T - T_p) \\ 1 \\ 1 \\ 0 \end{bmatrix} \tag{2.107}$$

The independent space-time variables and characteristic coordinate variables are included as an illustration; they are generally necessary only if the transformation from characteristic coordinates to space time is not known because the velocities of propagation of discontinuities are functions of the dependent variables. The space-time variables may be included if the parameters are dependent on them; for example, when Hw or T_w varies with x. The characteristic coordinates may be included as a check on numerical techniques, to determine at what point in the y-z plane intermediate calculations required by the particular numerical scheme are made. In practice, c_A and T are usually the only necessary components of c [δ is a known constant, from equation (2.103)], and T_p is the only necessary component of u.

Vector notation is used here to simplify the expressions obtained and to relate general numerical techniques to the two cases

considered previously. In the following development, c and u can be considered as scalars or vectors; the resulting equations can be considered as scalar equations which apply to each component of c or u.

To obtain the desired solution of c and u as functions of y and z, the system equations (2.105) and (2.106) are integrated. For the general case in which f and g are nonlinear functions, the equations can be integrated numerically. For numerical integration, the unsteady state region in the y-z plane can be divided into a network or lattice of rectangles, of the form of Figure 10. The sides of the rectangles parallel to the z-axis have length h, and the sides of the rectangles parallel to the y-axis have length k. The location of the lower left corner of a rectangle is $y = ik$, $z = jh$.

The values of c and u, and thus f and g, at the points (i,j), $(i+1,j)$, and $(i,j+1)$, are known, and with a proper numerical integration scheme, the values of c and u at $(i+1,j+1)$ can be calculated. This conforms with the specified boundary conditions, by which c and u are known along the y- and z-axes. These boundary conditions give the values of the variables c and u on the boundaries, at all points $(0,j)$ and $(i,0)$.

A method of integration which can be used in this two-dimensional region is the modified Euler method,[11] which is a predictor and iterated corrector method. The predictor is

$$c^{(1)}_{i+1,j+1} = c_{i+1,j} + kf(c_{i+1,j}, u_{i+1,j}) \tag{2.108}$$

$$u^{(1)}_{i+1,j+1} = u_{i,j+1} + hg(c_{i,j+1}, u_{i,j+1}) \tag{2.109}$$

The corrector is

$$c^{(m+1)}_{i+1,j+1} = c_{i+1,j} + \tfrac{1}{2}\left[k\, f(c_{i+1,j}, u_{i+1,j}) + f(c^{(m)}_{i+1,j+1}, u^{(m)}_{i+1,j+1})\right] \tag{2.110}$$

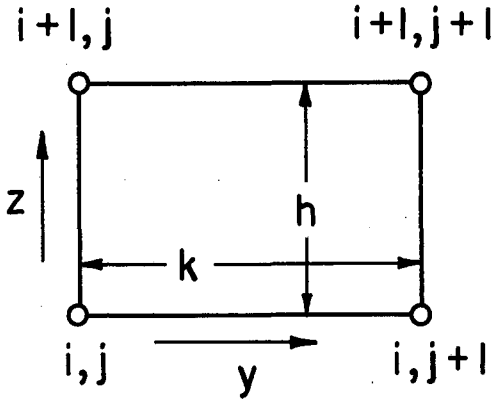

MU-34913

Fig. 10. Lattice rectangle in two-dimensional numerical integration.

$$u_{i+1,j+1}^{(m+1)} = u_{i,j+1} + \tfrac{1}{2} h\left[g(c_{i,j+1}, u_{i,j+1}) + g(c_{i+1,j+1}^{(m)}, u_{i+1,j+1}^{(m)})\right] \tag{2.111}$$

where the superscript indicates the number of the iteration. The iteration is usually continued until the difference between $c_{i+1,j+1}^{(m+1)}$ and $c_{i+1,j+1}^{(m)}$ and the difference between $u_{i+1,j+1}^{(m+1)}$ and $u_{i+1,j+1}^{(m)}$ are negligible or until m reaches a particular value, the choice of which should be based upon experience with other systems in which $f, g, h,$ and k have magnitudes similar to those of the present system.

Because the truncation error in this method is proportional to the third and higher powers of h and k, the method is third order.[7] Its main disadvantages are the truncation errors and the selection of an appropriate number of iterations. Truncation errors can be decreased by decreasing h and k, at the expense of computing time. The proper choice of the number of iterations is important, because each iteration involves another calculation of f and g, usually a time-consuming step. Too many iterations waste time, and too few iterations allow the accumulation of iteration errors.

To overcome these disadvantages, a new method for the numerical integration of the system equations was developed here. It is a two-dimensional Runge-Kutta method; it is a noniterative method which requires only two calculations of f and g at each step, and is theoretically a fourth-order method. This method has these theoretical advantages over the modified Euler method because it uses information at point (i, j) to estimate higher derivatives.

The algorithm of this method is

$$c^* = c_{i+1,j} + kf_{i+1,j} + \left[(1-a)(c_{i,j+1} - c_{i,j}) + \tfrac{1}{2} ak(f_{i,j+1} + f_{i,j})\right] - kf_{i,j}$$

$$u^* = u_{i,j+1} + hg_{i,j+1} + \left[(1-b)(u_{i+1,j} - u_{i,j}) + \tfrac{1}{2} bh(g_{i+1,j} + g_{i,j})\right] - hg_{i,j} \tag{2.112}$$

$$c_{i+1,j+1} = c_{i+1,j} + \tfrac{1}{2} k[f_{i+1,j} + f(c^*, u^*)] + [(c_{i,j+1} - c_{i,j}) - \tfrac{1}{2} k(f_{i,j+1} + f_{i,j})]$$

$$u_{i+1,j+1} = u_{i,j+1} + \tfrac{1}{2} h[g_{i,j+1} + g(c^*, u^*)] + [(u_{i+1,j} - u_{i,j}) - \tfrac{1}{2} h(g_{i+1,j} + g_{i,j})]$$

(2.113)

In equations (2.112), c^* and u^* are intermediate values of the variables; they are arguments of f and g in equations (2.113), in which the desired values $c_{i+1,j+1}$ and $u_{i+1,j+1}$ are calculated. In equations (2.112), a and b are adjustable parameters (a feature common to Runge-Kutta methods) that may have any value between zero and one. These parameters have no general effect upon the error of the method, and their values are chosen by the computer solely for computational convenience.

To compare this method with the modified Euler method, both methods were applied to a sample linear problem which has a known solution and which is similar in form to a plug flow chemical reactor which is dominated by heat transfer. This comparison showed that the modified Euler method is superior in all respects. The reason that the Runge-Kutta method does not have its theoretical advantages was not investigated. The development of the method is presented in Appendix A, together with the comparison of the two methods, because the Runge-Kutta method involves some potentially useful concepts. The Runge-Kutta method was used satisfactorily in a prototype plug-flow program which was written before the two methods were directly compared. In the final plug-flow program, the modified Euler method was used because of its overall practical superiority.

For the case of finite Hp, the linear form of the particle temperature equation allowed a simplification of the modified Euler method, as noted by Gonzales and Spencer.[13] The result of an infinite number of iterations of the corrector equation (2.111) applied to the particle temperature is

$$T_{p_{i+1,j+1}} = T_{p_{i,j+1}} + \tfrac{1}{2} h \left[\left(\frac{Hp}{\beta - 1}\right) (T_{i,j+1} - T_{p_{i,j+1}}) + \left(\frac{Hp}{\beta-1}\right) (T_{i+1,j+1} - T_{p_{i+1,j+1}}) \right] \tag{2.114}$$

Solution for $T_{p_{i+1,j+1}}$ gives

$$T_{p_{i+1,j+1}} = \frac{T_{p_{i,j+1}} + \left(\frac{1}{2} \frac{hHp}{\beta-1}\right) T_{i+1,j+1} + \left(\frac{1}{2} \frac{hHp}{\beta-1}\right) (T_{i,j+1} - T_{p_{i,j+1}})}{1 + \frac{1}{2} \frac{hHp}{\beta-1}} \tag{2.115}$$

$$Hp(T_{p_{i+1,j+1}} - T_{i+1,j+1}) = Hp \left[\frac{T_{p_{i,j+1}} - T_{i+1,j+1} + \left(\frac{1}{2} \frac{hHp}{\beta-1}\right) (T_{i,j+1} - T_{p_{i,j+1}})}{1 + \frac{1}{2} \frac{hHp}{\beta-1}} \right] \tag{2.116}$$

Thus the corrector equation (2.111) for the fluid temperature at $(i+1, j+1)$ can be written and used independently of the unknown value of $T_{p_{i+1,j+1}}$; the corrector equations for c_A and T can be iterated simultaneously to find $C_{A_{i+1,j+1}}$ and $T_{i+1,j+1}$; and then $T_{p_{i+1,j+1}}$ can be found directly, without iteration, from $T_{i+1,j+1}$ with equation (2.115). Thus, although there are three variables, only two expressions need be iterated simultaneously at each lattice point for the numerical integration of this system.

The boundary conditions necessary for numerical integration in the unsteady state region can be obtained by any method suitable

for numerical integration of first-order ordinary differential equations.[7] This method must give the values of c and u at every point, (0, i) and (j, 0), along the boundaries. This method is completely independent of the two-dimensional integration method used inside the boundaries. The boundary values are found as described in the previous section. For example, for the case of finite Hp, the steady state equations are integrated to obtain the initial steady state profiles; the initial steady state temperature profile is the particle temperature profile along the y-axis, and the concentration and fluid temperature equations are integrated simultaneously, using this particle temperature profile. In all cases the equations integrated along the boundaries can be considered as first-order ordinary differential equations.

In the present PLGFLO program, the initial and final steady state profiles and the profiles along the boundaries are calculated with the Runge-Kutta-Gill method, equations (2.67).

CHAPTER 3

CORRELATION BETWEEN WALL HEAT TRANSFER COEFFICIENTS OF THE ONE-DIMENSIONAL AND THE TWO-DIMENSIONAL FINITE STAGE MODELS

Part A. Continuous Approximation of Finite Stage Models

As indicated in Chapter 1, the wall heat transfer coefficient of the two-dimensional finite stage model is equivalent to the wall film heat transfer coefficient (in dimensionless form) of the reactor being modeled. The wall heat transfer coefficient of the one-dimensional finite stage model, however, is equivalent to the overall heat transfer coefficient (in dimensionless form) of the reactor being modeled. The overall heat transfer coefficient reflects not only the resistance to heat flow through the wall, but also the resistance to heat flow radially through the bed to the wall. Thus, even if there were no resistance to heat flow through the wall, and the two-dimensional wall heat transfer coefficient were infinite, the wall heat transfer coefficient for the equivalent one-dimensional finite stage model would be finite, because of the radial resistance to heat flow through the bed.

The radial resistance to heat flow through the bed and through the wall causes radial temperature gradients in the reactor being modeled. The formation of these radial gradients is accounted for in the formulation of the two-dimensional finite stage model. However, because the one-dimensional model does not have radial gradients, it does not allow for radial resistance to heat and mass transport, except through its wall heat transfer coefficient.

Because no material is lost through the wall, radial gradients in concentration result only from the coupling of concentration and temperature through the reaction term. If there were no radial temperature gradients (i.e., if the reactor were adiabatic), or if the temperature did not affect the rate of reaction, then there would be no radial concentration gradients. Thus the present problem of correlation of heat transfer coefficients is a heat transfer problem and is basically independent of concentration and reaction effects.

However, just as radial temperature gradients cause radial concentration gradients through the reaction terms, so the radial concentration gradients affect the radial temperature gradients through the reaction term. These coupling effects are expected to appear as nonlinear distortion of the radial temperature gradients without reaction. It is unrealistic to expect, however, that the one-dimensional wall heat transfer coefficient should also be adjusted to compensate for these non-linear effects. In this case the one-dimensional wall heat transfer coefficient would be a function not only of the two-dimensional wall heat transfer coefficient and the resistance to radial flow through the bed, but also of the reaction parameters, i.e., the activation energy, the pre-exponential factor, and the heat of reaction. The one-dimensional wall heat transfer coefficient cannot be expected to compensate for all differences in the one-dimensional and the two-dimensional finite stage models. The differences in the two models resulting from the effect of reaction on radial gradients reflect inherent differences of the two models.

Further, the one-dimensional wall heat transfer coefficient cannot necessarily compensate for differences in the unsteady state behavior of the two models. Again, these differences are inherent in the two models. The models should agree, however, in the steady state, which can be considered as the limiting case of the unsteady state.

Therefore the problem reduces to a wall heat transfer coefficient correlation for finite stage models of a reactionless packed bed tubular heat exchanger at steady state.

For the models, the best criterion for the wall heat transfer correlation is the equivalence of heat loss through the walls; that is, the wall heat transfer coefficient of the one-dimensional finite stage model should be found such that the heat loss through the wall of the one-dimensional model is equal to the heat loss through the wall of the two-dimensional finite stage model. The radially averaged temperature of the two-dimensional model is a measure of the heat content

of the fluid at any axial position, because it is obtained from the sum of the temperatures of the fluid at each stage, weighted by the amount of fluid in each stage. Further, the difference between the radially averaged temperature at a given axial position and the radilly averaged temperature at the preceding axial position is a measure of the heat lost through the walls at that axial position. Thus, the value of the desired one-dimensional wall heat transfer coefficient is the one for which the axial temperature profile of the one-dimensional model is equivalent to the radially averaged axial temperature profile of the two-dimensional model.

Because this finite stage heat exchanger problem is linear with temperature, the fluid temperature can be scaled, and any convenient temperature can be used as a reference temperature. Therefore, in this analysis the inlet temperature is taken as unity, and the wall temperature is taken as zero.

This correlation concerns the one-dimensional and the two-dimensional finite stage models. However, because of difficulties involved in the analysis of the discrete equations of the finite stage models, these models may first be approximated by the more familiar continuous models described by partial differential equations. A study of these continuous models will lead to some insight into the correlation of the wall heat transfer coefficients of the finite stage models, and will also illustrate some differences between the finite stage models and the continuous models.

The partial differential equation which expresses the conservation of heat in a packed bed tubular heat exchanger at steady state is:

$$\frac{1}{Pe_x} \frac{\partial^2 T}{\partial x^2} + \frac{1}{r Pe_r} \frac{\partial}{\partial r} \left(r \frac{\partial T}{\partial r} \right) - \frac{\partial T}{\partial x} = 0 . \qquad (3.1)$$

This equation is assumed here to be a suitable continuous first approximation of the two-dimensional finite stage equations (Chapter 2). Here, the particle temperatures and the fluid temperatures are equal. The variable x is the axial distance from the inlet, and r is the radial

distance from the axis of the reactor. Both x and r are dimensionless variables, the characteristic dimensional length being d_p; thus x is the continuous form of the discrete finite stage variable i, and r is similarly related to $\frac{1}{2}j$.

The appropriate boundary conditions are:

$$\text{at } r = 0, \qquad \frac{\partial T}{\partial r} = 0; \tag{3.2}$$

$$\text{at } r = \tfrac{1}{2}M, \qquad \frac{1}{Pe_r}\frac{\partial T}{\partial r} + Hw_2\, T = 0; \tag{3.3}$$

$$\text{at } x = 0, \qquad T = 1; \tag{3.4}$$

$$\text{at } x = \infty, \qquad T = 0\,. \tag{3.5}$$

The first boundary condition is an expression of axial symmetry at the axis. The second boundary condition is an expression of a heat balance at the interface between the fluid and the wall: the rate of heat flow into the interface from the fluid, as expressed by Fourier's law of heat conduction, is equal to the rate of heat flow from the interface through the wall, as expressed by Newton's law of cooling.

The third and fourth boundary conditions are representative of the finite stage model, which is independent of downstream conditions. Wehner and Wilhelm[14] have discussed more appropriate boundary conditions for a packed bed chemical reactor, but equation (3.1) is used here not as an approximation of a chemical reactor, but rather as an approximation of the finite stage model. Further, it will be seen that the heat transfer coefficient correlation results from the roots of the characteristic equation associated with the ordinary differential equation in x which results from the solution of equation (3.1) by the standard method of separation of variables. Thus the correlation is independent of the axial boundaries conditions, because the roots of this characteristic equation are.

The solution[15] of this partial differential equation is:

$$T = \sum_{n=1}^{\infty} \exp\left[-\tfrac{1}{2} Pe_x \left(\sqrt{1 + \frac{16\beta_n^2}{M^2 Pe_r Pe_x}} - 1 \right) x \right] \frac{2BiJ_0(\frac{2r}{M}\beta_n)}{(Bi^2+\beta_n^2)J_0(\beta_n)}, \tag{3.6}$$

where β_n is defined as the nth positive root of

$$\beta J_1(\beta) - BiJ_0(\beta) = 0 \tag{3.7}$$

J_0 and J_1 are Bessel's functions of the first kind and of order zero and one, respectively, and

$$Bi = \tfrac{1}{2} M\, Pe_r\, Hw_2 \tag{3.8}$$

Bi is the Biot number, the ratio between the resistance to heat transfer through the bed ($\frac{1}{2}M\ Pe_r$ in dimensionless terms) and the resistance to heat transfer at the wall ($1/Hw_2$ in dimensionless terms).

The radially averaged temperature is defined as

$$\overline{T} \equiv \frac{8}{M^2} \int_0^{\frac{1}{2}M} Tr\, dr\,. \tag{3.9}$$

Then

$$\overline{T} = \sum_{n=1}^{\infty} \exp\left[-\tfrac{1}{2} Pe_x \left(\sqrt{1 + \frac{16\beta_n^2}{M^2 Pe_r Pe_x}} - 1 \right) x \right] \frac{4Bi^2}{\beta_n^2(Bi^2 + \beta_n^2)}\,. \tag{3.10}$$

The axial temperature profiles described by this equation are similar to a continuous form of those in Figure 12. Except in a region near the inlet of the reactor, all of the terms of the series are negligible

except for the first term. Therefore, the temperature profile can be represented by

$$\overline{T} = \frac{4Bi^2}{\beta_1^{\,2}(Bi^2+\beta_1^{\,2})} \exp\left[-\tfrac{1}{2}\,Pe_x\left(\sqrt{1+\frac{16\beta_1^{\,2}}{M^2 Pe_r Pe_x}}-1\right)x\right] \tag{3.11}$$

throughout most of the reactor.

The corresponding one-dimensional differential equation is

$$\frac{1}{Pe_x}\frac{d^2T}{dx^2} - \frac{dT}{dx} - \frac{4Hw_1}{M}\,T = 0. \tag{3.12}$$

This equation is assumed here to be a suitable continuous first approximation to the one-dimensional finite stage model. The equivalent boundary conditions are

$$\text{at } x = 0, \qquad T = 1; \tag{3.13}$$

$$\text{at } x = \infty, \qquad T = 0. \tag{3.14}$$

The solution is

$$T = \exp\left[-\tfrac{1}{2}\,Pe_x\left(\sqrt{1+\frac{16Hw_1}{MPe_x}}-1\right)x\right]. \tag{3.15}$$

Comparison of the two solutions, equations (3.11) and (3.15), shows that the temperature profiles decrease exponentially with distance, except in the inlet region of the two dimensional model. In this inlet region, the rate of heat loss in the two-dimensional reactor is relatively greater than that downstream. This initial high rate of heat loss results from the easy extraction of large amounts of heat from fluid near the wall. The extraction is easy because only a fraction of the bed's total thermal resistance is effective. Fluid in the inner core is essentially unaffected in this inlet region.

However, in the chemical reactors considered further in this study, the feed temperature is usually very close to the wall temperature, so the heat loss through the wall in the inlet region is

usually negligible. The feed temperature and the wall temperature are taken as unequal in this correlation because there is no heat generation inside the reactionless heat exchanger considered here, and because the profiles in such heat exchangers are caused solely by the heat loss at the wall. In a chemical reactor, the rate of heat generation in the chemical reaction is usually much greater than the rate of heat loss through the wall in the inlet region, in which the radial profiles are developing. Further, in many cases the overall heat transfer coefficient is only slightly less than the wall film heat transfer coefficient. That is, the effect of resistance to heat flow through the bed is small, compared with the resistance of the wall. Then the effect of the apparent lower bed resistance at the entrance is usually negligible, since the bed resistance is small throughout the reactor. Finally, the effect of this inlet region is expected to be negligible compared with the inherent differences of the two models, such as the distortion of the radial profiles of the two-dimensional model by the temperature-concentration coupling and the differences in unsteady state behavior. Therefore the inlet region, in which the radial profiles are not fully developed, need not be considered further for this correlation.

Before the effects of the inlet region are dismissed entirely, it is of interest to determine the length of this inlet region. A study of the radially averaged temperature profiles of the two-dimensional finite stage model which are shown graphically in Figure 12 reveals that for $M = 10$, the sum of all other terms is 4.3% of the dominant exponential term at $i = M$, and 0.8% at $i = 2M$; for $M = 15$, the sum of the other terms is 8.1% of the dominant term at $i = M$, and 2.9% at $i = 2M$; and for $M = 20$, the sum of the other terms is 10.9% at $i = M$ and 5.0% at $i = 2M$. Therefore the inlet region extends one or two reactor diameters downstream from the entrance of the reactor, or slightly longer for reactors of larger diameter.

The pre-exponential factor in equation (3.11) reflects the relatively higher heat loss in the inlet region, and thus can be disregarded. Comparison of the two profiles described by equations (3.11) and (3.15) yields the heat transfer coefficient correlation

$$Hw_1 = \frac{\beta_1^2(Bi)}{MPe_r} \quad . \tag{3.16}$$

As discussed previously, this correlation is independent of axial boundary conditions, because the exponential terms involved come from the characteristic roots of the differential equations (3.1) and (3.12). It can be shown that the same correlation would result if axial diffusion were neglected in both models, or if a heat generation term which is linear with temperature and otherwise independent of position were included in both models.

Equation (3.7) expresses β_1^2 as a function of Bi; then the correlation (3.16) predicts that $MPe_r Hw_1$ is a universal function of $MPe_r Hw_2$. Figure 11 shows $\beta_1^2(Bi)$ as a function of Bi. For large Bi, β_1^2 approaches a limiting value, $\beta_{1\infty}^2 = 5.783186\cdots$, the square of the smallest positive root of J_0. This limit is the horizontal asymptote to β_1^2. For large Bi, the overall heat transfer coefficient is influenced primarily by the resistance to heat flow through the bed, which is much greater than the resistance to heat flow through the wall. For large Bi, the temperature of the fluid near the wall is approximately equal to the temperature of the wall, thus in two-dimensional models, the wall boundary condition can be expressed as:

$$\text{at} \quad r = \tfrac{1}{2}M, \quad T = 0, \tag{3.17}$$

instead of by equation (3.3).

At the other extreme, in the nearly adiabatic heat exchanger, the overall heat transfer coefficient is approximately equal to the wall film heat transfer coefficient. In this case the resistance to heat flow through the wall is much greater than the resistance to heat flow through the bed, and Bi is small. As Bi becomes very small, Hw_1 approaches Hw_2, and β_1^2 approaches the 45° asymptote shown in Figure 11. For small Bi, the Bessel's functions of equation (3.7) may be approximated with truncated Taylor's series:

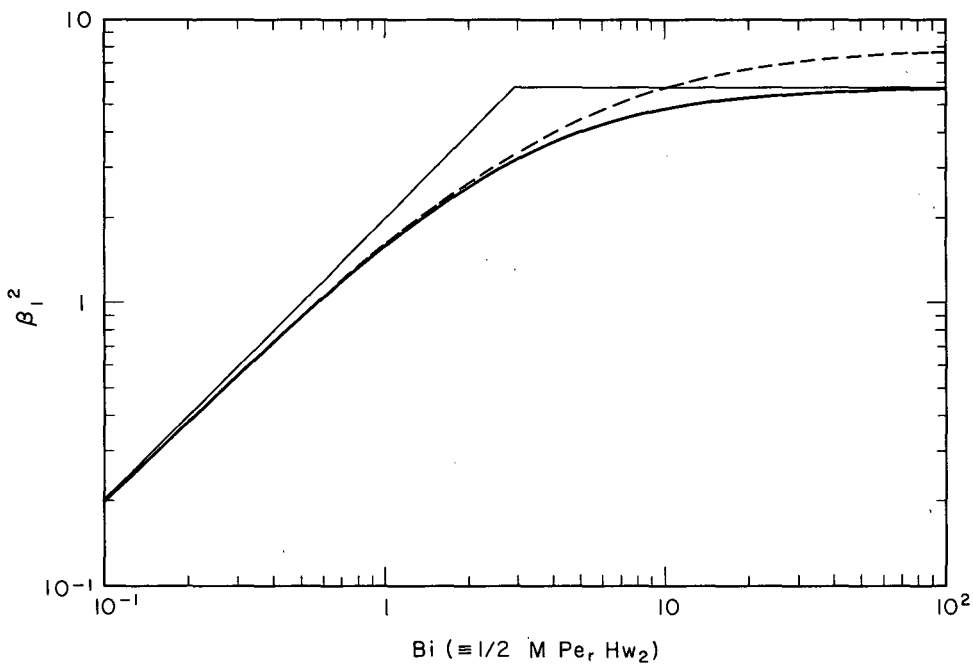

MU-34912

Fig. 11. The function β_1^2 (Bi). β_1 is defined as the smallest positive root of the equation $\beta\ J_1(\beta)$ - Bi $J_0(\beta) = 0$. ▬ is β_1^2(Bi); ----- is Beck's correlation, 8Bi/(Bi + 4); — are asymptotes of β_1^2(Bi).

$$\left(\tfrac{1}{2}B_1^{\,2} - \frac{1}{16}\,\beta_1^{\,4}\right) - Bi\left(1-\tfrac{1}{4}\,\beta_1^{\,2} + \frac{1}{64}\,\beta_1^{\,4}\right) \cong 0. \qquad (3.18)$$

The smallest root of this equation is

$$\beta_1^{\,2} = \frac{8Bi}{Bi+4} = \frac{2Bi}{1+\frac{1}{4}Bi}\,. \qquad (3.19)$$

With this approximation, equation (3.16) becomes

$$Hw_1 = \frac{Hw_2}{1 + \frac{1}{8}\,M\,Pe_r\,Hw_2}\,. \qquad (3.20)$$

or

$$\frac{1}{Hw_1} = \frac{1}{Hw_2} + \frac{1}{8}\,M\,Pe_r\,. \qquad (3.21)$$

Equations (3.20) and (3.21) express Beek's correlation.[2] Equation (3.21) states that the overall radial resistance to heat flow is equal to the sum of the resistance to heat flow through the wall and the radial resistance to heat flow through the bed. Beek derived these expressions by approximating radial temperature profiles with a parabola, which is equivalent to approximating the Bessel's functions with a truncated Taylor's series which is of second degree in $\beta_1^{\,2}$ (see equation (3.6)).

Beek's correlation is shown graphically in Figure 11. It is accurate for small Bi, but is only qualitatively correct for large Bi. It is very useful in practice, however, because in many cases Bi is small.

The correlation expressed in equation (3.16), and its approximation, given by Beek's correlation, are derived here because they give insight into the relationship of the heat transfer coefficients of one-dimensional and two-dimensional models. However, these correlations are useful for comparison of the finite stage models only if equations (3.1) and (3.12) are satisfactory approximations of the finite stage models. (Of course, these correlations are also useful if the

continuous mathematical models described by equations (3.1) and (3.12) are used to describe an actual reactor; but in this study the finite stage models and the plug flow model are of foremost interest.) Therefore the applicability of the correlation (3.16) to the finite stage models must now be determined.

The radial Peclet number, Pe_r, needed in the correlation (3.16), is not a parameter fundamental to the finite stage model, as it is to the partial differential equation model. For the two-dimensional finite stage model, Deans[3] has shown, by approximation of finite stage profiles with a finite difference form of equation (3.1), that the average Pe_r is 8.2. This value is a result of the radial geometry of the two dimensional finite stage model. Deans also shows that Pe_x is 2.

Radially averaged temperature profiles calculated with the FS2D program, for particular values of the input data M and Hw_1, are shown in Figure 12. These profiles exhibit an exponential decrease in temperature with distance except in the region near the inlet of the reactor. The corresponding values of Hw_1 were found from the slope of the exponential portion of the profiles. From these profiles it was found that equations (3.16) and (3.20) were valid for small values of Hw_2, but that, for infinite Hw_2, the reciprocal of Hw_1 was not proportional to M. An empirical relationship was found, with which Hw_1 (for infinite Hw_2) can be calculated with an error of less than 1%:

$$Hw_{1\infty} \equiv \lim_{Hw_2 \to \infty} Hw_1 \cong \frac{0.726}{M-2} \quad . \tag{3.22}$$

Here, the reciprocal of $Hw_{1\infty}$ is not proportional to M, but rather is a linear function of M. It is easily seen that for a finite stage model in which M = 2, $Hw_{1\infty}$ is infinite, whereas for M = 3, $Hw_{1\infty}$ is finite. The factor 0.726 was found by curve fitting techniques.

It is desirable, as will be seen, that the correlation (3.16) be applicable to the finite stage models. Because Pe_r is not a fundamental parameter of the finite stage model, its value may depend

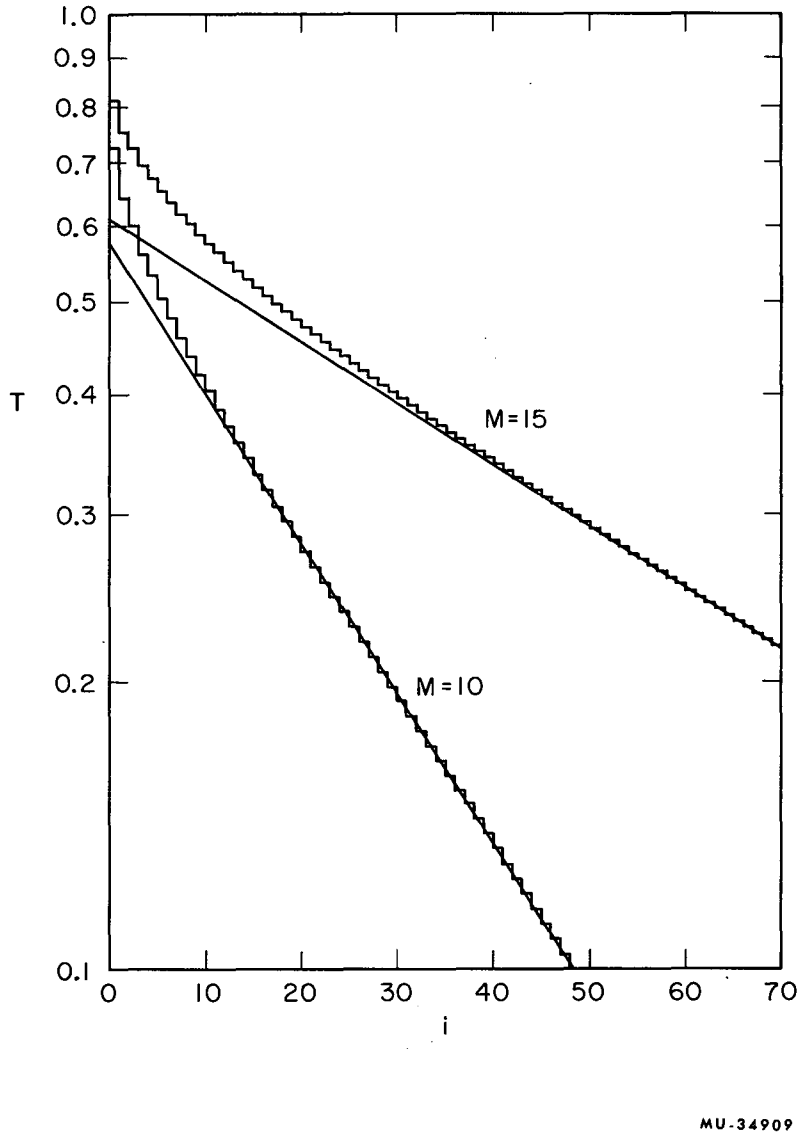

Fig. 12. Temperature profiles for the two-dimensional finite stage models without chemical reaction (infinite Hw_2).

somewhat upon the method of calculation. Deans' calculations[3] showed that Pe_r varied radially and axially by at least 10%. It is not unreasonable to assume that for the finite state model, Pe_r is a function of M, in which case the correlation (3.16) can be reconciled with the empirical relation (3.22). Then these equations require the following functionality of Pe_r with M:

$$Pe_r = \frac{\beta_{1\infty}^2}{MHw_{1\infty}} = 7.97\ (1 - \frac{2}{M}) \tag{3.23}$$

Pe_r must be assumed to be independent of x and r in this development, otherwise the solution (3.6) and the resulting correlation (3.16) would not be correct. This development is in fact another method of determining Pe_r for the two dimensional finite stage model. The reasons for the disagreement between equation (3.23) and Deans' calculations have not been investigated; however, his calculations involved an intermediate finite difference form of equation (3.1) and were made for a value of M = 19 only.

Equation (3.23) can be used to eliminate Pe_r from the correlation, in which case equation (3.16) becomes

$$\frac{Hw_1}{Hw_{1\infty}} = \frac{\beta_1^2 (Bi)}{\beta_{1\infty}^2} \tag{3.24}$$

where

$$Bi = \tfrac{1}{2}\, \beta_{1\infty}^2 \frac{Hw_2}{Hw_{1\infty}}$$

and $Hw_{1\infty}$ is given by equation (3.22). This correlation (3.24) is empirical as applied to the finite stage models because it was obtained by approximating the finite stage models with differential equation models.

This approach has revealed some useful relationships. For example, the difference in the functionality of $Hw_{1\infty}$ with M for the partial differential equation model (inverse proportionality) and for the finite stage model (equation (3.22)) may be used with a

careful experimental study of packed bed heat exchangers to determine which of the two mathematical models is more accurate in this respect. Such a study may give insight into the development of a better finite stage model.

Part B. Matrix Solution of the Finite Stage Equations

A more fundamental understanding of the finite stage models may be obtained by further study of steady state temperature profiles of the finite stage models. Expression of the model equations in matrix notation is helpful in this study.

For a finite stage model at steady state without chemical reaction, the temperature equations reduce to:

for the general stage (i, j),

$$T_{i,j} = \left(\frac{2j-3}{4j-4}\right) T_{i-1,j-1} + \left(\frac{2j-1}{4j-4}\right) T_{i-1,j+1}; \tag{3.25}$$

if the center stage on row (or axial position) i is a half stage,

$$T_{i,1} = T_{i-1,2} \; ; \tag{3.26}$$

if the wall stage on row i is a whole stage,

$$T_{i,M} = \left(\frac{2M-3}{4M-4+4MHw_2}\right) T_{i-1,j-1} + \left(\frac{2M-1}{4M-4+4MHw_2}\right) T_{i-1,j+1}; \tag{3.27}$$

if the wall stage on row i is a half stage,

$$T_{i,M+1} = \left(\frac{2M-1}{2M-1+4MHw_2}\right) T_{i-1,M} \; . \tag{3.28}$$

Here, as previously, the wall temperature is taken as zero, and the inlet temperature is taken as unity, so

$$T_{0,j} = 1, \qquad 1 \leq j \leq M+1 \; . \tag{3.29}$$

These equations for a given row i can be expressed in a matrix form:

$$T_i = S\, T_{i-1}\,, \tag{3.30}$$

where

$$S \equiv \begin{bmatrix} 0 & 1 & 0 & 0 & & & & & \\ \frac{1}{4} & 0 & \frac{3}{4} & 0 & & & & & \\ 0 & \frac{3}{8} & 0 & \frac{5}{8} & & & & & \\ & & \cdots & & & & & & \\ \cdot & \cdot & \cdot & \frac{2j-3}{4j-4} & 0 & \frac{2j-1}{4j-4} & & \cdots & \\ & & \cdots & & & & & & \\ & & & & & \frac{4M-3}{4M-4+4MHw_2} & 0 & \frac{4M-1}{4M-4+4MHw_2} & \\ & & & & & 0 & \frac{2M-1}{2M-1+4MHw_2} & 0 & \end{bmatrix}$$

and

$$T_i = \begin{bmatrix} T_{i,1} \\ T_{i,2} \\ \cdot \\ \cdot\cdot \\ \cdot \\ T_{i,j} \\ \cdot \\ \cdot \\ \cdot \\ T_{i,M} \\ T_{i,M+1} \end{bmatrix}, \quad T_0 = \begin{bmatrix} 1 \\ 1 \\ 1 \\ 1 \\ 1 \\ 1 \\ 1 \\ 1 \end{bmatrix}. \tag{3.32}$$

T_i is a column matrix, the elements of which are temperatures in all the radial stages at axial position i. T_0 is the column matrix which represents the temperature of the feed stream; here, the feed stream is treated as the output of a row of hypothetical radial stages preceding the stages of row 1. The matrix of coefficients, S, is a square matrix with several interesting properties, among which are:

1. The matrix is bidiagonal: all elements of the matrix except those on the two diagonals adjacent to the main diagonal are zero. This property is a result of the manner in which the stages of the model are arrayed.
2. The sum of all elements on any row (except the last two rows) is unity. This property expresses the conservation of energy in the system. The last two rows would not be exceptions if the reactor were adiabatic, in which case $Hw_2 = 0$.

The system described by equations (3.30), (3.31), and (3.32) is actually a different system from the finite stage model described previously. In the finite stage model, the odd numbered rows include only the odd numbered radial stages, and the even numbered rows include only the even numbered radial stages. There is also a conjugate model in which the odd numbered rows include only even numbered radial stages, and the even numbered rows include only the odd numbered radial stages; this model has not been previously considered. The system described by equations (3.30), (3.31), and (3.32) includes both of these models, as shown by the definition of T_i in equation (3.32); the elements of T_i include both even and odd numbered radial stages. The bidiagonal property of S insures the complete independence of the two models; the temperature of a stage in one model will never affect the temperature in any stage of the other model.

In the simulation of the behavior of a chemical reactor by one of these models of the finite stage type, there is no reason why one model should be preferred to the other. There is a slight difference in the behavior of the two models, since the first row of one consists of odd numbered radial stages, with a half-stage at the center, and the first row of the other consists of even numbered radial stages, with a whole stage at the center; but the behavior of an actual chemical reactor is probably best simulated by an average of the two models.

The system presently under consideration does afford an averaged behavior of the two models; in addition, the notation is simplified. This present system is not used in the general FS2D program because it actually involves the calculations for both models, thus doubling the computing time.

Equation (3.30) is a simple difference equation; its solution is:

$$T_i = S^i T_0 \quad . \tag{3.33}$$

To obtain the radially averaged temperature, an averaging operator V, a row vector, is defined:

$$V = \left[\frac{1}{2M^2} \quad \frac{4}{2M^2} \quad \frac{8}{2M^2} \quad \cdots \quad \frac{4j-4}{2M^2} \quad \cdots \quad \frac{4M-4}{2M^2} \quad \frac{2M-1}{2M^2} \right] . \tag{3.34}$$

The radially averaged temperature profile is

$$\overline{T_i} = VT_i \quad . \tag{3.35}$$

For the feed stream,

$$\overline{T_0} = VT_0 = 1 \; . \tag{3.36}$$

The weight assigned in V to the temperature of each stage is equal to the relative size of each stage. Equation (3.36) shows that the sum of the elements of V is unity.

The unity column vector T_0 can be considered as a post-multiplicative operator which sums the elements of each row of a matrix. Thus, in equation (3.36), the elements of V are summed, and from equation (3.33), each element of T_i can be considered as the sum of the corresponding row of S^i.

The radially averaged temperature profile, in terms of S, is

$$\overline{T_i} = VS^i \, T_0 \quad . \tag{3.37}$$

Sylvester's theorem[16] states that for any polynomial function, P(S), of a square matrix S,

$$P(S) = \sum_{r=1}^{s} P(\lambda_r) \frac{J(\lambda_r)}{\psi'(\lambda_r)} , \tag{3.38}$$

where s is the order of S; $\psi(\lambda) = \left| S - \lambda I \right|$, the characteristic polynomial of S; λ_r are the characteristic roots of S, the roots of

$$\psi(\lambda) = 0;$$
$$\psi'(\lambda_r) = \frac{d\psi}{d\lambda} \quad \text{at} \quad \lambda = \lambda_r;$$

and

$$J(\lambda) = -\psi(\lambda)[S-\lambda I]^{-1},$$

the adjoint matrix, or matrix of cofactors, of $S-\lambda I$.

$$S^i = \sum_{r=1}^{M+1} \lambda_r^{\,i} \frac{J(\lambda_r)}{\psi'(\lambda_r)} , \tag{3.39}$$

and therefore

$$\overline{T}_i = \sum_{r=1}^{M+1} \lambda_r^{\,i} \frac{VJ(\lambda_r)T_0}{\psi'(\lambda_r)} . \tag{3.40}$$

This equation should be compared with equation (3.12), which describes the radially averaged temperature profile for the partial differential equation model. In both cases, temperature is expressed as a series of exponential functions of x, or i; but in the finite stage case, this series is finite. The number of terms in the series is $M+1$, which is the total number of radial stages in any two adjacent rows of either of the two-dimensional finite stage models, and is the order of S and of all other matrices considered here. In both the finite stage and the partial differential equation models, only the first term of each series is important except in the region near the inlet of the reactor, as is seen in Figure 2. Then

$$T_i = \lambda_1^{\,i} \frac{J(\lambda_1)\, T_0}{\psi'(\lambda_1)} , \tag{3.41}$$

and

$$\overline{T_i} = \lambda_1^{\,i} \frac{VJ(\lambda_1)\, T_0}{\psi'(\lambda_1)} , \tag{3.42}$$

where λ_1 is the largest characteristic root of S.

To establish the correlation between heat transfer coefficients of the two-dimensional and the one-dimensional finite stage models, this radially averaged temperature profile is compared with the corresponding temperature profile of the one-dimensional finite stage model. For a one-dimensional finite stage model at steady state without chemical reaction, the temperature equations become:

$$\left(1 + \frac{4Hw_1}{M}\right) T_i = T_{i-1} . \tag{3.43}$$

The solution of this difference equation is the temperature profile of the one dimensional finite stage model:

$$T_i = \left(\frac{1}{1 + \frac{4Hw_1}{M}}\right)^i . \tag{3.44}$$

Because the T_i are scalar, and T_0 is unity, T_0 need not be explicit in this equation.

As in the differential equation approach, comparison of the slopes of these profiles yields

$$Hw_1 = \tfrac{1}{4} M \left(\frac{1-\lambda_1}{\lambda_1}\right) . \tag{3.45}$$

This equation expresses the correlation of Hw_1 with M and Hw_2, although λ_1 cannot generally be expressed explicitly in terms of M and Hw_2, because λ_1 is the largest characteristic root of S.

The numerical methods of calculating λ_1 can be simplified because of the special properties of S. The characteristic polynomial is

$$\psi(\lambda) = \begin{vmatrix} -\lambda & 1 & 0 & 0 & & & & \\ \frac{1}{4} & -\lambda & \frac{3}{4} & 0 & & & & \\ 0 & \frac{3}{8} & -\lambda & \frac{5}{8} & & & & \\ & & \cdots & & & & & \\ \cdots & & \frac{2j-3}{4j-4} & -\lambda & \frac{2j-1}{4j-4} & & & \\ & & & & \cdots & \frac{2M-3}{4M-4+4MHw_2} & -\lambda & \frac{2M-1}{4M-4+4MHw_2} \\ & & \cdots & & & & \frac{2M-1}{2M-1+4MHw_2} & -\lambda \end{vmatrix}$$

(3.46)

This determinant can be considered as the (M+1)th term in a sequence of determinants of submatrices of S:

$$p_1(\lambda) = \begin{vmatrix} -\lambda \end{vmatrix} = -\lambda ,$$

$$p_2(\lambda) = \begin{vmatrix} -\lambda & 1 \\ \frac{1}{4} & -\lambda \end{vmatrix} = \lambda^2 - \tfrac{1}{4},$$

$$p_3(\lambda) = \begin{vmatrix} -\lambda & 1 & 0 \\ \frac{1}{4} & -\lambda & \frac{3}{4} \\ 0 & \frac{3}{8} & -\lambda \end{vmatrix} = -\lambda^3 + \frac{17}{32}\lambda ,$$

(Eq. (3.47) continued)

$$P_4(\lambda) = \begin{vmatrix} -\lambda & 1 & 0 & 0 \\ \frac{1}{4} & -\lambda & \frac{3}{4} & 0 \\ 0 & \frac{3}{8} & -\lambda & \frac{5}{8} \\ 0 & 0 & \frac{5}{12} & -\lambda \end{vmatrix} = \lambda^4 - \frac{19}{24}\lambda^2 + \frac{25}{384} ,$$

$$\ldots$$

$$p_{M+1}(\lambda) = |\mathbf{S} - \lambda I| = \psi(\lambda) . \tag{3.47}$$

The polynomial $p_n(\lambda)$ is the determinant of the submatrix composed of the n^2 elements common to the first n rows and the first n columns of $S - \lambda I$. By expanding this determinant by cofactors of the elements of either the last row or the last column of the submatrix, the following recursion relation of the polynomials in this sequence is obtained:

$$p_n(\lambda) = -\lambda p_{n-1}(\lambda) - \gamma_n p_{n-2}(\lambda) , \qquad 3 \leq n \leq M+1,$$

where

$$p_1(\lambda) = -\lambda, \quad p_2(\lambda) = \lambda^2 - \tfrac{1}{4} ,$$

$$\gamma_n = \frac{(2n-3)^2}{(4n-4)(4n-8)} , \qquad 3 \leq n \leq M-1 ,$$

$$\gamma_M = \frac{(2M-3)^2}{(4M-4+4MHw_2)(4M-8)} ,$$

and

$$\gamma_{M+1} = \frac{(2M-1)^2}{(4M-4+4MHw_2)(2M-1+4MHw_2)} . \tag{3.48}$$

The characteristic polynomial $\psi(\lambda)$ is of degree M+1. Because of the bidiagonal form of S, $\psi(\lambda)$ contains terms of either even powers of λ, or odd powers of λ, but not both. Then if M+1 is even, ψ is a polynomial of degree $\frac{1}{2}(M+1)$ in λ^2; and if M+1 is odd, $\lambda_{M+1} = 0$ is a characteristic root, and ψ/λ is a polynomial of degree $\frac{1}{2}M$ in λ^2. In either case, if λ_1 is the largest root of $\psi(\lambda)$, then $-\lambda_1(=\lambda_2)$ is also a root of $\psi(\lambda)$. It can be shown by examples that, although λ_1 and λ_2 are of equal magnitude, the term containing λ_2 in equation (3.40) is negligible, because the coefficient of this term,

$$\frac{VJ(\lambda_2)T_0}{\psi'(\lambda_2)} ,$$

is much smaller than the corresponding coefficient of the λ_1 term. For small values of M, this λ_2 term is large enough to cause a small saw-tooth effect in the finite stage temperature profile.

Because the elements of S are positive, and the sum of the elements in each row of S is less than or equal to unity, the magnitudes of the characteristic roots are less than one. For the special case of the adiabatic reactor, Hw_2 is zero, so the sum of the elements in each row of S is unity, and λ_1 is exactly one.

The largest root, λ_1, is generally slightly less than one. For an accurate determination of Hw_1, the difference between λ_1 and unity must be found accurately, as equation (3.45) shows. The reciprocal of this difference, a very large number, may be more accurately obtained than can λ_1 directly:

$$\mu_1 = \frac{1}{1-\lambda_1} ;$$

then (3.49)

$$\lambda_1 = 1 - \frac{1}{\mu_1} .$$

By expanding $\psi(\lambda)$ in a Taylor's series about $\lambda = 1$,

$$\psi(1-\frac{1}{\mu_1}) = \psi(\lambda_1) = 0$$

$$= \psi(1)-\psi'(1)\left(\frac{1}{\mu_1}\right) + \frac{1}{2!}\psi''(1)\left(\frac{1}{\mu_1}\right)^2 + \cdots + \frac{(-1)^n}{n!}\psi^{(n)}(1)\left(\frac{1}{\mu_1}\right)^n$$

$$+ \cdots + \frac{(-1)^{M+1}}{(M+1)!}\psi^{(M+1)}(1)\left(\frac{1}{\mu_1}\right)^{M+1} , \qquad (3.50)$$

a polynomial equation is obtained,

$$\psi(1)\mu_1^{M+1} - \psi'(1)\mu_1^{M} + \frac{1}{2!}\psi''(1)\mu_1^{M-1} + \cdots + \frac{(-1)^n}{n!}\psi^{(n)}(1)\mu_1^{M+1-n}$$

$$+ \cdots + \frac{(-1)^{M+1}}{(M+1)!}\psi^{(M+1)}(1) = 0 , \qquad (3.51)$$

of which μ_1 is the largest root. This root can be found by standard numerical methods.[7] The necessary derivations of $\psi(\lambda)$ can be found from the recursion relation of the derivatives of the polynomials $p_n(\lambda)$:

$$p_n^{(i)}(\lambda) = -\lambda p_{n-1}^{(i)}(\lambda) - i p_{n-1}^{(i-1)}(\lambda) + \gamma_n p_{n-2}^{(i)}(\lambda), \qquad (3.52)$$

which follows from equation (3.48).

In terms of μ_1, the heat transfer correlation is

$$Hw_1 = \frac{1}{4} M \left(\frac{1}{\mu_1 - 1}\right) . \qquad (3.53)$$

The first major calculation in the FS2D program is the calculation of Hw_1 in the manner described above for the particular values of M and Hw_2 obtained from the input data.

The root, λ_1, or the difference, $1 - \lambda_1$, can instead be found from the appropriate polynomial equation in λ^2, as mentioned previously; in this manner, the degree of the polynomial equation of interest is either $\frac{1}{2}$ M or $\frac{1}{2}$ (M + 1), whichever is an integer.

At one extreme of heat transfer coefficients, the reactors are adiabatic and Hw_1 and Hw_2 are zero; at the other extreme, Hw_2 is infinite. This case is important because it yields the maximum values of Hw_1 and the minimum values of λ_1 for a given M. The values of λ_1 and Hw_1 as a function of M for infinite Hw_2 are given in Table 3.1. For finite values of Hw_2, λ_1 is nearer to one than the values given in Table 3.1, and Hw_1 is smaller.

Then Hw_1 can be calculated for given values of Hw_2 and M by either of two methods: exactly, from the root of the characteristic equation of the finite stage coefficient matrix; or empirically, from equation (3.24), with $Hw_{1\infty}$ from equation (3.22) or Table 3.1, and $\beta_1^2(Bi)$ from Figure 11 or from an approximation such as equation (3.19).

The wall heat transfer coefficient, Hw_p, of the plug flow model may be adjusted slightly to effect agreement between the continuous temperature profile of the plug flow model and the step-wise profile of the finite stage model. The differential equation which describes the steady state temperature profile of a plug flow reactor without reaction is

$$\frac{dT}{dx} + \frac{4Hw_p}{M} T = 0 \quad . \tag{3.54}$$

The temperature profile is

$$T = e^{-\frac{4Hw_p}{M} x} \quad . \tag{3.55}$$

Comparison of the slope of this profile with the slope of the corresponding one dimensional finite stage temperature profile described in equation (3.44) (with x = i) yields

$$\frac{1}{1+\frac{4Hw_1}{M}} = e^{-\frac{4Hw_p}{M}} \quad ,$$

or

$$\frac{4Hw_p}{M} = \ln\left(1+\frac{4Hw_1}{M}\right) \quad . \tag{3.56}$$

Table 3.1

λ_1 and Hw_1 as a function of M for the case of infinite Hw_2

M	λ_1		Hw_1		$\frac{4Hw_1}{M}$	
3	0.5000	000	0.7500	000	1.0000	000
4	0.7288	690	0.3719	887	0.3719	887
5	0.8357	362	0.2456	873	0.1965	498
6	0.8911	695	0.1831	814	0.1221	209
7	0.9229	926	0.1460	065	0.0834	3226
8	0.9427	821	0.1213	808	0.0606	9042
9	0.9558	722	0.1038	712	0.0461	6499
10	0.9649	594	0.0907	8250	0.0363	1300
11	0.9715	160	0.0806	2747	0.0293	1908
12	0.9763	976	0.0725	1867	0.0241	7289
13	0.9801	279	0.0658	9381	0.0202	7502
14	0.9830	413	0.0603	7944	0.0172	5127
15	0.9853	594	0.0557	1776	0.0148	5807
16	0.9872	338	0.0517	2500	0.0129	3125
17	0.9887	706	0.0482	6670	0.0113	5688
18	0.9900	462	0.0452	4237	0.0100	5386
19	0.9911	165	0.0425	7492	0.0089	6314
20	0.9920	232	0.0402	0474	0.0080	4095
21	0.9927	980	0.0380	8473	0.0072	5423
22	0.9934	653	0.0361	7723	0.0065	7768

Thus, when Hw_1 corresponding to particular values of M and Hw_2 is found, the corresponding Hw_p is easily found with equation (3.56).

These correlations can be used not only in the near adiabatic region (where Beek's correlation, equation (3.21), is sufficient) but also in regions of high heat transfer coefficients, where the radial gradients are large. The one-dimensional models have flat radial profiles, zero gradients. The seeming contradiction that such models can approximate two-dimensional models with large radial gradients can be explained by the fact that in the two-dimensional models, after a short entrance region, the radial temperature profiles are similar; that is, the relationship between any temperature on the profile and the radially averaged temperature, is independent of axial position. This similarity is seen in equation (3.41) and in the corresponding equation for the partial differential equation model, from equation (3.8), with the first term of the series:

$$T \cong \exp\left[-\tfrac{1}{2}\,Pe_x\left(\sqrt{1+\frac{16\beta_1^{\,2}}{M^2 Pe_r Pe_x}}-1\right)x\right]\frac{2Bi\,J_0\left(\frac{2r}{M}\beta_1\right)}{(Bi^2+\beta_1^{\,2})J_0(\beta_1)} \quad . \tag{3.57}$$

In each case, the temperature is expressed as the product of two factors, one a function of axial position only, the other a function of radial position only. With similar radial profiles, the heat loss at the wall can be expressed in terms of the average temperature, so a one-dimensional model is sufficient. The wall heat transfer coefficient of the one-dimensional model thus represents not only the resistance to heat transfer to the wall but also resistance to heat transport radially through the bed; these terms determine the similar radial profiles.

Therefore one-dimensional models can provide adequate approximation of two dimensional models which have similar radial

profiles. Correlation of wall heat transfer coefficients of one-dimensional and two-dimensional models is obtained from comparison of axial temperature profiles of the two models. The correlations show that when resistance to heat transfer at the wall is large, the radial gradients are small and the two heat transfer coefficients are approximately equal; and when resistance to heat transfer at the wall is small, the one-dimensional heat transfer coefficient reflects the radial resistance of heat transport through the bed.

A correlation for differential equation models shows that a dimensionless group including the one dimensional heat transfer coefficient, $M\ Pe_r\ Hw_1$, is a universal function of the Biot number, which includes the two-dimensional heat transfer coefficient. Study of the finite stage models reveals that radial transport of heat cannot be simply expressed in terms of Pe_r, as is done in the partial differential equation model; but the Pe_r may be used as a sufficient approximation in finite stage models, because in actual tubular reactors the major resistance to radial heat transport is usually at the wall.

This correlation allows reasonable compensation for lack of radial gradients in one-dimensional models. Further comparison of the behavior of the one-dimensional and the two-dimensional models, in unsteady state and with chemical reaction, should reveal the adequacy of the one-dimensional models for description of the dynamics of a tubular chemical reactor.

CHAPTER 4

GENERAL FEATURES OF THE COMPUTER PROGRAMS

The techniques and algorithms used to solve the equations which describe the three reactor models, as presented in Chapter 2, were coded in Fortran IV. Calculations were performed according to the programs on an IBM 7090 computer and an IBM 7094 computer, each having 32 K storage locations.

The three programs are: FS2D (describing the two-dimensional finite stage reactor); FS1D (describing the one-dimensional finite stage reactor); and PLGFLO (describing the plug flow reactor). Each program contained several subroutines, each of which performed particular functions of steady state calculations, output, etc. Also, a subroutine, PLCT, was written for use with each of the three programs to produce output in graphical form, through the off-line plotting facilities of the University of California Computer Center.

The calculations of these programs describe the dynamic behavior of the reactor discussed in Chapter 1. The programs accept input data in either dimensioned or dimensionless form. The output, which includes concentrations and temperatures at specified times and positions in the reactor, is available in printed form, in graphical form, or both. The format of the output is flexible, and is controlled by input data parameters. The printed output may include the concentration of each reactant, the fluid temperature, and the solid temperature; however, only the concentration of the primary reactant and the fluid temperature are included in the graphical output. The two forms of graphs are: c_A and T are plotted against time at selected axial positions (for example, Figures 13 and 14, and c_A and T are plotted against axial position at selected (equally spaced) times (for example, Figures 15 and 16).

The FS2D program was designed to describe reactors with maximum dimensions of 300 (particle diameters) axially and 15 across the diameter. The printed output of this program may include

concentrations and temperatures at any stage, thus giving complete axial and radial profiles during the transient. Only radially averaged concentrations and temperatures are plotted, however.

The FS2D program includes a subroutine in which the overall heat transfer coefficients, Hw_1 and Hw_p, are calculated according to the methods described in Chapter 3. These heat transfer coefficients must be used in the respective programs based on the one-dimensional models, FS1D and PLGFLO, in order to compare the computed results of these programs with the computer results of the FS2D program.

The FS2D program was designed to handle cases of both finite and infinite Hp (in the latter case, the fluid temperatures and the particle temperatures are equal), as well as cases of either finite or infinite Hw_2 (in the latter case, the temperatures of the wall stages are equal to the wall temperature). This program cannot handle the case of an adiabatic reactor (i.e., with zero Hw_2). However, in an adiabatic reactor there are no radial gradients, in which case the two-dimensional finite stage reactor is identical to the one-dimensional finite stage reactor.

For the reactor described by the parameter values presented in Chapter 6 (i.e., L = 100, M = 8, and maximum time = 260) the FS2D program (including plotting) required approximately 11 minutes on the IBM 7094. The numerical integration time step was taken as 1 (particle residence time). Instabilities occurred for a time step of 2, and the differences between the results for a time step of 1 and those for a time step of 1/2 were less than 0.01%.

The FS1D program was designed to describe reactors with a maximum length of 300 (particle diameters). It was designed to handle cases of both finite and infinite Hp, as well as cases of both zero and positive Hw_1.

For the reactor described by the parameter values presented in Chapter 6, the FS1D program (including plotting) required slightly more than 3 minutes on the IBM 7094. The above remarks concerning the numerical integration time step in the FS2D program also apply to the FS1D program. The size of this time step depends upon the

reaction rate; either program used for a reactor with a higher rate of reaction would require a smaller integration time step.

The PLGFLO program was designed to describe reactors with lengths which can be divided into a maximum of 1000 increments. Because the plug flow model is a continuous, rather than a discrete, model, these increments need not correspond to packing particles; the discretization in the program is necessary only for the numerical integration techniques. However, in the coding of this program, the particle diameter was used as a natural unit of length, to afford correspondence among the results of the three programs. Therefore, the increment size is represented as a fraction, or a multiple, of the particle diameter.

The PLGFLO program was designed for cases of both zero and positive Hw_1, but only for finite values of Hp. As is discussed in Chapter 6, the plug flow model with infinite Hp predicts physically unreasonable behavior. Furthermore, there is difficulty in converting the data in this case to a form easily plotted, because of the position of the characteristics in this case.

For the reactor described by the parameter values presented in Chapter 6, convergence of the numerical integration scheme used in the PLGFLO program was excellent for three iterations and for the space increment and the time increment equal to one particle diameter and one particle residence time, respectively. For this case, the PLGFLO program (including plotting) required slightly more than $7\frac{1}{2}$ minutes on the IBM 7094. It may be concluded from the computer times required by runs with prototype programs that much of this time is used in rearranging the results to a form suitable for plotting. It is expected that the time required by the PLGFLO program without plotting of axial profiles (but with plotting of dynamic behavior at selected axial positions) is comparable with the time required by the FS1D program for the same case.

The computer times given above include preparation of a plotting tape on the IBM 7094. The actual plotting is done off-line, and requires

approximately 15 minutes on the IBM 1401 for the production of four graphs including a total of 70 curves representing about 7500 data points.

CHAPTER 5

SELECTION OF NUMERICAL VALUES OF PARAMETERS

The values of the parameters used in the numerical calculations of this study were chosen as those of the experimental reactor studied by Sinai.[6] These parameters are summarized in Tables 5.1 and 5.2.

The reaction of this study is that of sodium thiosulfate and hydrogen peroxide in aqueous solution:

$$Na_2S_2O_3 + \gamma H_2O_2 \longrightarrow \text{products.}$$

This is a homogenous, liquid-phase reaction. This reaction has been studied by Spencer,[17] who obtained the values of the energy of activation, E; the pre-exponential coefficient, k^*; the heat of reaction, $(-\Delta H)$; and the stoichiometric coefficient, γ. Spencer also found that the rate of reaction is proportional to the concentration of each reactant:

$$\text{rate} = k^* c_A^* c_B^* e^{-\frac{E}{RT}} . \tag{5.1}$$

The reactor studied by Sinai was a tube of 1-inch-ID and 3 feet long packed with 3-mm-diameter borosilicate glass beads. The length used in these calculations is taken as 30 cm (100 particle diameters), approximately one-third the length of Sinai's reactor. The reactor of 30 cm length has a residence time of 3.59 sec, and the particle residence time is 0.0359 sec. According to the dynamic calculations on the models, steady state is reached in less than 10 seconds after a step in feed concentration or feed temperature.

The modified Reynolds number, $\frac{\epsilon v \rho d_p}{\mu}$, is approximately 93, in which case[1] the fluid is in the transition region between fully laminar flow and fully turbulent flow. The velocity profile may not be uniform, as assumed in this development, because of the low Reynolds number and because of the low ratio of reactor diameter to particle diameter, which is 8.47. Beek[2] states that this ratio must be

Table 5.1. Numerical Values of Parameters

Parameter	Symbol	Value	Source[a]
$Na_2S_2O_3$ feed concentration	$c^*_{A_f}$	0.325×10^{-3} moles/cm^3	Sinai[6]
H_2O_2 feed concentration	$c^*_{B_f}$	1.3×10^{-3} moles/cm^3	Sinai[6]
Feed temperature	T^*_f	27°C	Sinai[6]
Wall temperature	T^*_w	27°C	Sinai[6]
Reactor length	N^*	30 cm	
Reactor diameter	M^*	2.54 cm	Sinai[6]
Particle diameter	d_p	0.3 cm	Sinai[6]
Volumetric flowrate	Q	15.67 cm^3/sec	Sinai[6]
Porosity	ϵ	0.37	Sinai[6]
Fluid velocity	v	8.36 cm/sec	
Particle residence time	$\frac{d_p}{v}$	0.0359 sec	
Fluid density	ρ_f	1. g/cm^3	Hodgman[18]
Fluid heat capacity	c_f	1. cal/g-°C	Hodgman[18]
Fluid volumetric heat capacity	$\rho_f c_f$	1. cal/cm^3-°C	
Particle density	ρ_p	2.23 g/cm^3	Perry[19]
Particle heat capacity	c_p	0.20 cal/g-°C	Perry[19]
Particle volumetric heat capacity	$\rho_p c_p$	0.446 cal/cm^3-°C	
Particle surface to volume ratio	a_p	20.0 cm^2/cm^3	

Table 5.1 (continued)

Parameter	Symbol	Value	Source
Particle-fluid heat transfer coefficient	h_p	0.0372 cal/sec-cm^2-°C	Sinai[6]
Wall heat transfer coefficient	h_w	0.09201 cal/sec-cm^2-°C	
Energy of activation	E	18.3 kcal/mole $Na_2S_2O_3$	Spencer[17]
Pre-exponential coefficient	k^*	0.685×10^{15} cm^3/sec-mole-$Na_2S_2O_3$	Spencer[17]
Heat of reaction	$(-\Delta H)$	132×10^3 cal/mole $Na_2S_2O_3$	Spencer[17]
Stoichiometric coefficient	γ	2.	Spencer[17]
Adiabatic temperature rise	ΔT_a	42.9°C	

[a]The values of parameters for which sources are not given are calculated from other parameters as discussed in this chapter or in Chaper 1, Part B.

Table 5.2. Numerical Values of Dimensionless Parameters[a]

Parameter	Symbol	Value
Reactor length	L	100
Reactor diameter	M	8.47 (rounded to integer: 8)
Heat capacity parameter	β	1.7594
Particle-fluid heat transfer coefficient	Hp	0.04983
Wall heat transfer coefficient (FS2D)	Hw_2	0.01101
Overall heat transfer coefficient (FS1D)	Hw_1	0.01038
(PLGFLO)	Hw_p	0.01035
Activation energy	A	30.69
Pre-exponential coefficient	k	0.7992×10^{10}
Reference temperature/adiabatic temperature rise	T_0	6.997
Stoichiometric coefficient	γ	2.

[a]The values of ΔT_a (Table 5.1), A, k, and T_0 are based upon a reference concentration of 0.325×10^{-3} moles/cm^3 and a reference temperature of 27°C.

greater than 10 before the assumption of a uniform velocity profile can be made. Although a reactor with a larger Reynolds number and a larger reactor diameter to particle diameter ratio may be more suitable for modelling with the mathematical models of this study, it is expected that the results of the calculations based upon these parameters will satisfactorily indicate the relative magnitudes of the effects of the phenomena under consideration here.

The wall heat transfer coefficient is equal to the reciprocal of the sum of the reciprocals of several heat conduction terms. These terms include the heat transfer coefficient between the reacting fluid and the wall, the heat conductivity at the wall, and the heat transfer coefficient between the wall and the coolant. In this study, the material of the reactor wall and the nature of the coolant are not specified; rather it is assumed that the wall remains always at a constant temperature (for cases of heat loss at the wall), or that the heat conductivity of the wall and the heat capacity of the wall are zero (for adiabatic cases). For cases of heat loss at the wall, the wall heat transfer coefficient is taken as the heat transfer coefficient between the fluid and the wall; i.e., the resistances to heat transfer through the wall and from the wall to the coolant, which would give a lower wall heat transfer coefficient, are disregarded. Calculations with this higher value illustrate greater differences between the one-dimensional and the two-dimensional models.

According to Beek,[2] the heat transfer coefficient between the fluid and the wall can be estimated as 80% of the heat transfer coefficient between the fluid and the packing particles. The wall heat transfer coefficient is taken here somewhat arbitrarily as 2.5 times h_p, to further illustrate the differences between the models. Then the wall heat transfer coefficient is 680 Btu/hr-ft^2-°F, or 0.09201 cal/sec-cm^2-°C.

CHAPTER 6

RESULTS OF PROGRAM CALCULATIONS

Computer calculations were made with the programs described in Chapter 4 to determine the effect upon the reactor dynamics of the phenomena considered in this study. The effect of these phenomena may be seen by comparing runs of cases in which the phenomena were present with those in which the phenomena were ignored.

Some phenomena were not eliminated from any of the runs. The effect of the heat capacity of the packing, for example, may be seen in all of the runs. However, its effect in slowing the speed at which temperature disturbances travel through the reactor is apparent from the discussion, in Chapter 2, of the characteristics in the plug flow model (with infinite Hp). The effect of axial dispersion can be seen by a comparison of the behavior of a finite stage model with that of a plug flow model. And the effect of radial gradients can be seen by a comparison of the behavior of the one-dimensional finite stage model with that of the two-dimensional finite stage model.

Thirteen computer runs were made in this study. In six of these runs, the feed temperature was stopped from 27°C to 37°C, while the feed concentration of the primary reactant (hereinafter called the feed concentration) remained at 0.325 moles/liter. In another six runs, the feed concentration was stepped from 0.325 moles/liter to 0.390 moles/liter (an increase of 20%), while the feed temperature remained at 37°C. The other run, Run 3, shows that for a feed temperature of 27°C, a change in feed concentration has little effect upon the temperature profile because the rate of reaction remains low in this case. In half of these runs, the reactor was taken as adiabatic; in the other half, there was heat loss through the wall of the reactor. Some runs were made with infinite Hp, others with finite Hp. The parameters which distinguish these runs are presented in Table 6.1. Parameters not mentioned in this table have the values presented in Chapter 5, which are the same for all runs.

Table 6.1. Summary of Computer Runs (Chronological Order)

Run number	Program used	Type of feed step	Feed temperature (°C)	Feed concentration (moles/liter)	Hw	Hp
0[a]	PLGFLO	temperature	27.-37.	.325	0	∞
1	FS1D	temperature	27.-37.	.325	0	∞
2	FS1D	temperature	27.-37.	.325	0	+
3	FS1D	concentration	27.	.325-.390	0	+
4	FS1D	concentration	37.	.3250.390	0	∞
5	FS1D	concentration	37.	.325-.390	0	+
6	PLGFLO	concentration	37.	.325-.390	0	+
7	PLGFLO	temperature	27.-37.	.325	0	+
8	FS2D	temperature	27.-37.	.325	+	+
9	FS1D	temperature	27.-37.	.325	+	+
10	PLGFLO	temperature	27.-37.	.325	+	+
11	FS2D	concentration	37.	.325-.390	+	+
12	FS1D	concentration	37.	.325-.390	+	+
13	PLGFLO	concentration	37.	.325-.390	+	+

[a]Run 0 was an early run made with a prototype PLGFLO program. The output of this run did not include machine-plotted graphs.

The plus signs (+) in the last two columns of this table, and in the second and third columns of Table 6.2, indicate that the value (dimensionless) of the respective heat transfer coefficients is:

Hp:	0.0498293	
Hw_2:	0.0110107	(FS2D)
Hw_1:	0.0103777	(FS1D)
Hw_p:	0.0103508	(PLGFLO)

The values of Hw_1 and Hw_p were calculated from M and Hw_2 according to equations (3.53) and (3.56).

In Table 6.2, the run numbers are arranged in an order which facilitates comparison of runs to determine the effect of the various phenomena. In Table 6.3, these run numbers are paired for direct comparison of the results.

The results of these runs, the dynamic behavior of the models, are presented in Figures 13 through 64. The results of each run include four graphs.

As an example, Run 5 may be considered. The results of this run are shown in Figures 29, 30, 31, and 32. These results show the response to a feed concentration step of the one-dimensional finite stage model with no heat loss at the wall and with finite Hp. Figure 29 shows concentration profiles at equally spaced values of time of 0, 10, 20, 30, 40, $\cdots$ (particle residence times). The curve that begins at c_A (CA)of 1.0 at $x = 0$ represents the initial steady state profile. The heavy curve that begins at $c_A = 1.2$ and crosses the initial steady state profile at $x = 67$ is the final steady state profile. This figure shows the concentration disturbance as it travels through the reactor. The flattening of the disturbance as it travels is due primarily to axial dispersion.

The corresponding dynamic temperature profiles for this run are shown in Figure 30. The lower curve is the initial steady state fluid temperature profile, and the upper curve is the final steady state profile. The other curves represent the dynamic profiles at the same equally spaced values of time as those of Figure 29.

Figure 31 shows the dynamic behavior of concentration for this run at selected axial positions of 20, 40, 60, 80, and 100. The effect of axial dispersion is apparent also here. It should be noted that, after the initial disturbance in concentration passes, the concentration changes monotonically to its final steady state value.

Figure 32 shows the dynamic behavior of fluid temperature for this run at the same axial positions of 20 (the lower curve), 40, 60, 80, and 100 (the upper curve). Because of the heat capacity of the packing, the major temperature change travels more slowly than the fluid velocity. Thus, at the exit of the reactor (axial position 100),

the major temperature change occurs at a time of approximately 176; the reactor residence time, and the time at which the initial concentration disturbance appears (see Figure 31, lower curve) is 100. The great amount of dispersion seen in this curve is due primarily to the finite rate of heat transfer between the particles and the fluid, but also partially to axial dispersion in turbulent mixing. The concentration continues to change (see Figure 31, lower curve) because it is affected by the temperature change through the coupling term in the mass balance equations.

From Table 6.3, it is seen that these four figures of Run 5 can be compared with the corresponding figures of Run 4 to show the effect of a finite rate of heat transfer between the particles and the fluid, Run 6 to show the effect of axial dispersion, and Run 12 to show the effect of heat loss at the wall. From the comparisons suggested in Table 6.3 and from considerations of the nature of the models, the effects of these and other phenomena can be determined.

The discontinuities inherent in the plug flow model are shown in the machine-plotted figures, for the runs with the PLGFLO model, as inclined lines rather than as vertical lines. These discontinuities are shown in this manner because the plotting subroutine was designed to accept values of concentration and temperature only at equally spaced values of distance or time. The discontinuities should more accurately appear in these figures as vertical lines at values x or t which are the nearest multiples of ten.

The Effect of Heat Capacity of the Packing Particles

As mentioned above, this effect was not eliminated in any of the runs. It was not eliminated because it is fundamental to the dynamic response of a packed-bed chemical reactor. This effect is seen most clearly in the plug flow model with infinite Hp, in which all other phenomena are eliminated except the coupling of concentration and temperature through the reaction, which is also fundamental to the dynamic response.

Table 6.2. Summary of Computer Runs (Logical Order)

Program used	Hw	Hp	Temperature Step	Concentration Step
PLGFLO	0	∞	0[a]	
FS1D	0	∞	1	4
FS1D	0	+	2	5
FLGFLO	0	+	7	6

[a]Run 0 was an early run made with a prototype PLGFLO program. The output of this run did not include machine-plotted graphs.

In this table, for runs with a temperature step, the feed concentration is 0.325 moles/liter and the feed temperature is stepped from 27°C to 37°C. For runs with a concentration step, the feed temperature is 37°C and the feed concentration is stepped from 0.325 moles/liter to 0.390 moles/liter.

Run 3 is omitted from this table because it is the only run with a concentration step for which the feed temperature is 27°C.

In all runs, the reference concentration is 0.325 moles/liter, and the reference temperature and the wall temperature are equal to the initial feed temperature. The maximum adiabatic temperature rise is 42.9°C in all runs.

Table 6.3 Pairing of Runs Revealing Effects of Phenomena

Phenomenon		Temperature step	Concentration step
Assumption of infinite Hp	without axial dispersion (PLGFLO)	7 and 0[a]	
	with axial dispersion (FS2D)	1 and 2	4 and 5
Axial dispersion	adiabatic case	2 and 7	5 and 6
	with heat loss at wall	9 and 10	12 and 13
Radial gradients		8 and 9	11 and 12
Heat loss at wall	with axial dispersion (FS1D)	2 and 9	5 and 12
	without axial dispersion (PLGFLO)	7 and 10	6 and 13
Effect of concentration step at different feed temperatures			3 and 5

[a]Run 0 was an early run made with a prototype PLGFLO program. The output of this run did not include machine-plotted graphs.

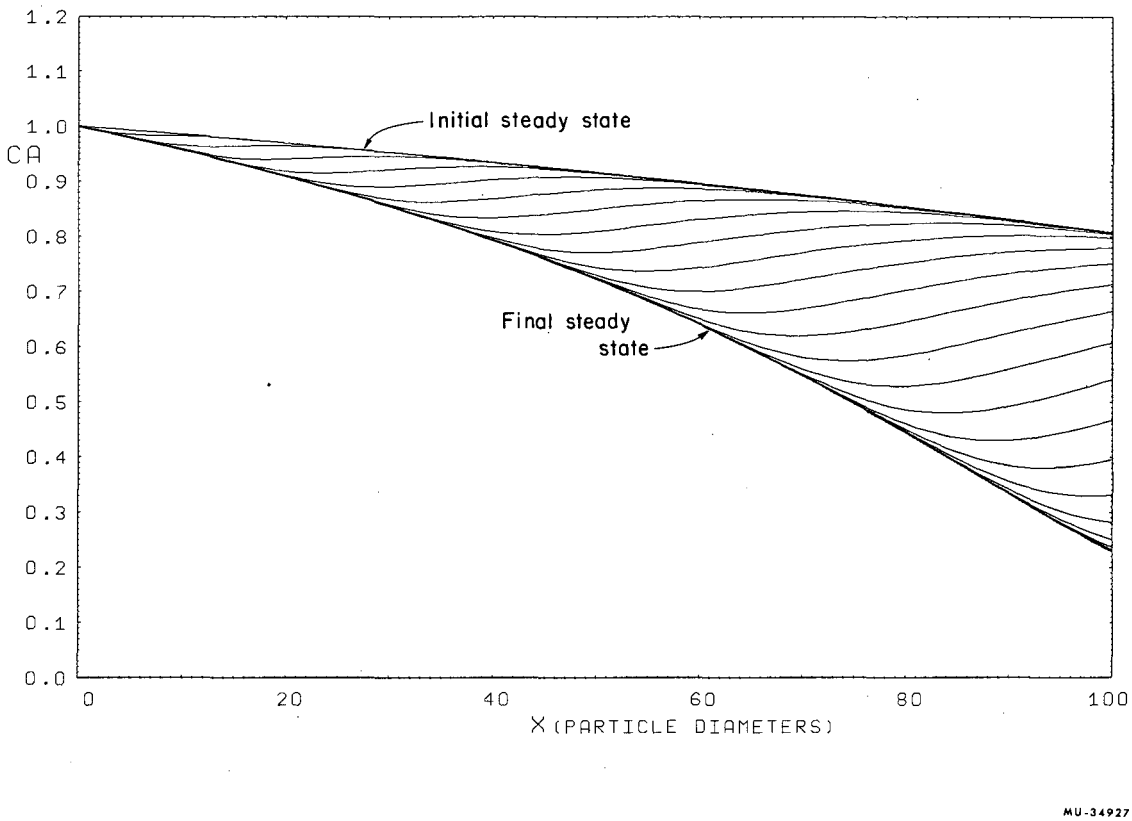

Fig. 13. Transient axial concentration profiles resulting from a temperature step (Run 1, FS1D program). Profiles are shown for times t = 10, 20, 30, 40,....

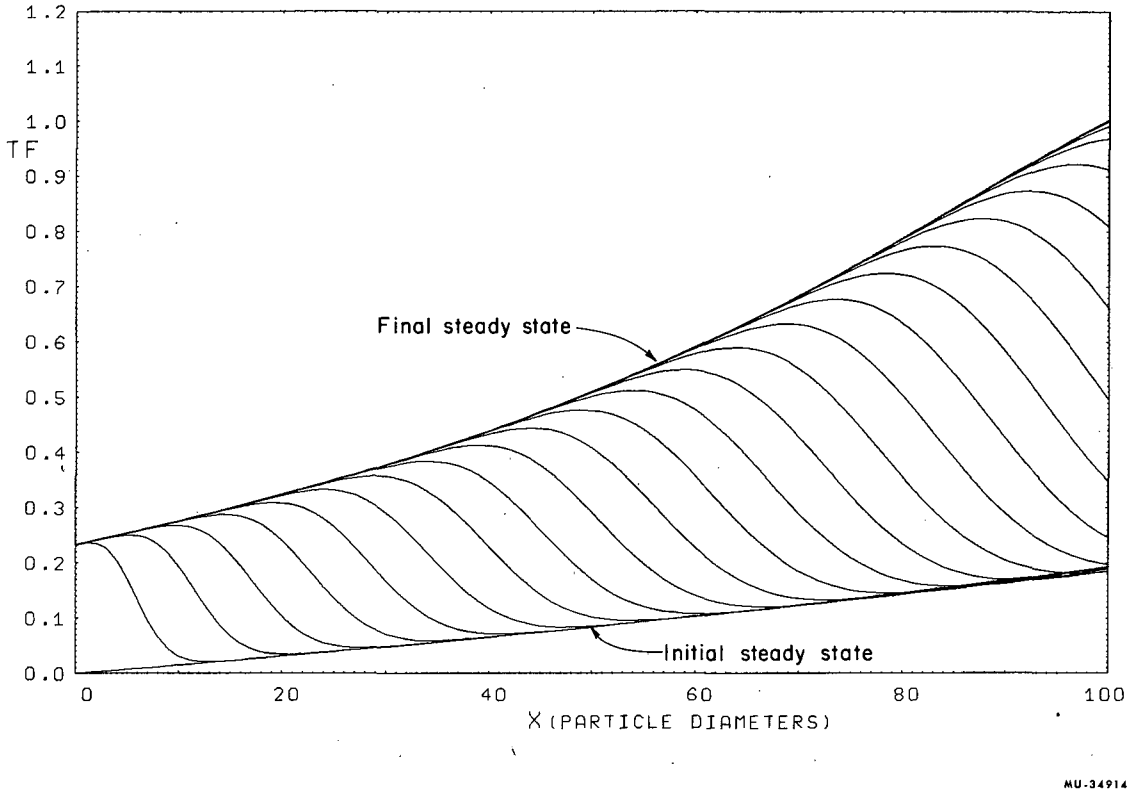

Fig. 14. Transient axial temperature profiles resulting from a temperature step (Run 1, FS1D program). Profiles are shown for times t = 10, 20, 30, 40,....

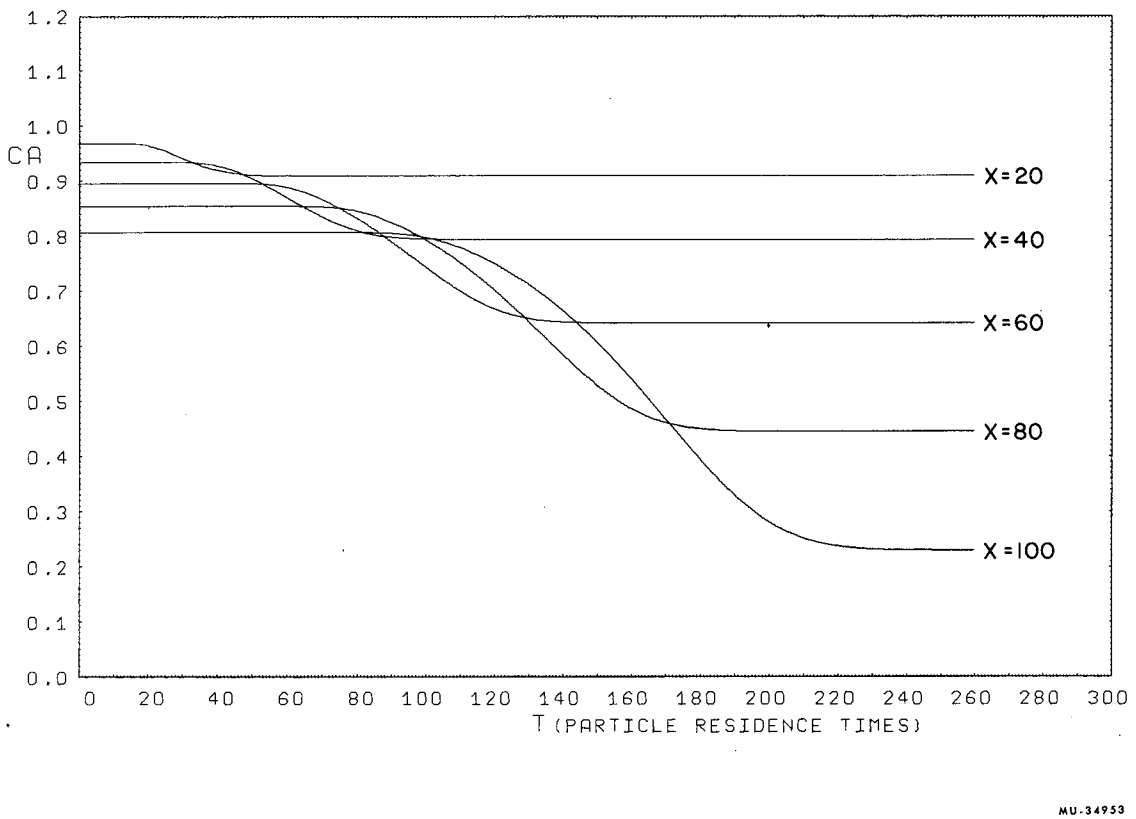

Fig. 15. Response of concentration at selected axial positions to a temperature step (Run 1, FS1D program).

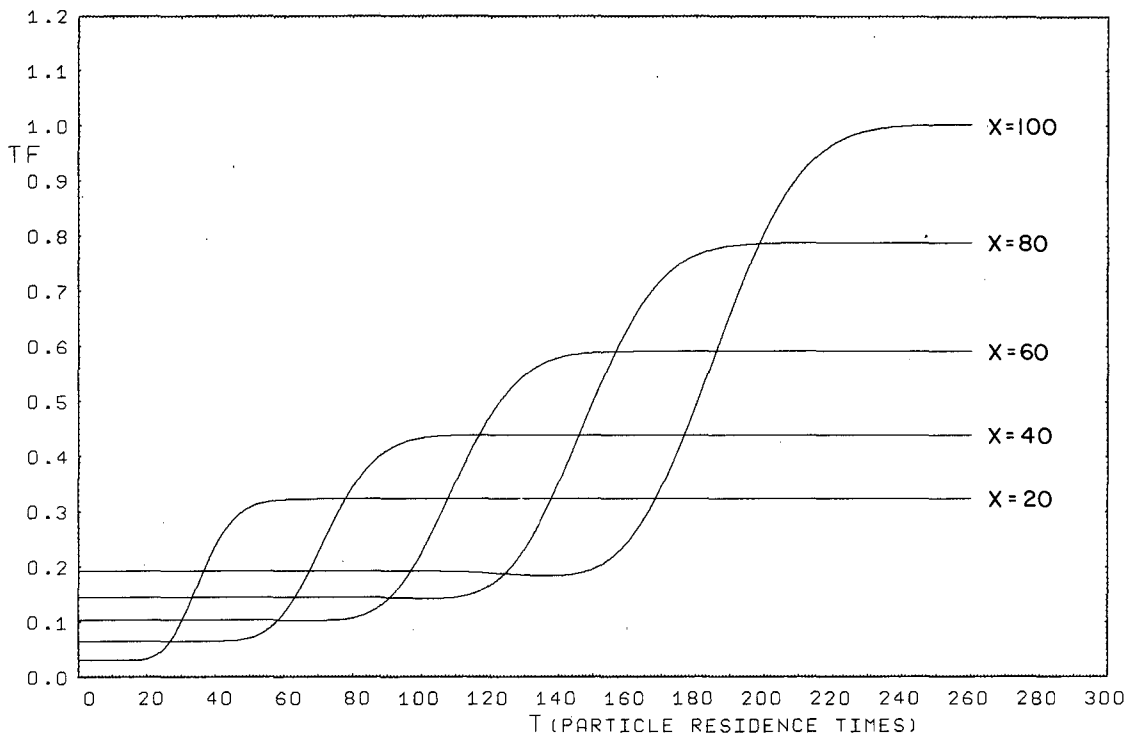

Fig. 16. Response of temperature at selected axial positions to a temperature step (Run 1, FS1D program).

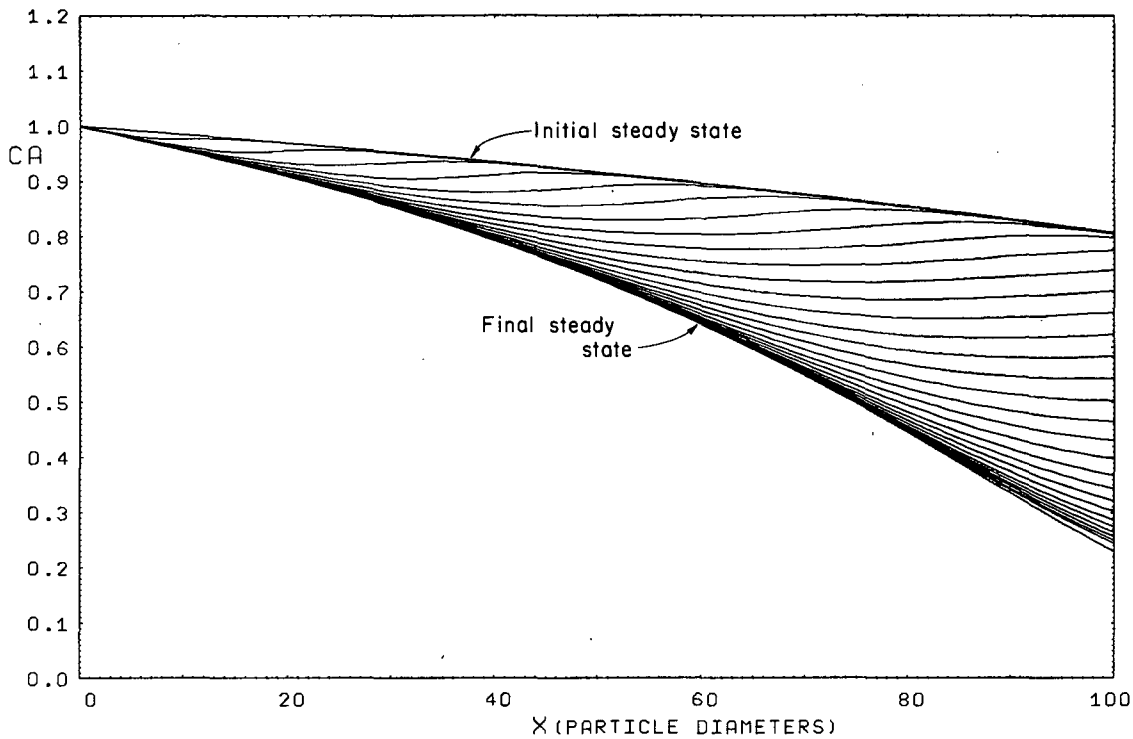

Fig. 17. Transient axial concentration profiles resulting from a temperature step (Run 2, FS1D program). Profiles are shown for times t = 10, 20, 30, 40,....

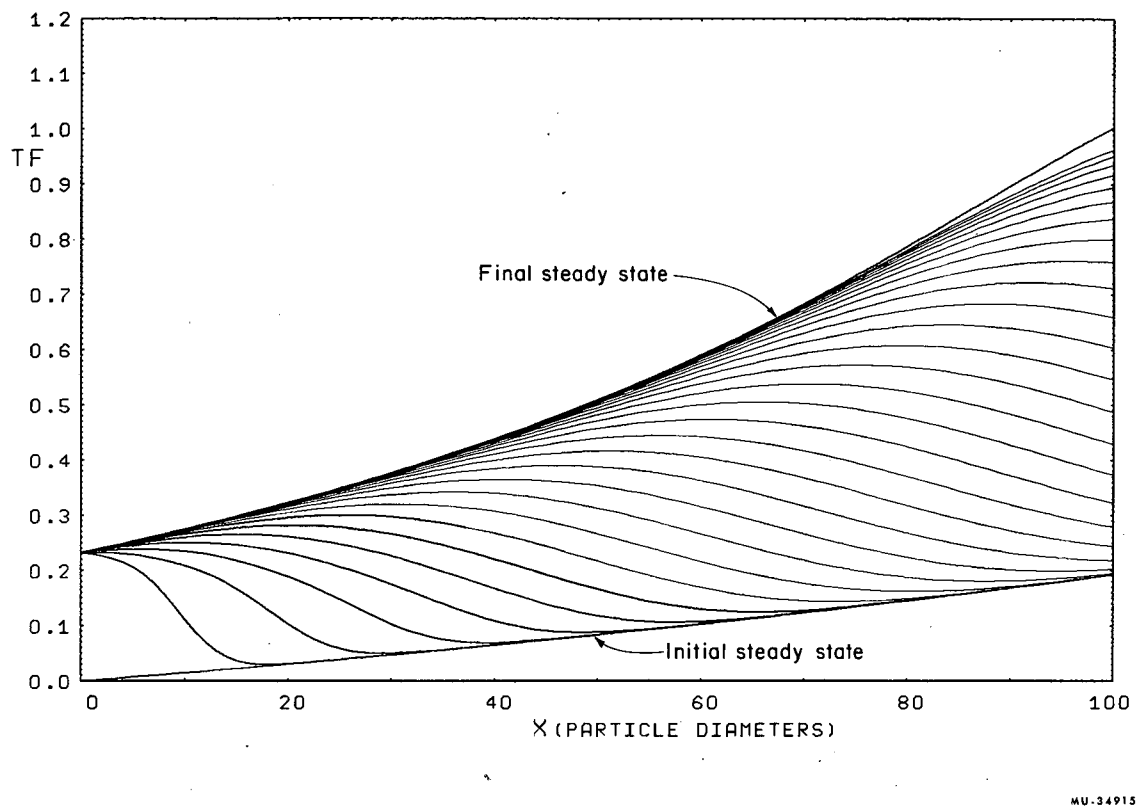

Fig. 18. Transient axial temperature profiles resulting from a temperature step (Run 2 FS1D program). Profiles are shown for times t = 10, 20, 30, 40,....

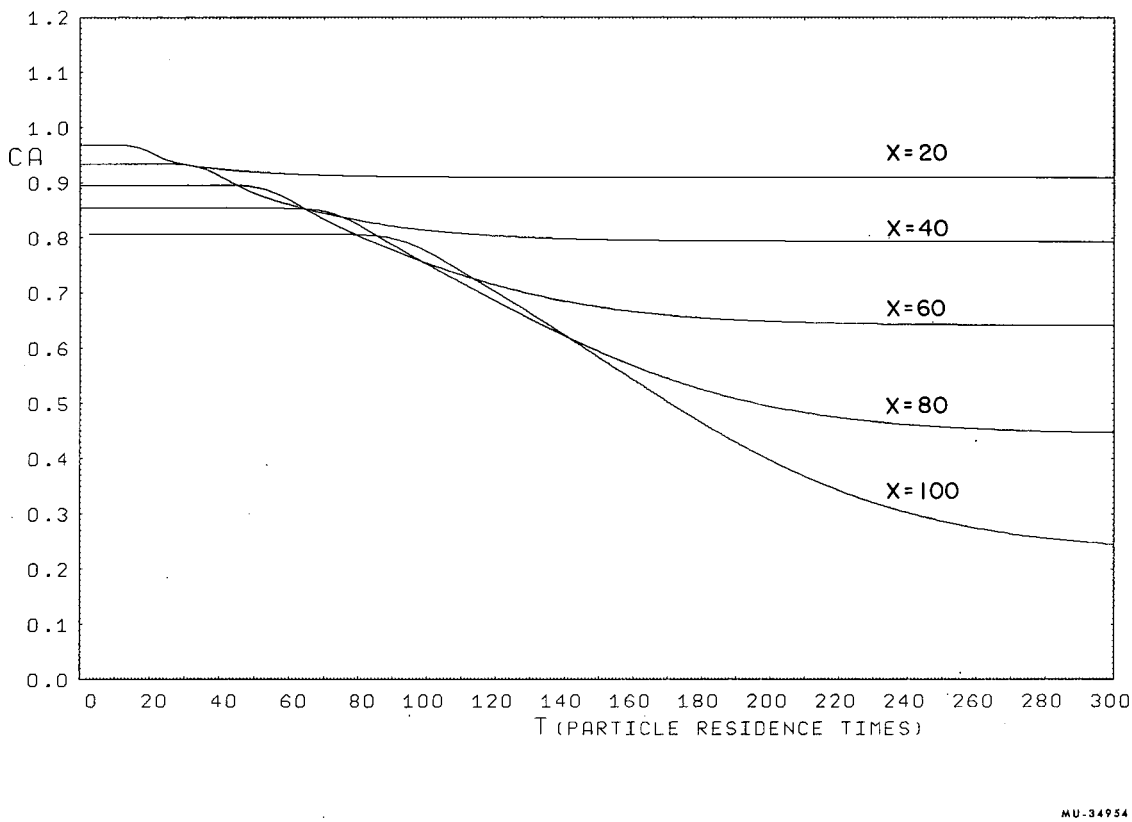

Fig. 19. Response of concentration at selected axial positions to a temperature step (Run 2, FS1D program).

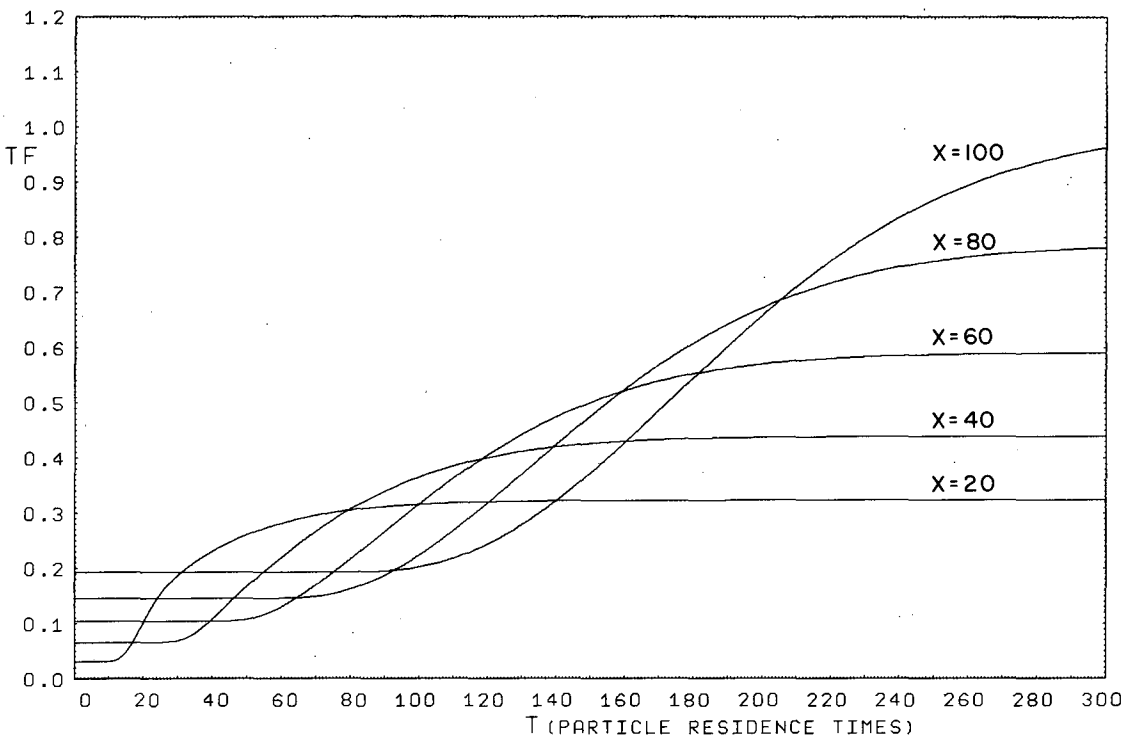

Fig. 20. Response of temperature at selected axial positions to a temperature step (Run 2, FS1D program).

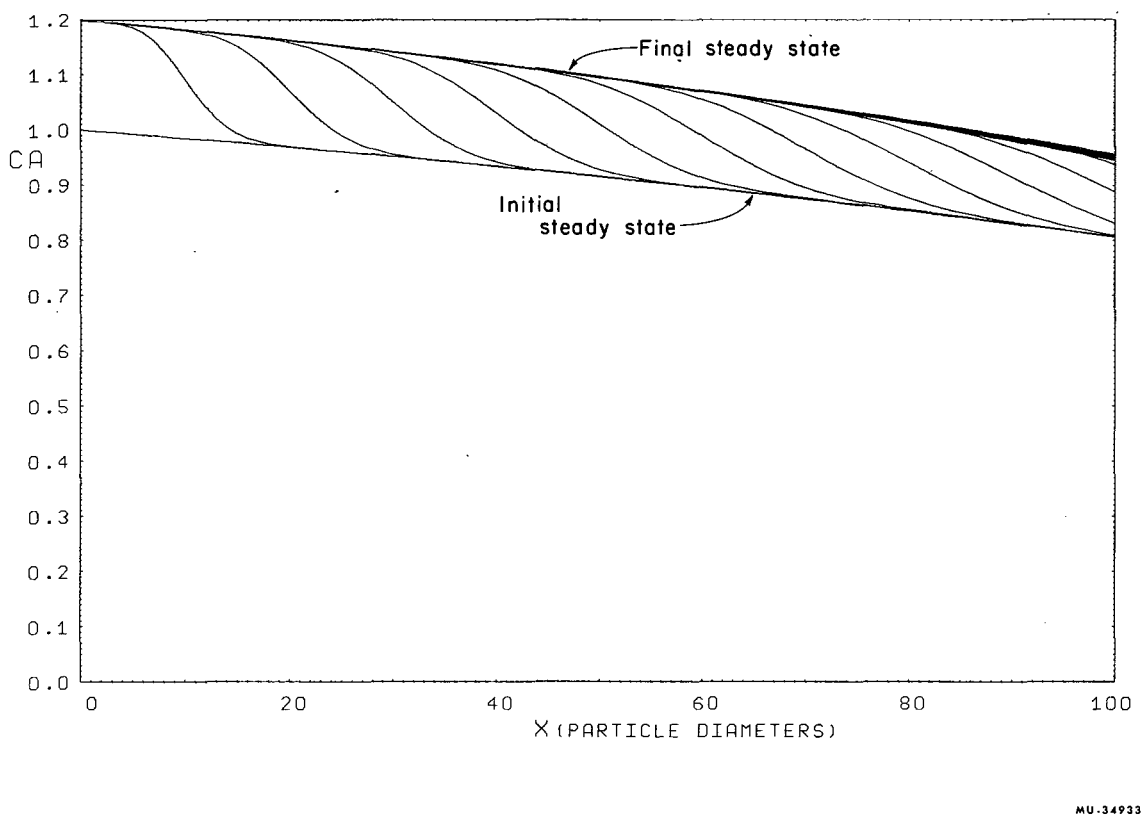

Fig. 21. Transient axial concentration profiles resulting from a concentration step (Run 3, FS1D program). Profiles are shown for times t = 10, 20, 30, 40.

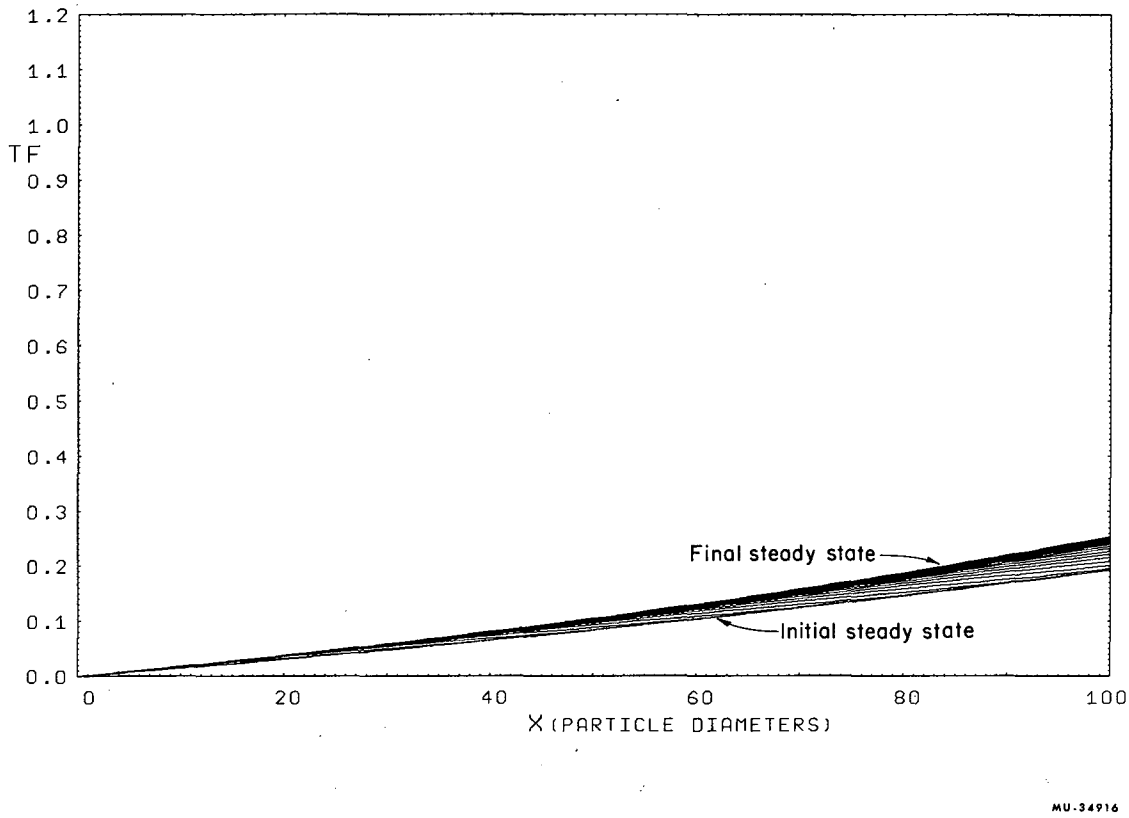

Fig. 22. Transient axial temperature profiles resulting from a concentration step (Run 3, FS1D program). Profiles are shown for times t = 10, 20, 30, 40,....

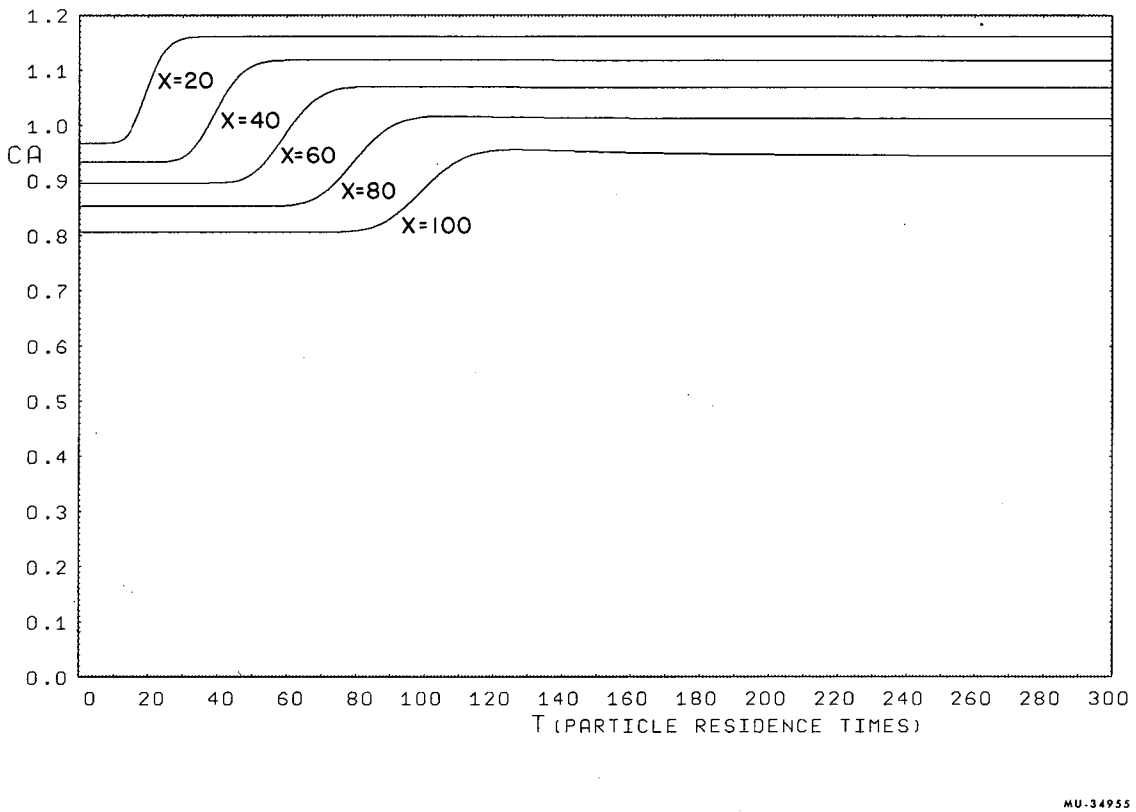

Fig. 23. Response of concentration at selected axial positions to a concentration step (Run 3, FS1D program).

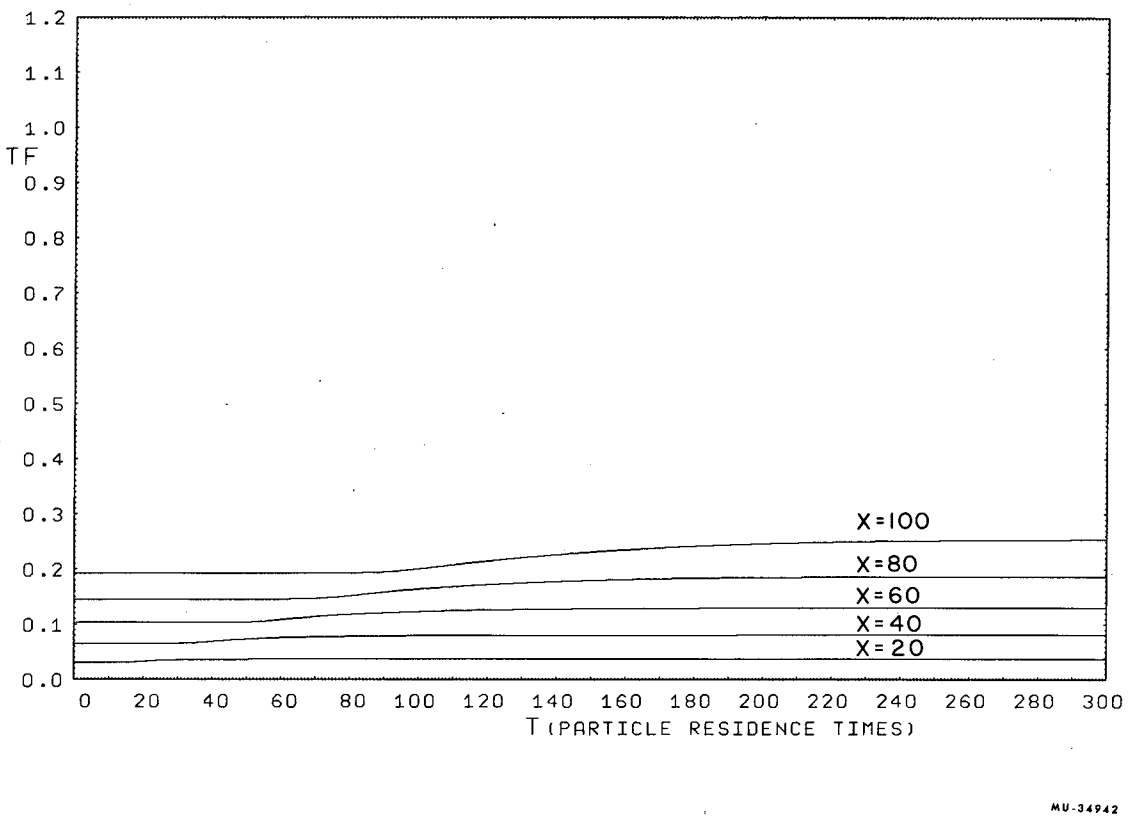

Fig. 24. Response of temperature at selected axial positions to a concentration step (Run 3, FS1D program).

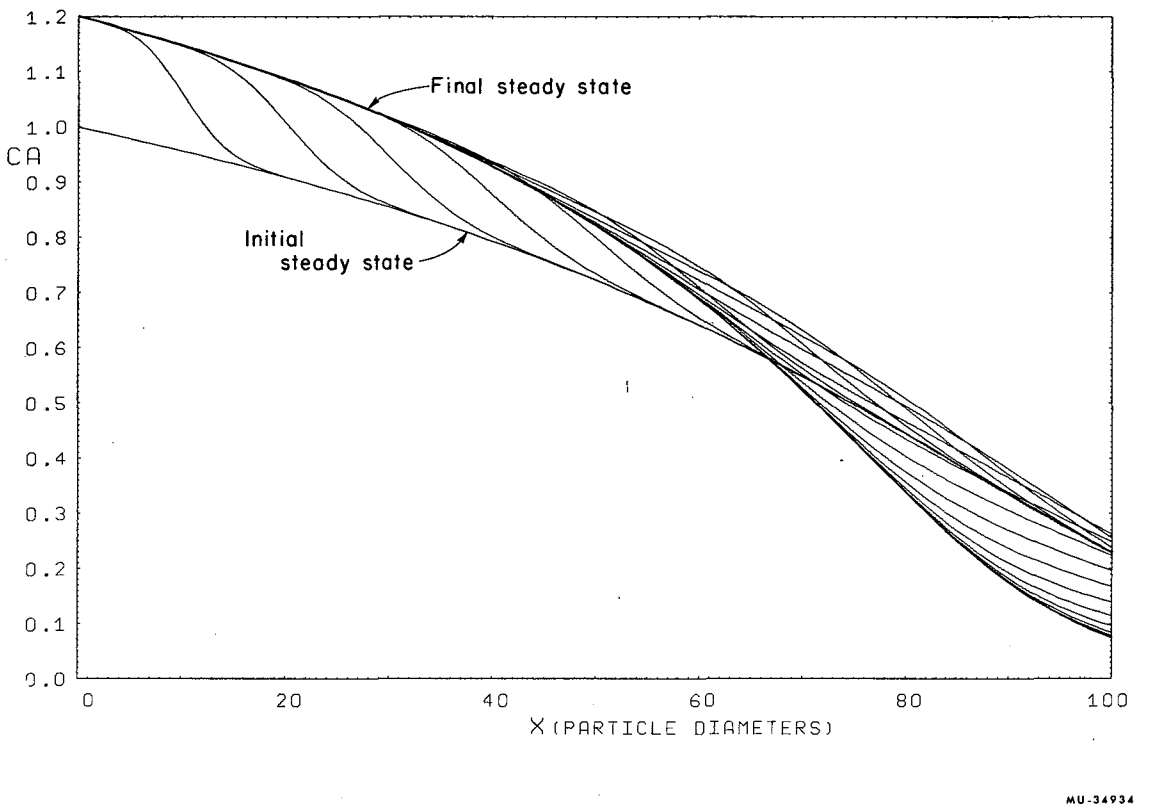

Fig. 25. Transient axial concentration profiles resulting from a concentration step (Run 4, FS1D program). Profiles are shown for times t = 10, 20, 30, 40,....

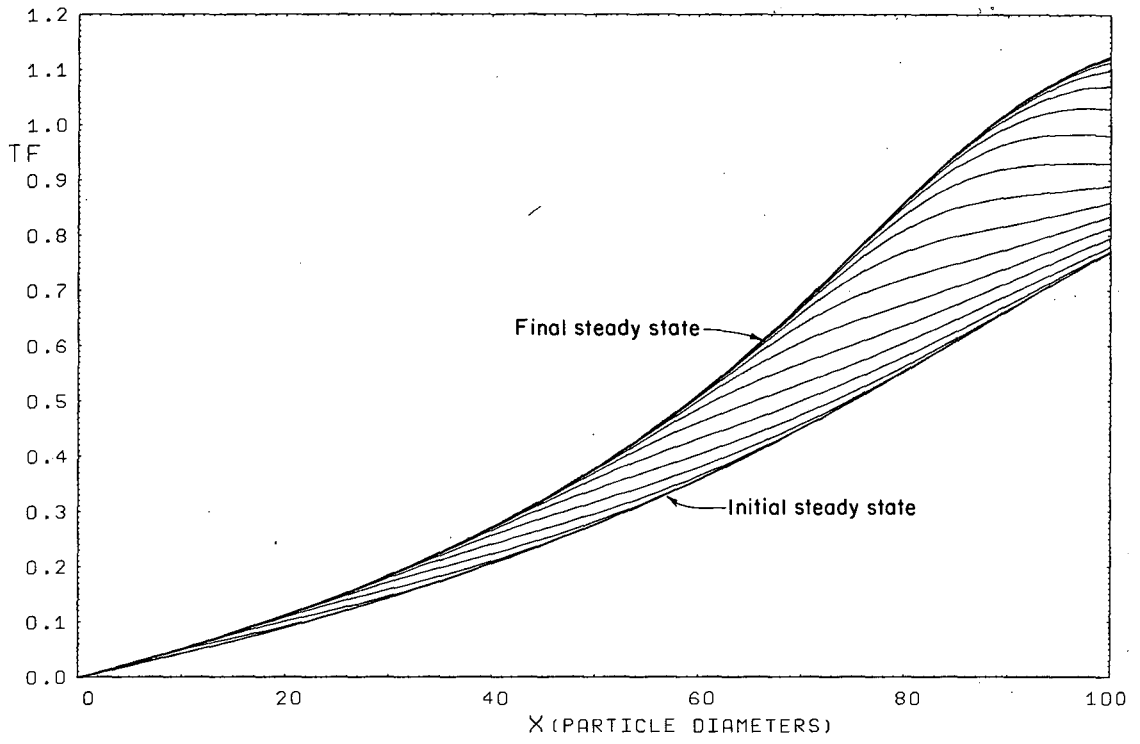

MU-34917

Fig. 26. Transient axial temperature profiles resulting from a concentration step (Run 4, FS1D program). Profiles are shown for times t = 10, 20, 30, 40,....

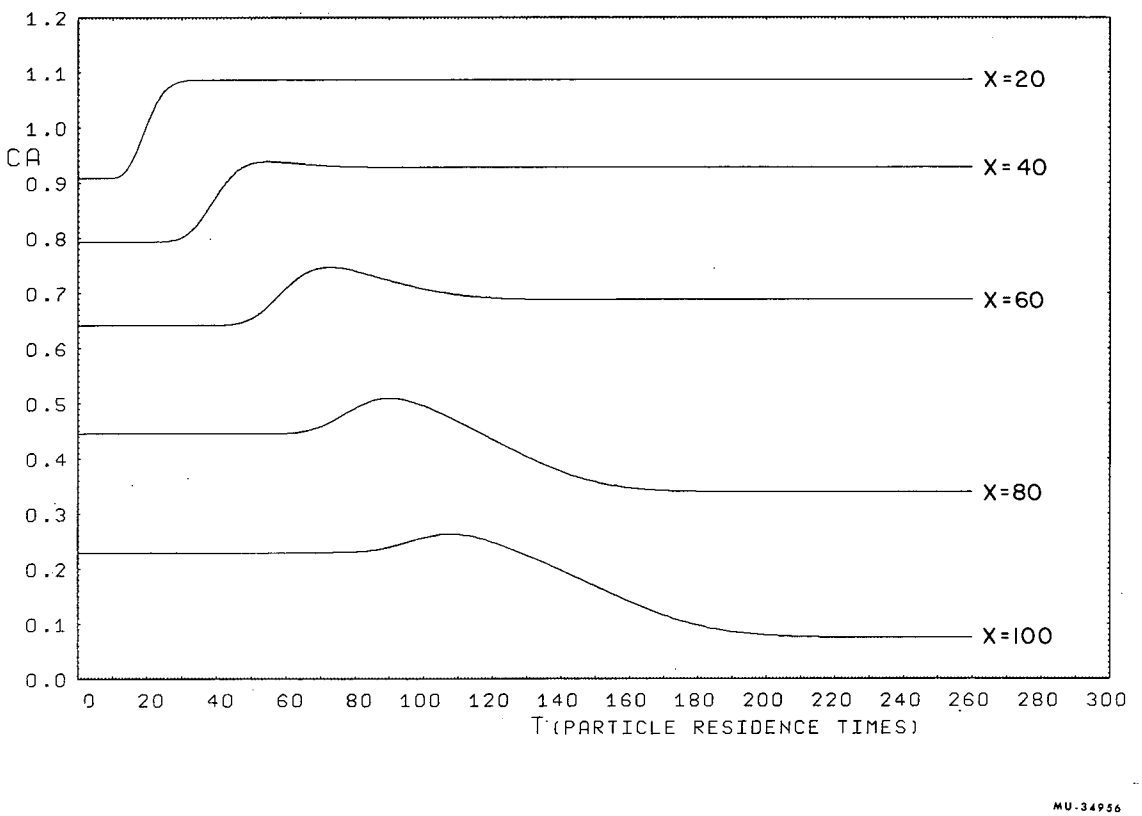

Fig. 27. Response of concentration at selected axial positions to a concentration step (Run 4, FS1D program).

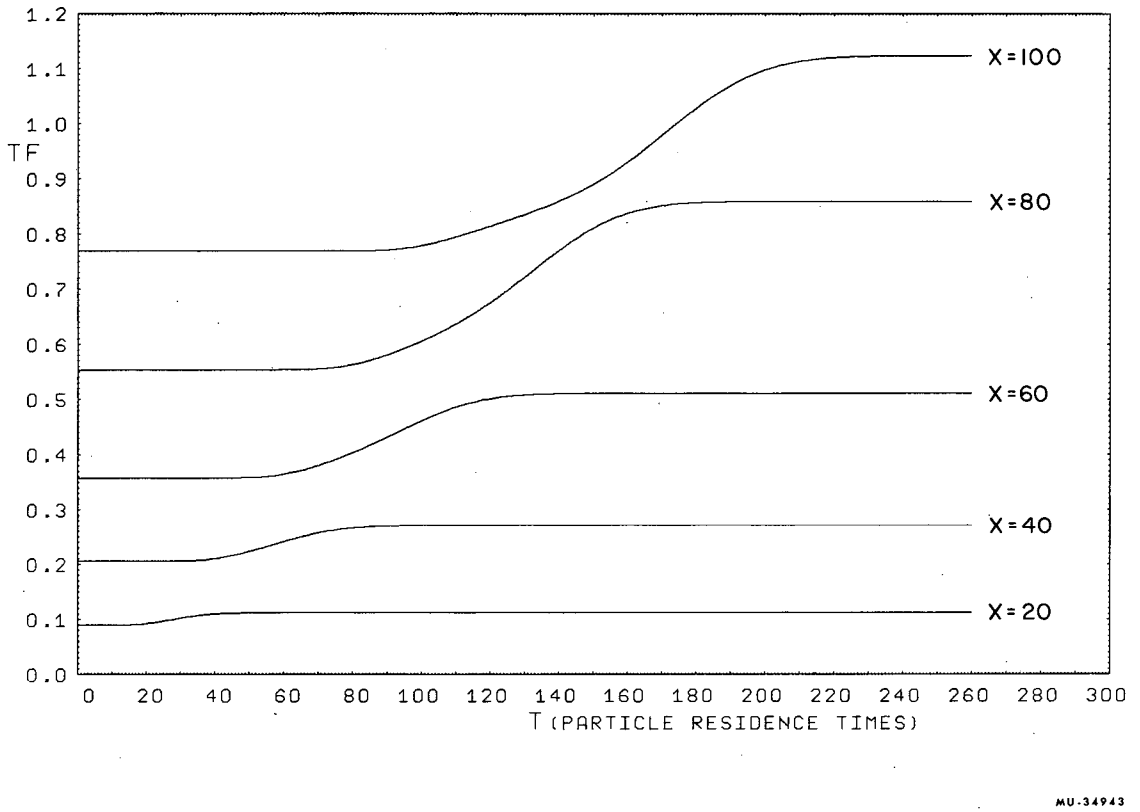

Fig. 28. Response of temperature at selected axial positions to a concentration step (Run 4, FS1D program).

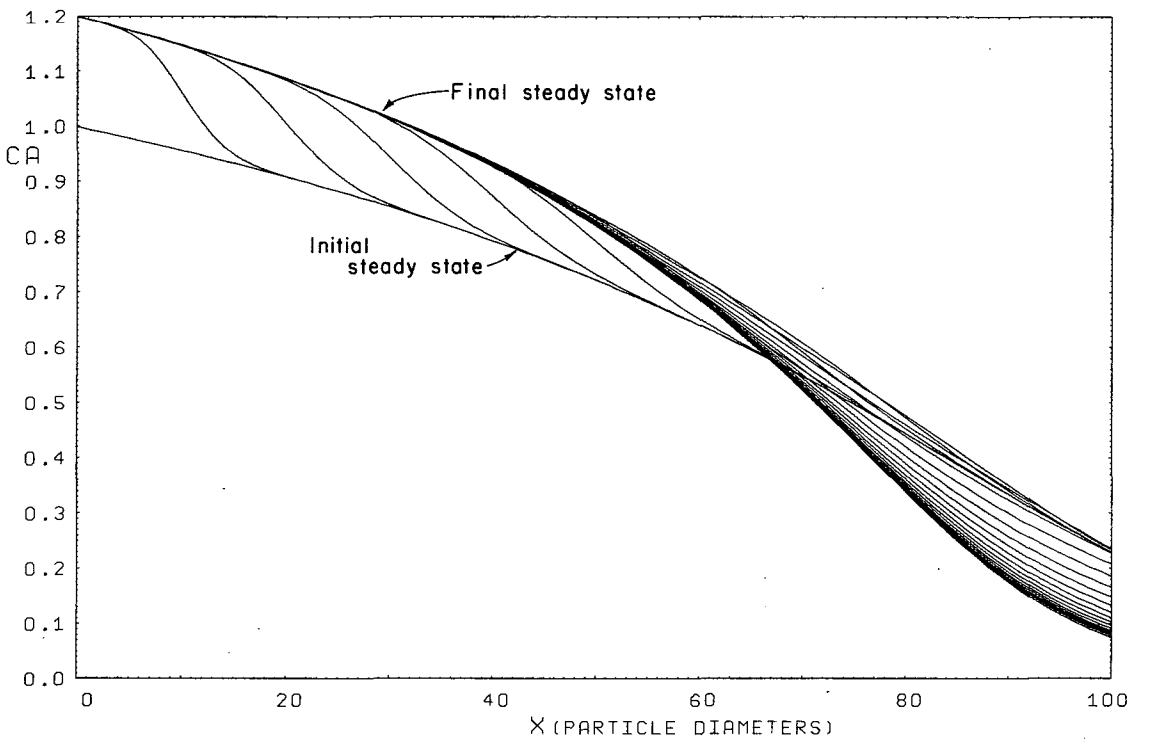

Fig. 29. Transient axial concentration profiles resulting from a concentration step (Run 5, FS1D program). Profiles are shown for times t = 10, 20, 30, 40,....

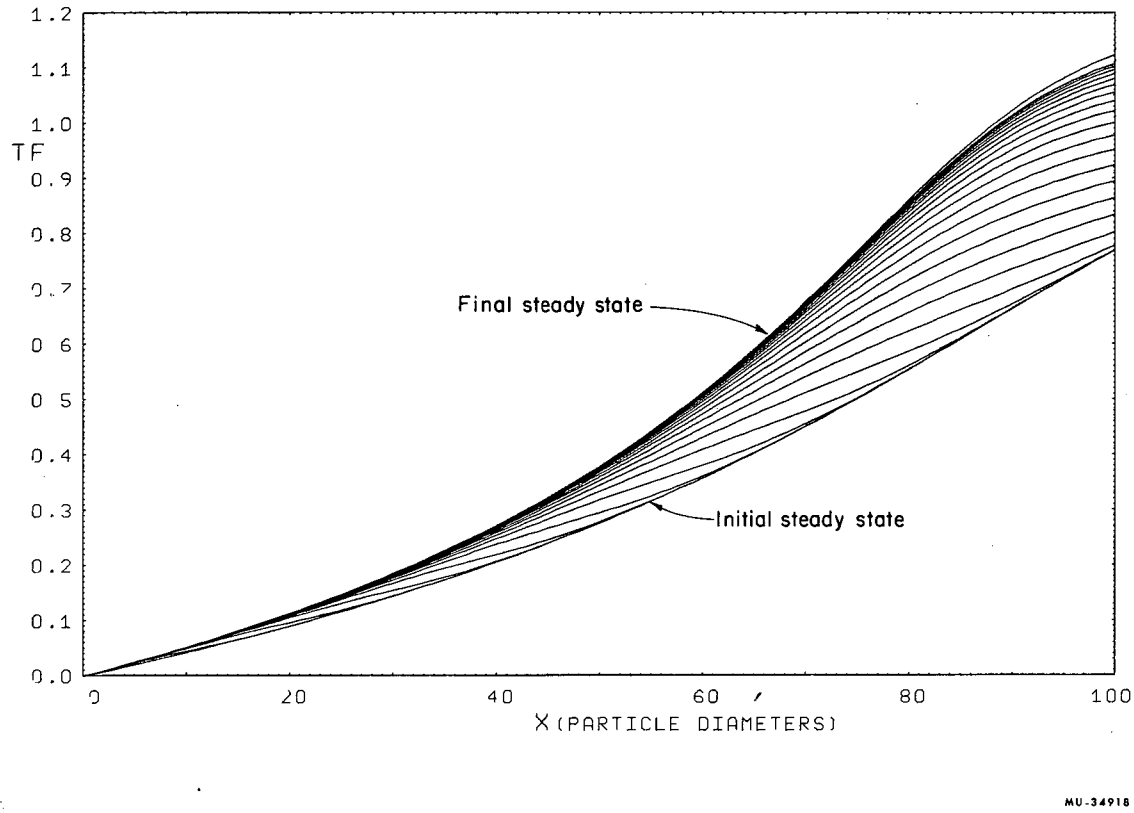

Fig. 30. Transient axial temperature profiles resulting from a concentration step (Run 5, FS1D program). Profiles are shown for times t = 10, 20, 30, 40,....

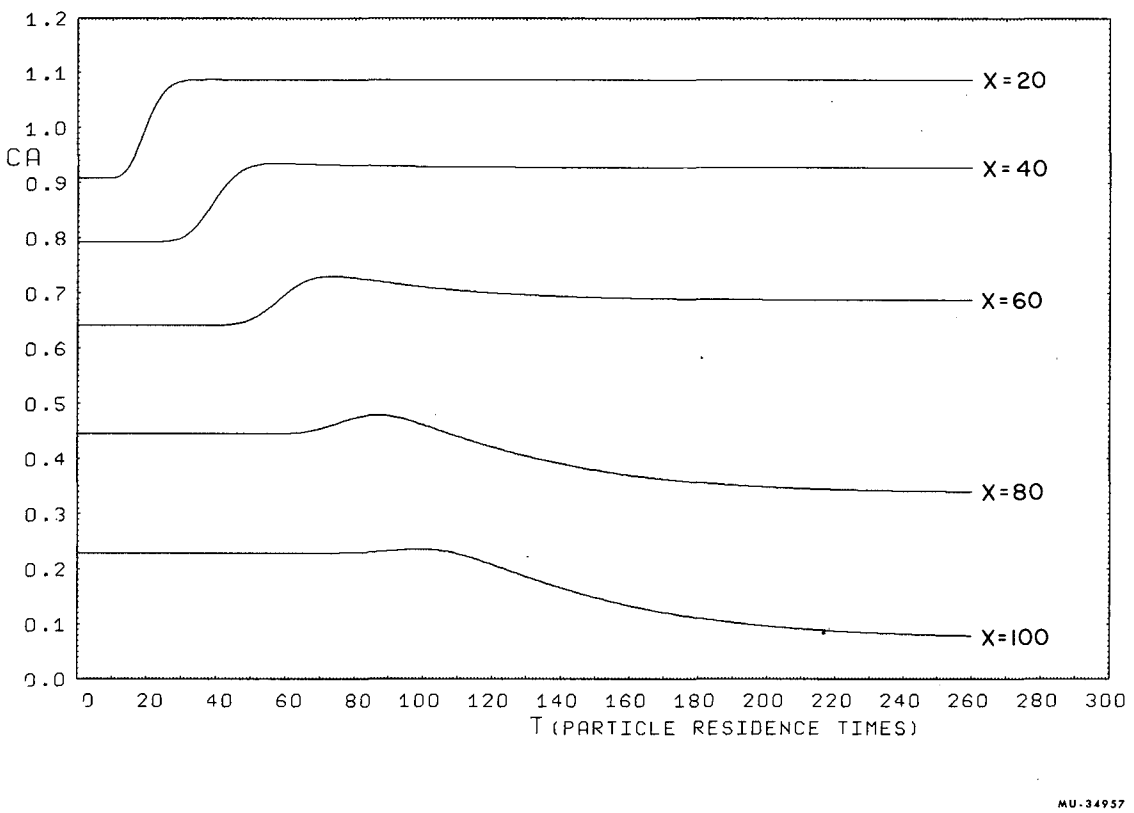

Fig. 31. Response of concentration at selected axial positions to a concentration step (Run 5, FS1D program).

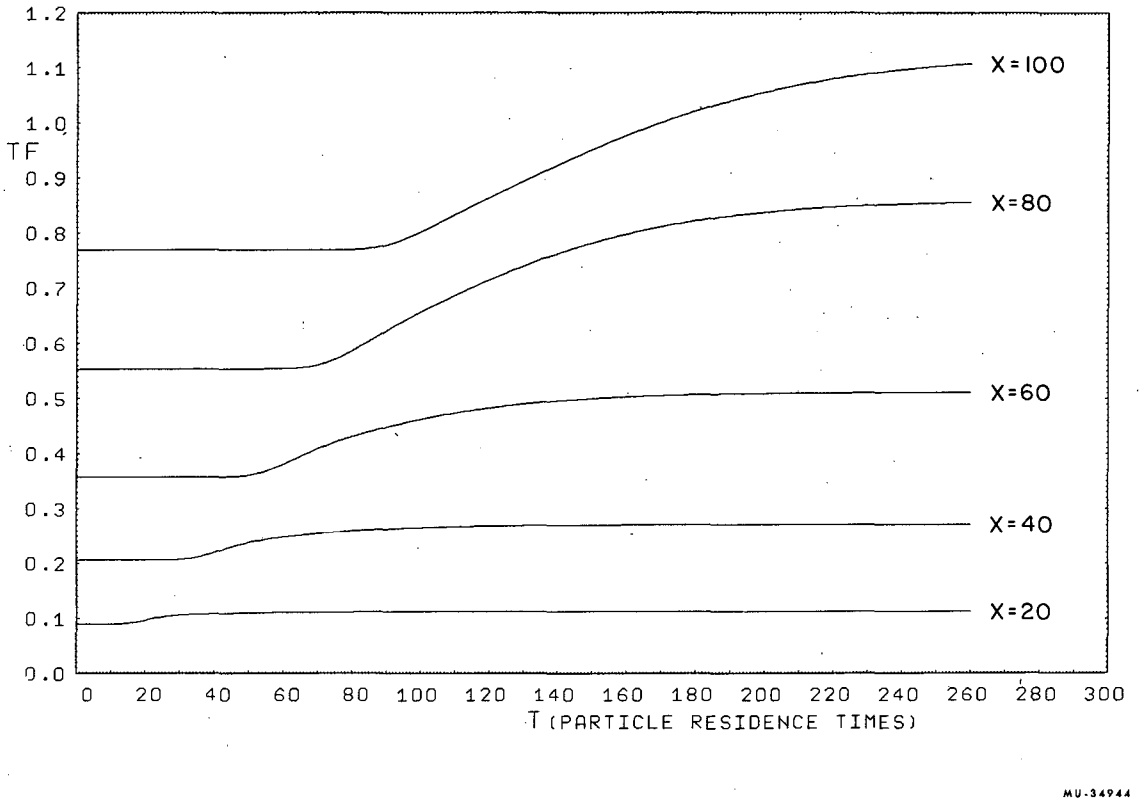

Fig. 32. Response of temperature at selected axial positions to a concentration step (Run 5, FS1D program).

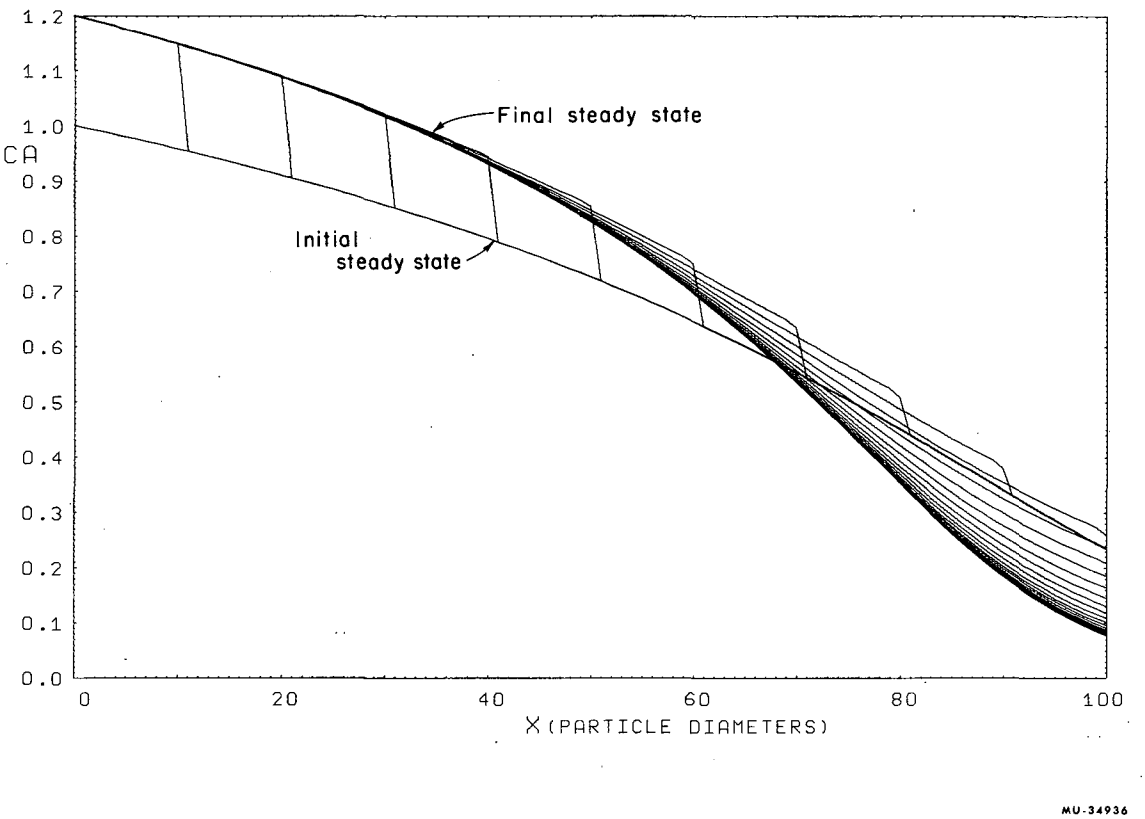

Fig. 33. Transient axial concentration profiles resulting from a concentration step (Run 6, PLGFLO program). Profiles are shown for times t = 10, 20, 30, 40,....

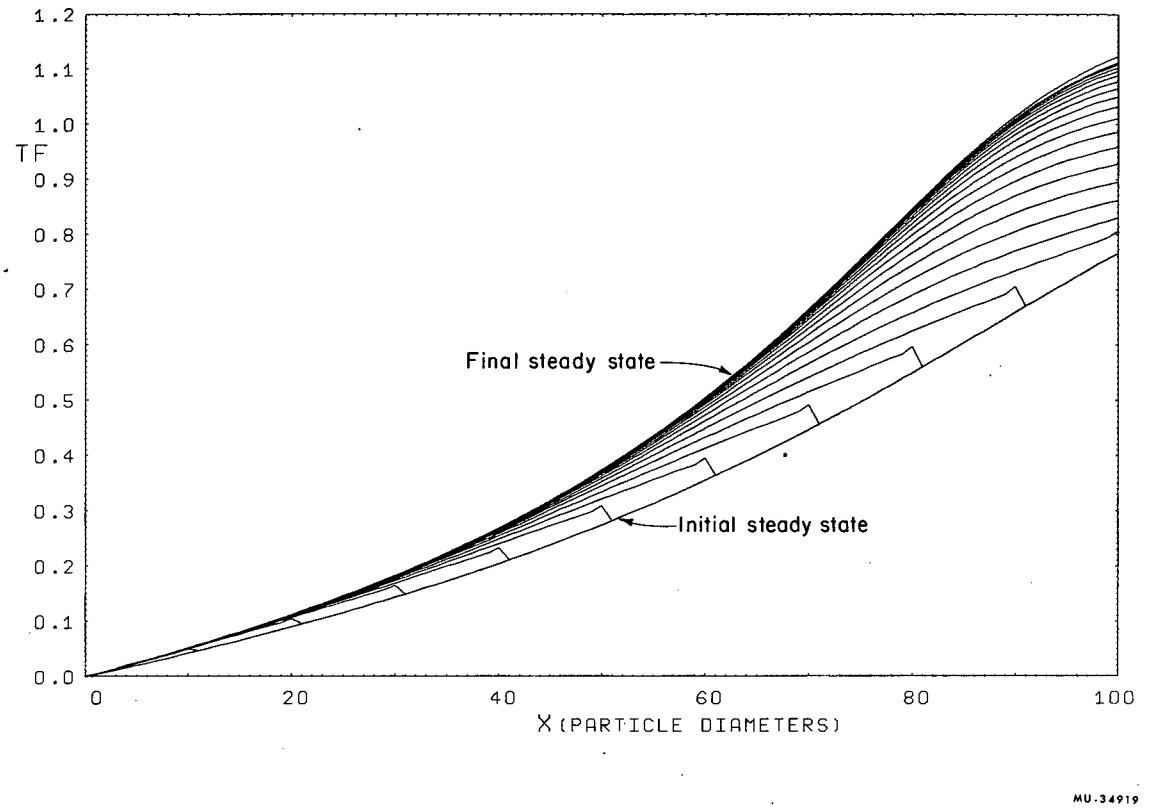

Fig. 34. Transient axial temperature profiles resulting from a concentration step (Run 6, PLGFLO program). Profiles are shown for times t = 10, 20, 30, 40,....

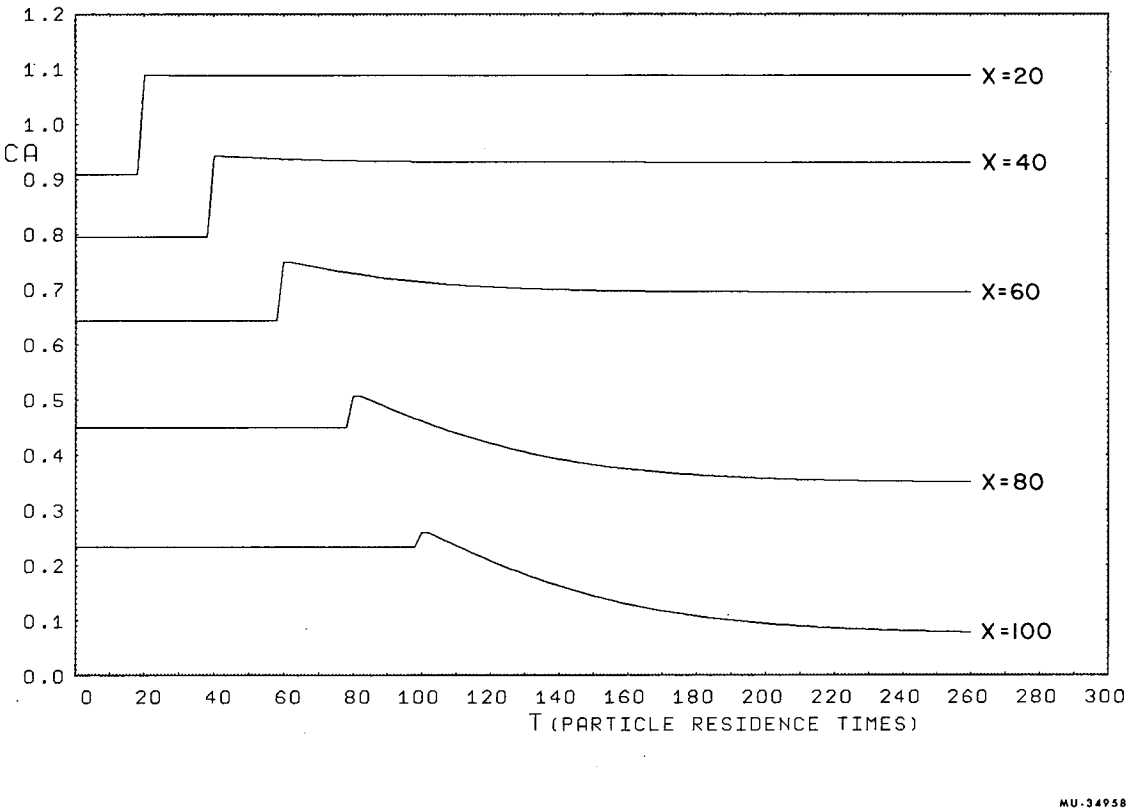

Fig. 35. Response of concentration at selected axial positions to a concentration step (Run 6, PLGFLO program).

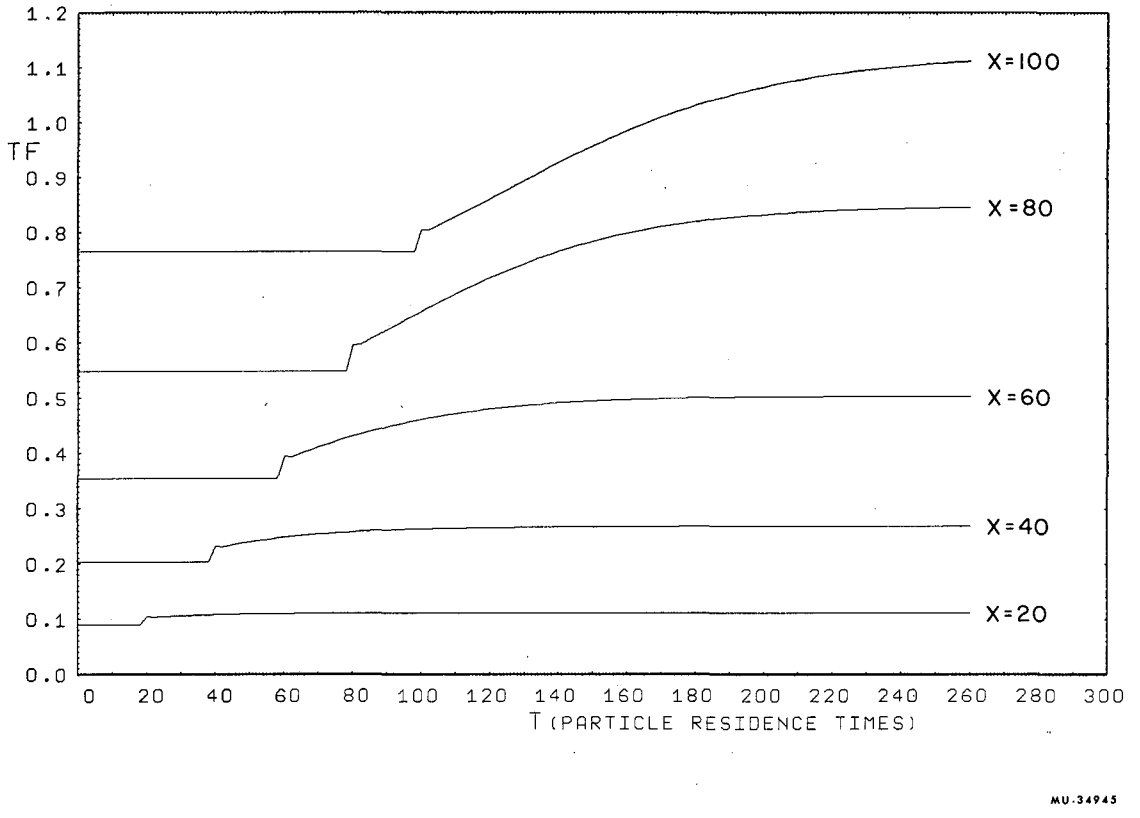

Fig. 36. Response of temperature at selected axial positions to a concentration step (Run 6, PLGFLO program).

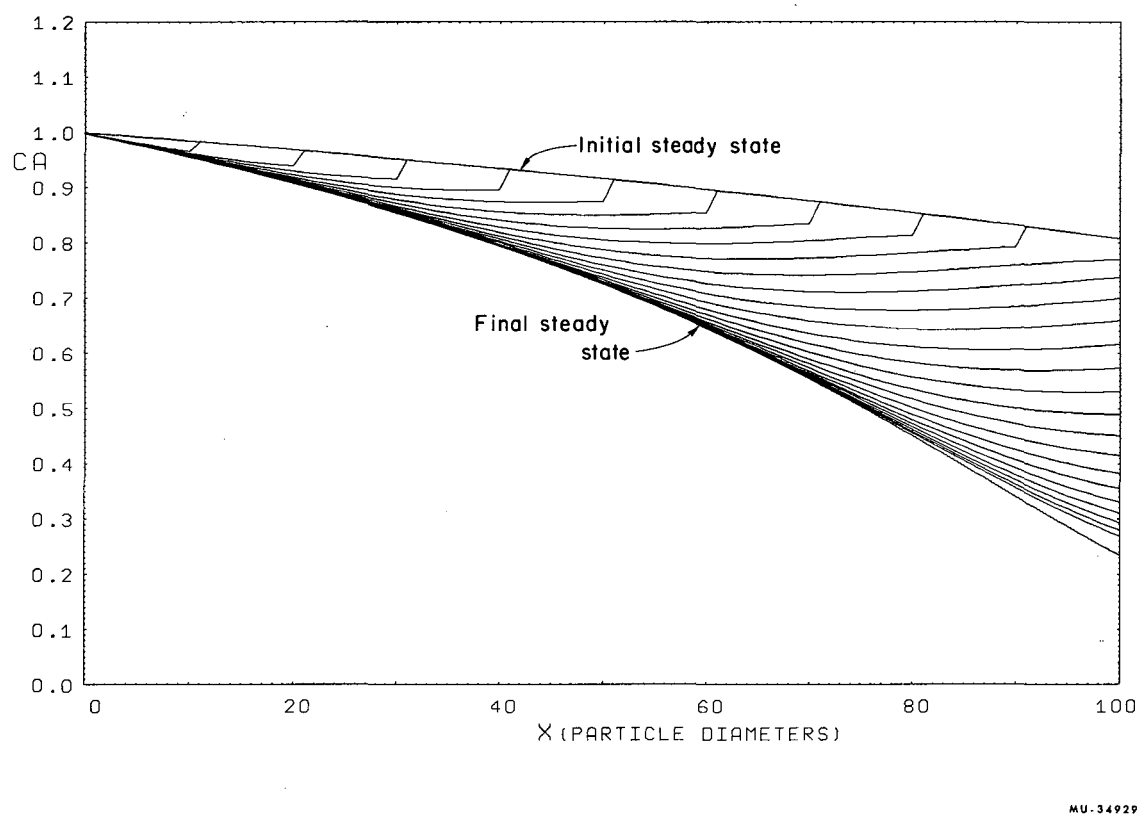

Fig. 37. Transient axial concentration profiles resulting from a temperature step (Run 7, PLGFLO program). Profiles are shown for times t = 10, 20, 30, 40,....

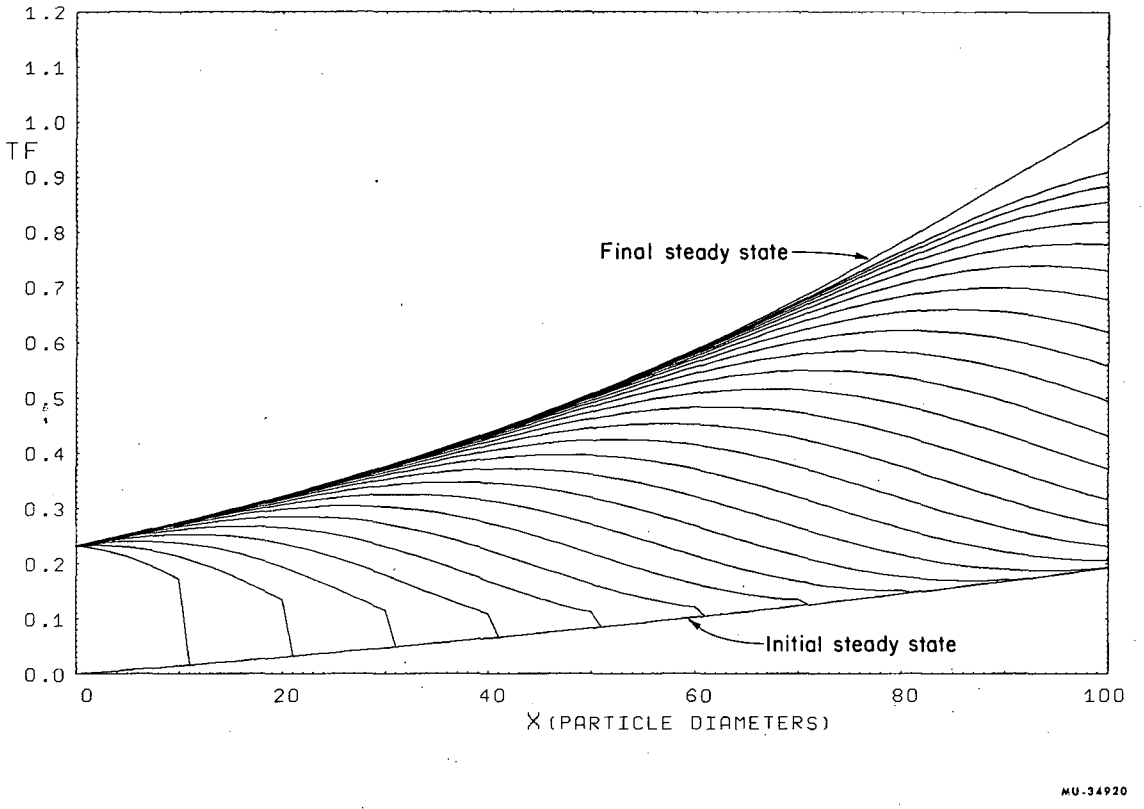

Fig. 38. Transient axial temperature profiles resulting from a temperature step (Run 7, PLGFLO program). Profiles are shown for times t = 10, 20, 30, 40,....

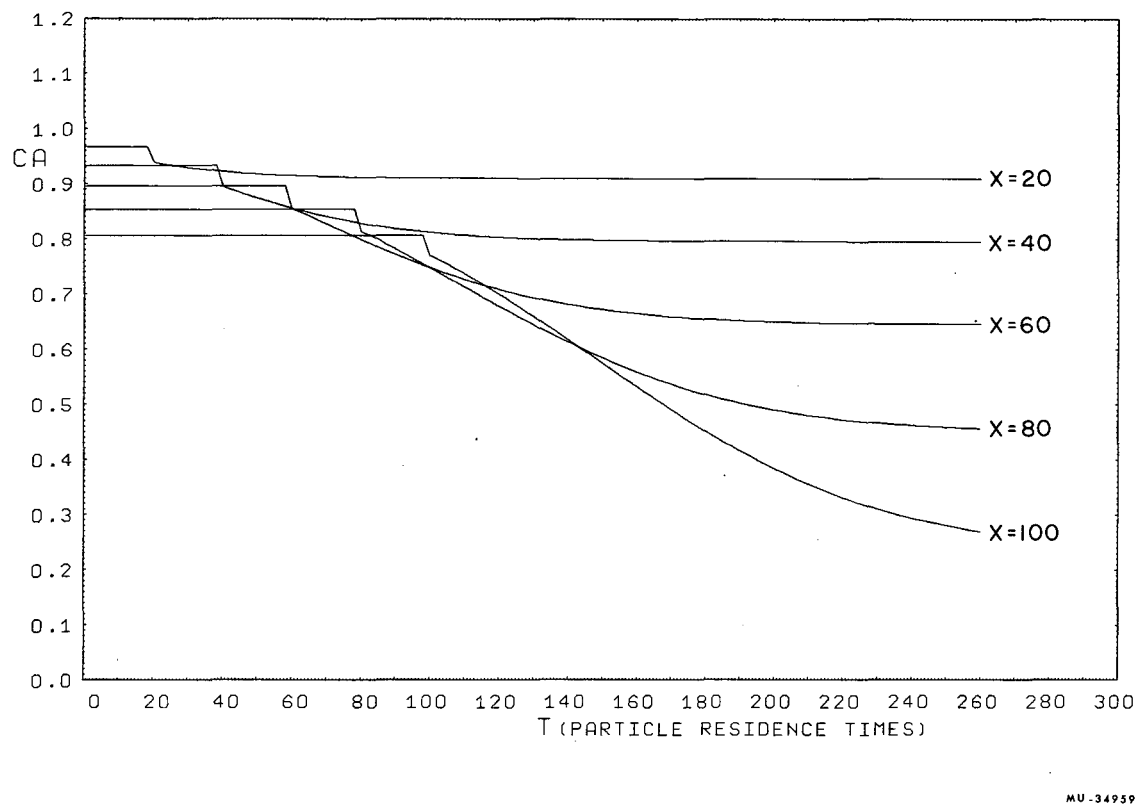

Fig. 39. Response of concentration at selected axial positions to a temperature step (Run 7, PLGFLO program).

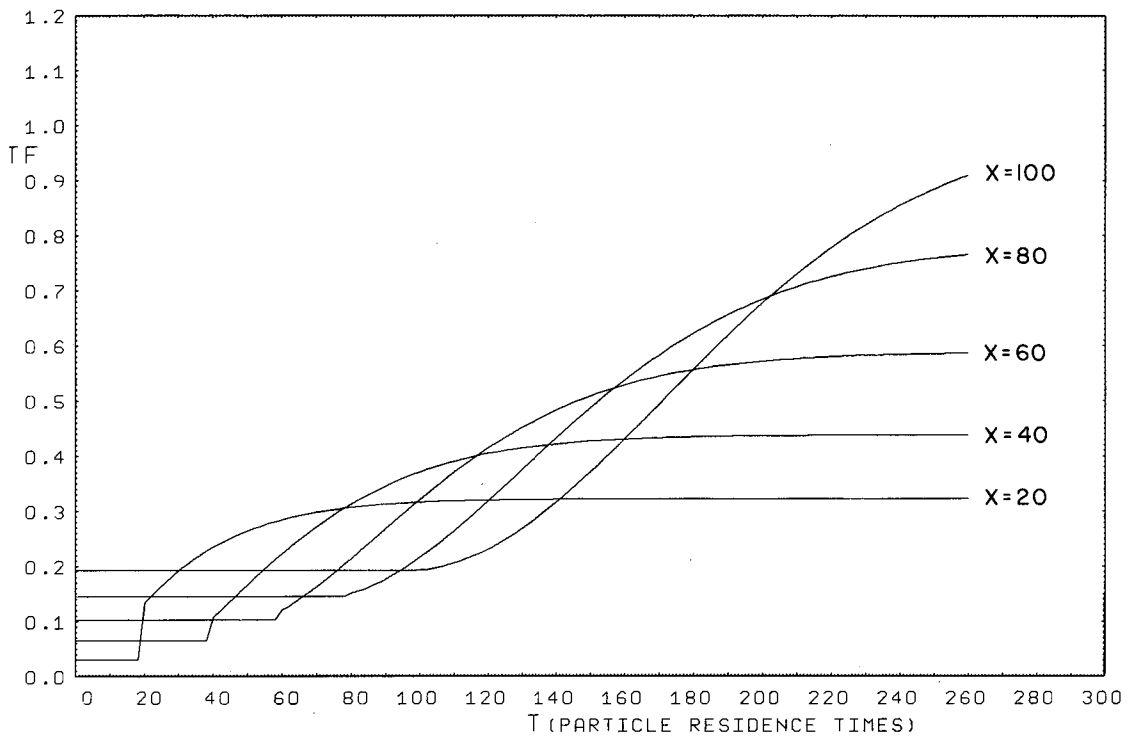

Fig. 40. Response of temperature at selected axial positions to a temperature step (Run 7, PLGFLO program).

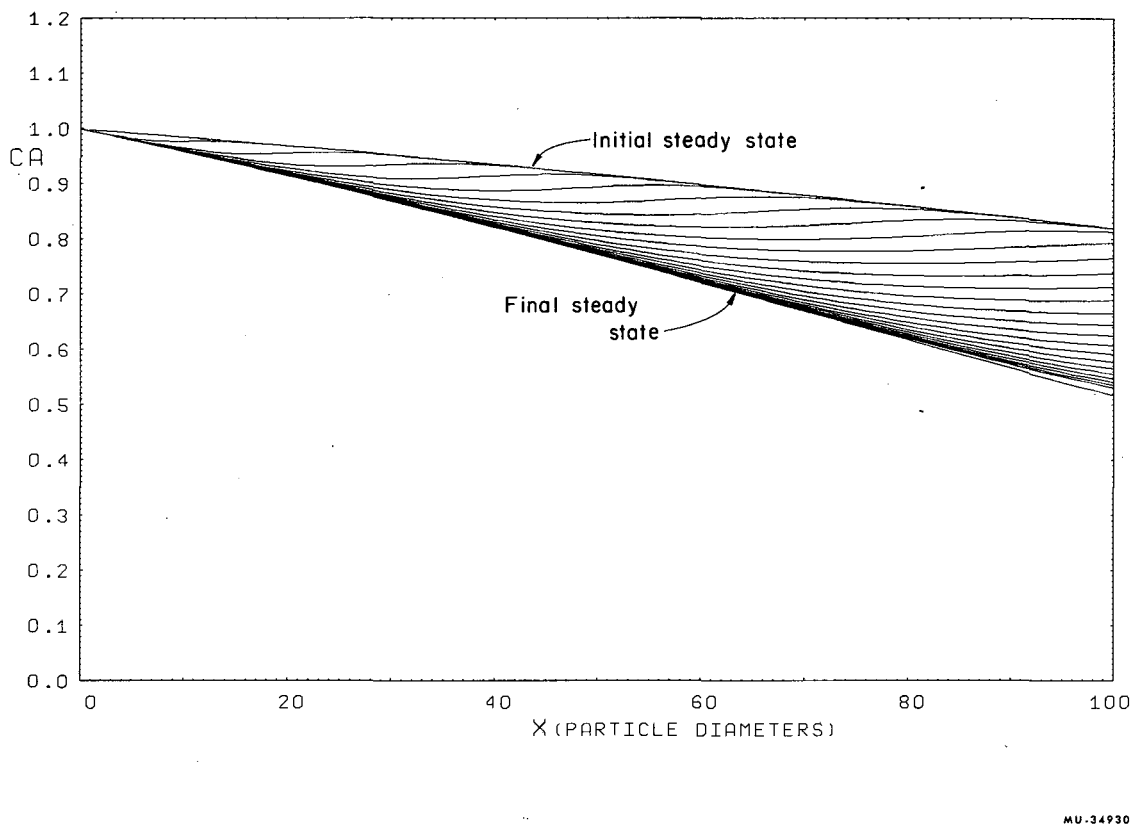

Fig. 41. Transient axial concentration profiles resulting from a temperature step (Run 8, FS2D program). Profiles are shown for times t = 10, 20, 30, 40,....

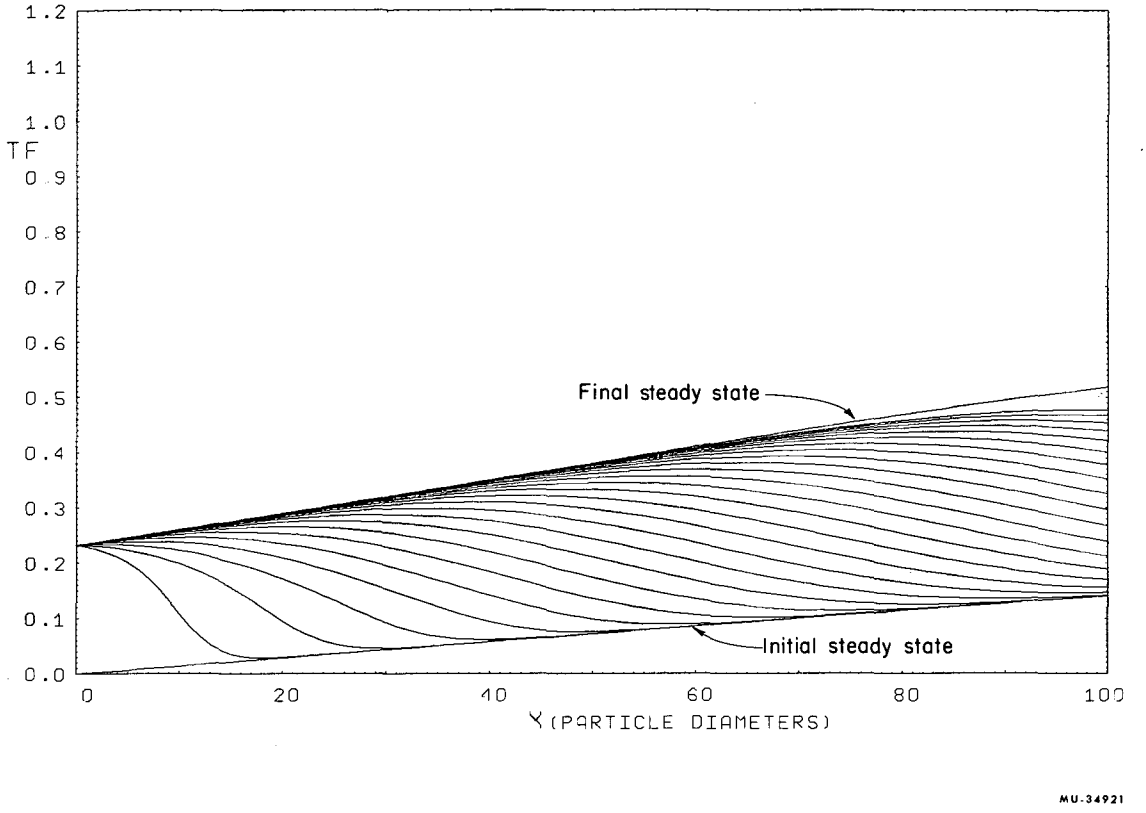

Fig. 42. Transient axial temperature profiles resulting from a temperature step (Run 8, FS2D program). Profiles are shown for times t = 10, 20, 30, 40,....

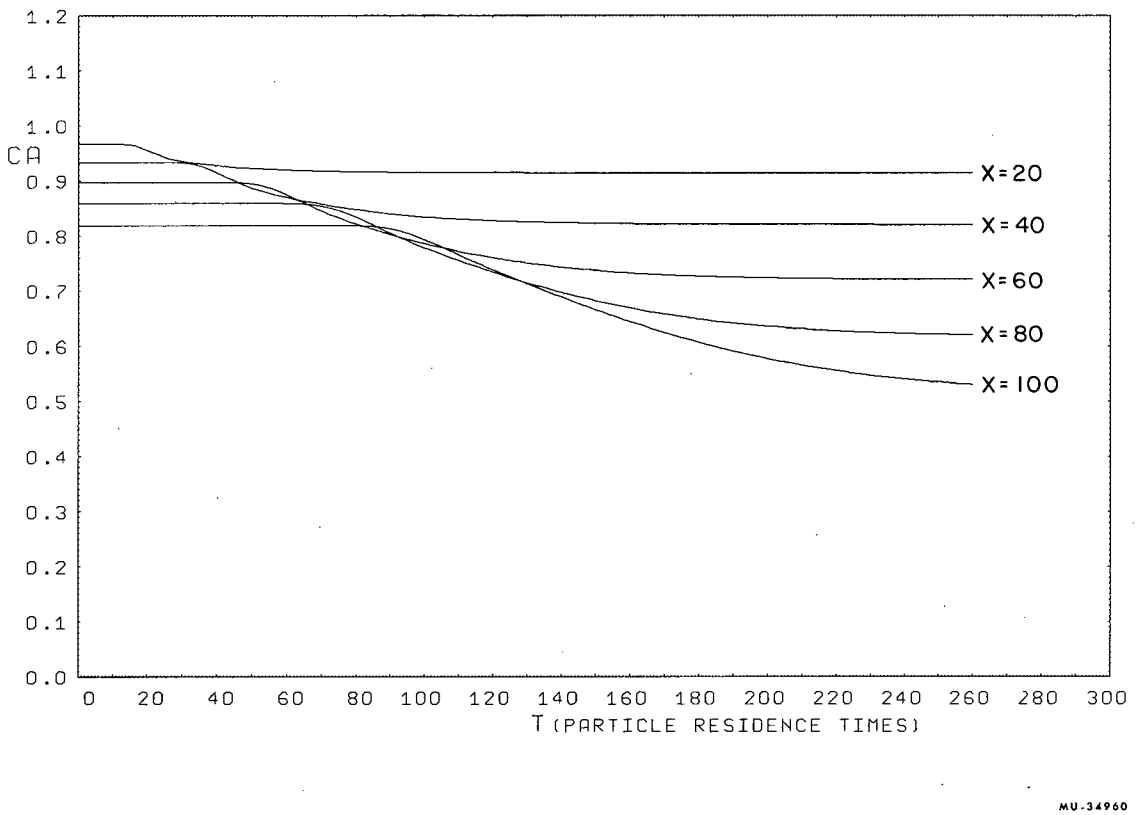

Fig. 43. Response of concentration at selected axial positions to a temperature step (Run 8, FS2D program).

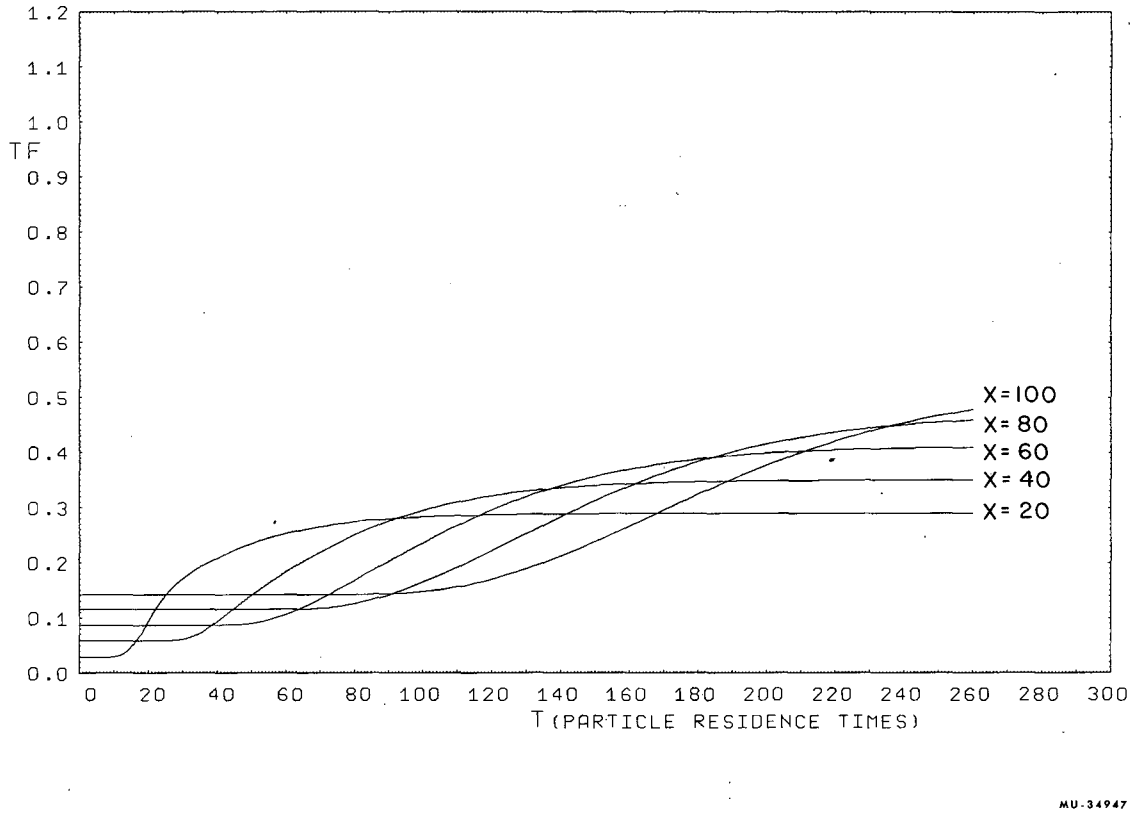

Fig. 44. Response of temperature at selected axial positions to a temperature step (Run 8, FS2D program).

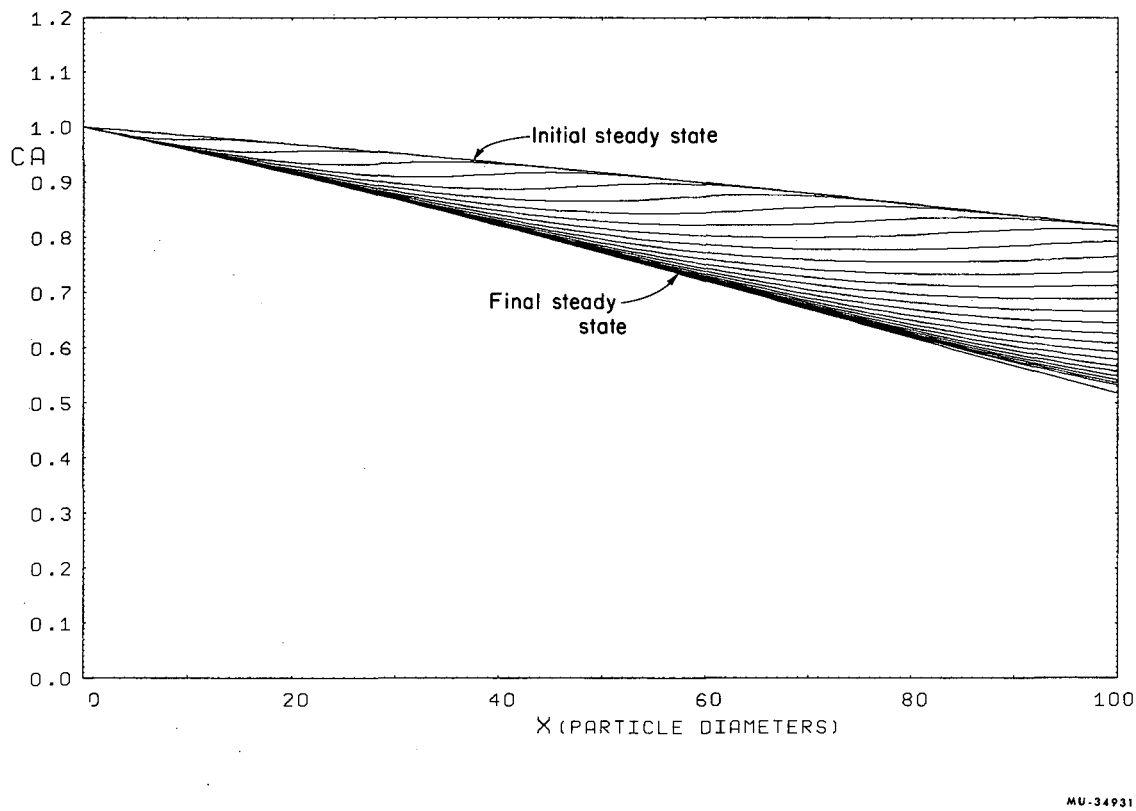

Fig. 45. Transient axial concentration profiles resulting from a temperature step (Run 9, FS1D program). Profiles are shown for times t = 10, 20, 30, 40,....

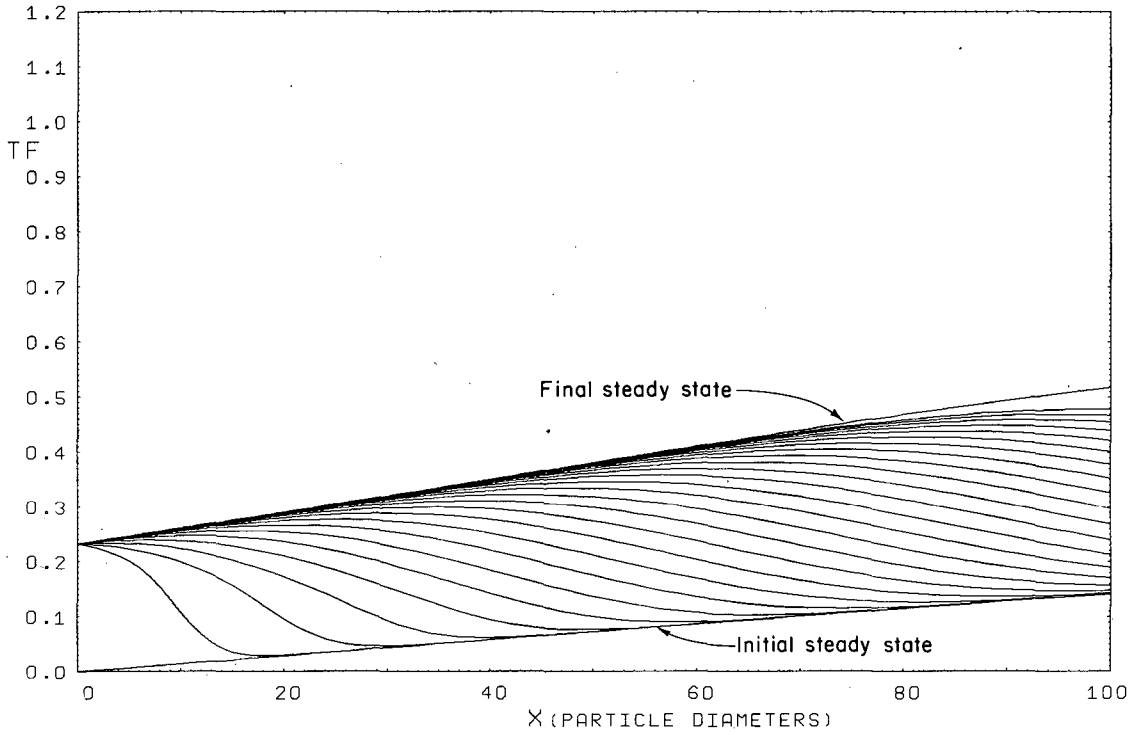

Fig. 46. Transient axial temperature profiles resulting from a temperature step (Run 9, FS1D program). Profiles are shown for times t = 10, 20, 30, 40,....

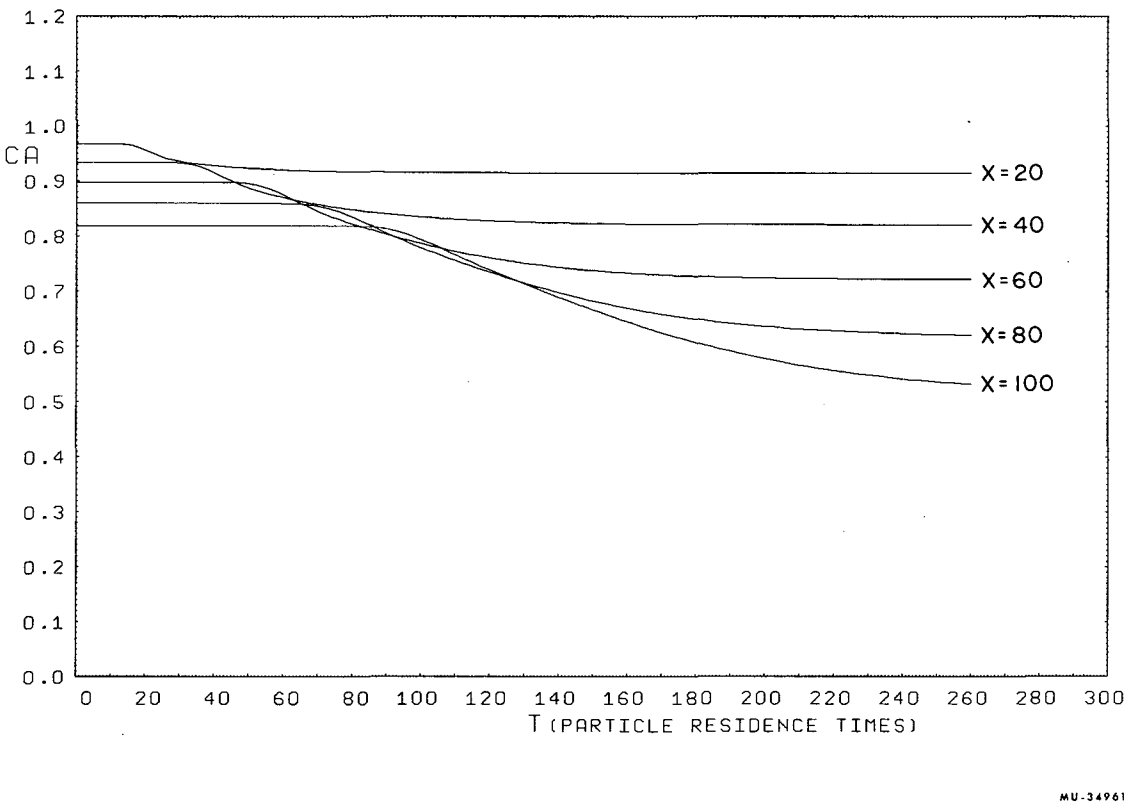

Fig. 47. Response of concentration at selected axial positions to a temperature step (Run 9, FS1D program).

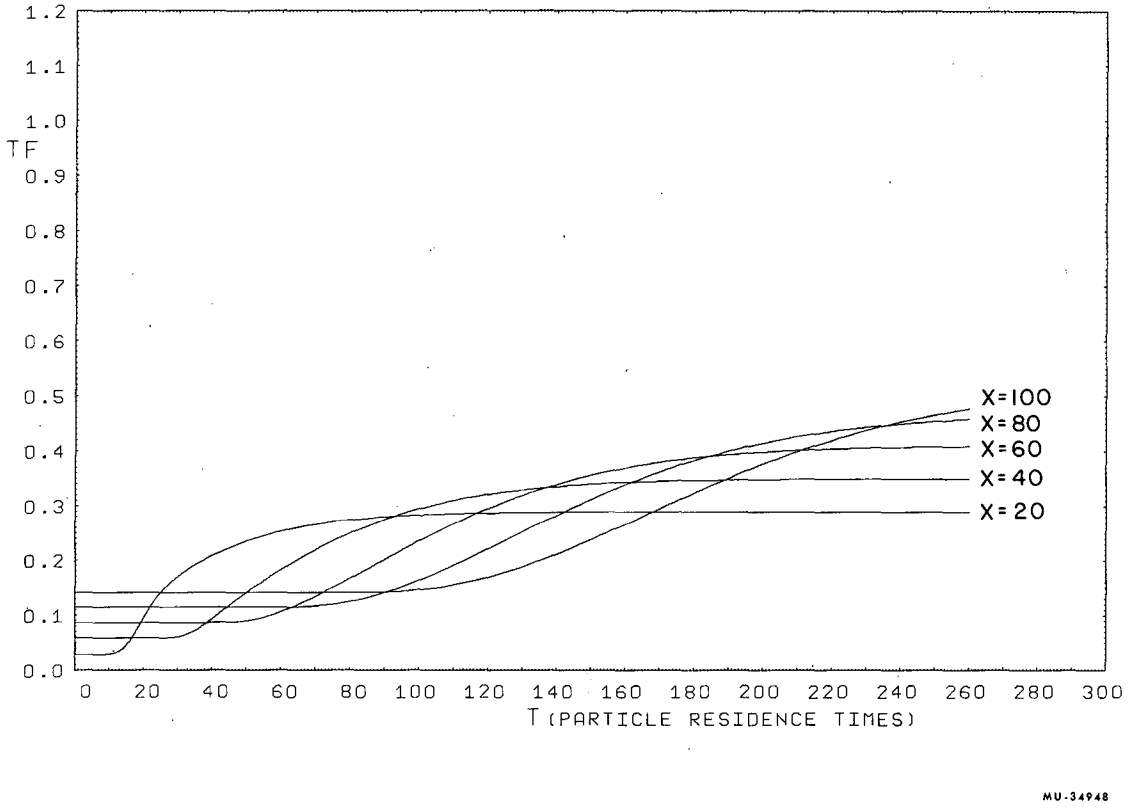

Fig. 48. Response of temperature at selected axial positions to a temperature step (Run 9, FS1D program).

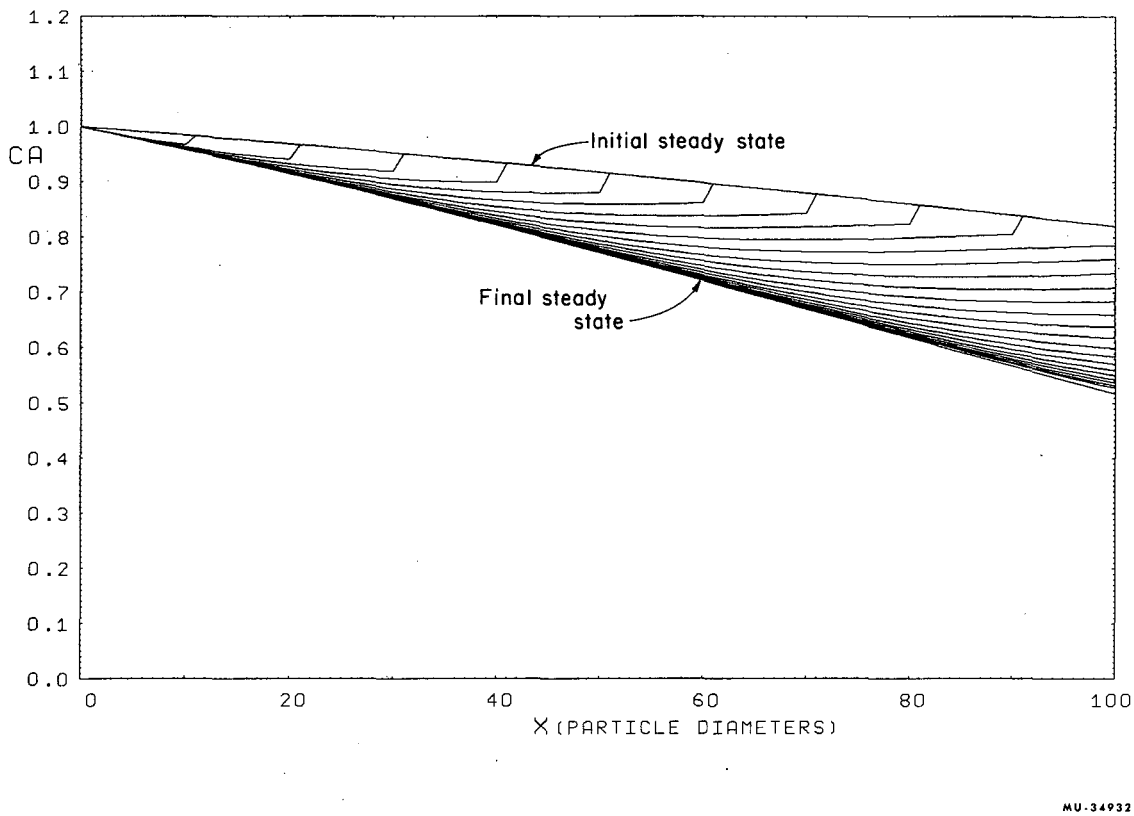

Fig. 49. Transient axial concentration profiles resulting from a temperature step (Run 10, PLGFLO program). Profiles are shown for times t = 10, 20, 30, 40,....

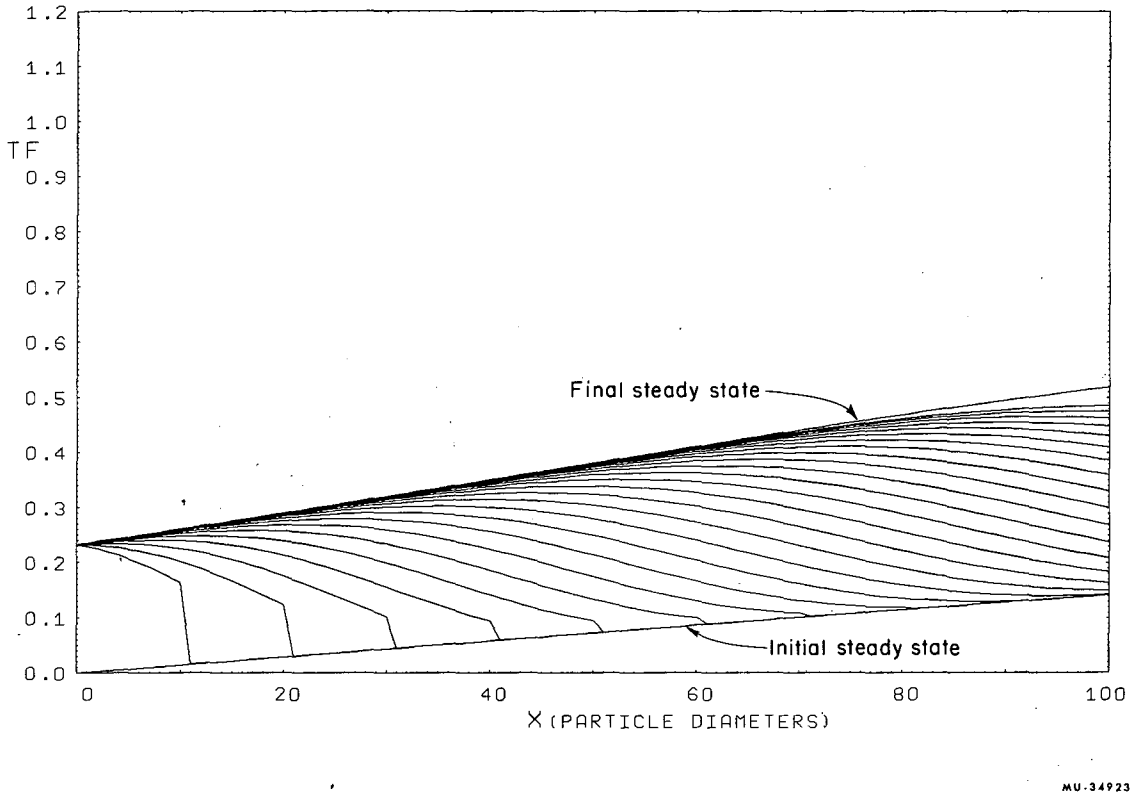

Fig. 50. Transient axial temperature profiles resulting from a temperature step (Run 10, PLGFLO program). Profiles are shown for times t = 10, 20, 30, 40,....

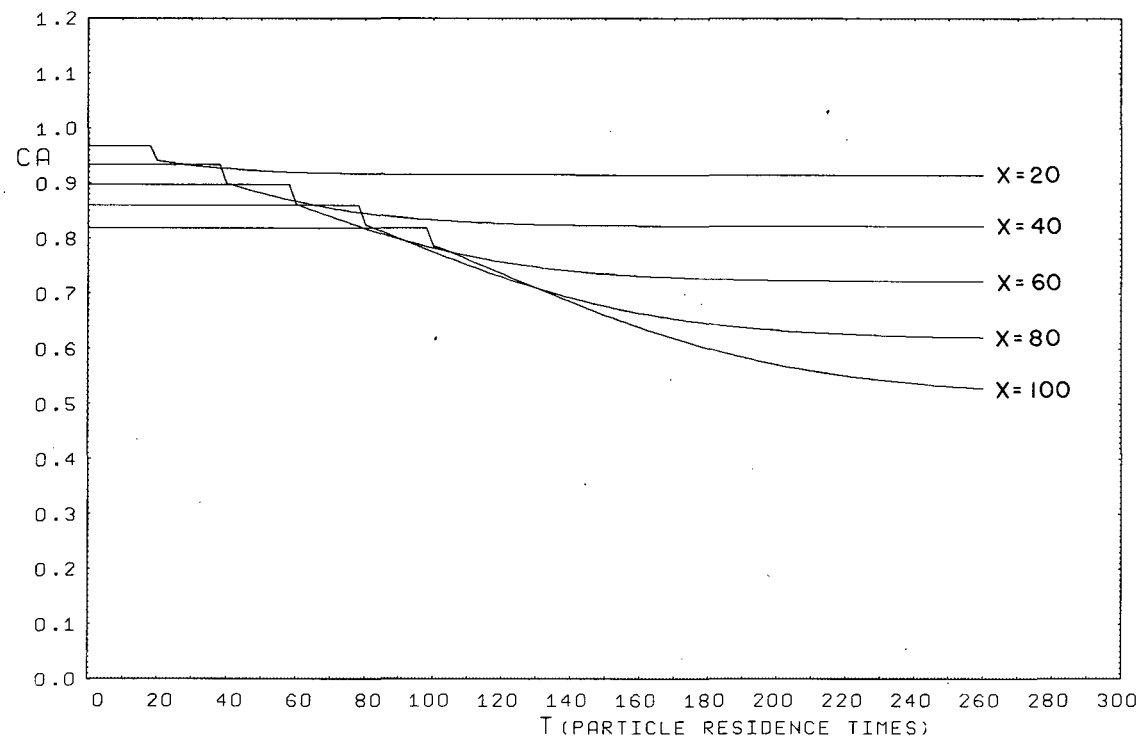

Fig. 51. Response of concentration at selected axial positions to a temperature step (Run 10, PLGFLO program).

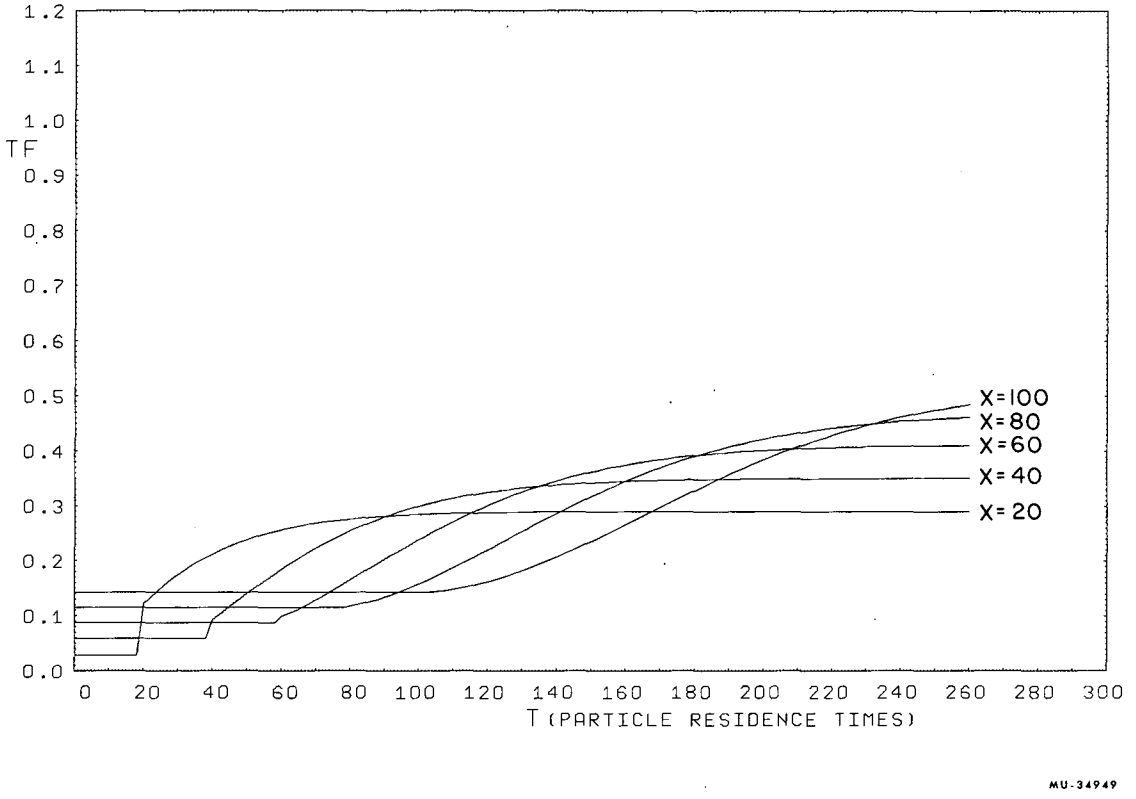

Fig. 52. Response of temperature at selected axial positions. to a temperature step (Run 10, PLGFLO program).

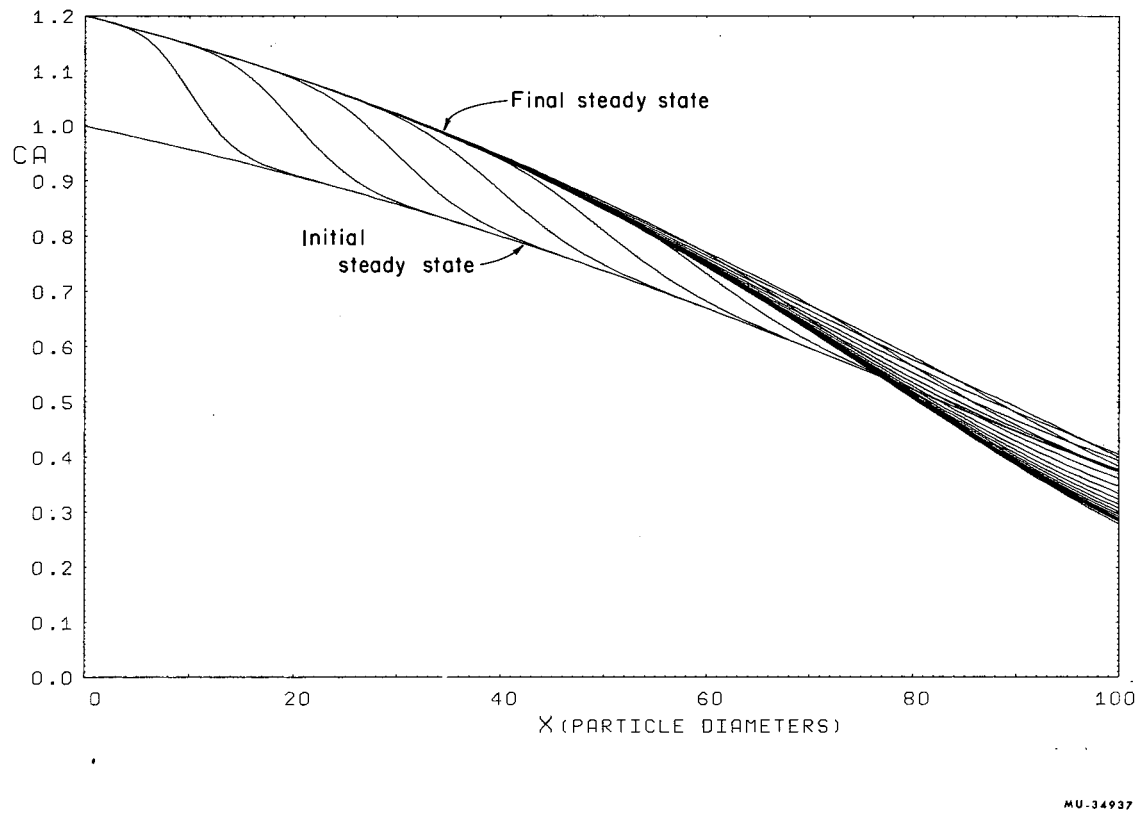

Fig. 53. Transient axial concentration profiles resulting from a concentration step (Run 11, FS2D program). Profiles are shown for times t = 10, 20, 30, 40,....

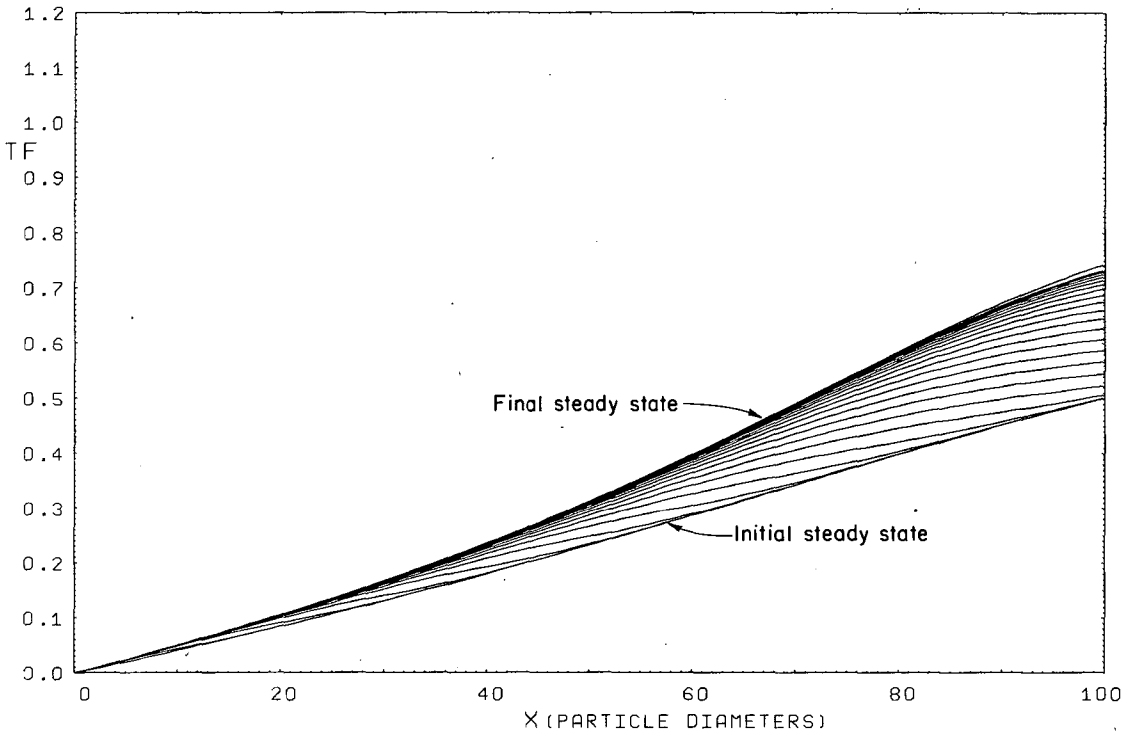

MU-34924

Fig. 54. Transient axial temperature profiles resulting from a concentration step (Run 11, FS2D program). Profiles are shown for times t = 10, 20, 30, 40,....

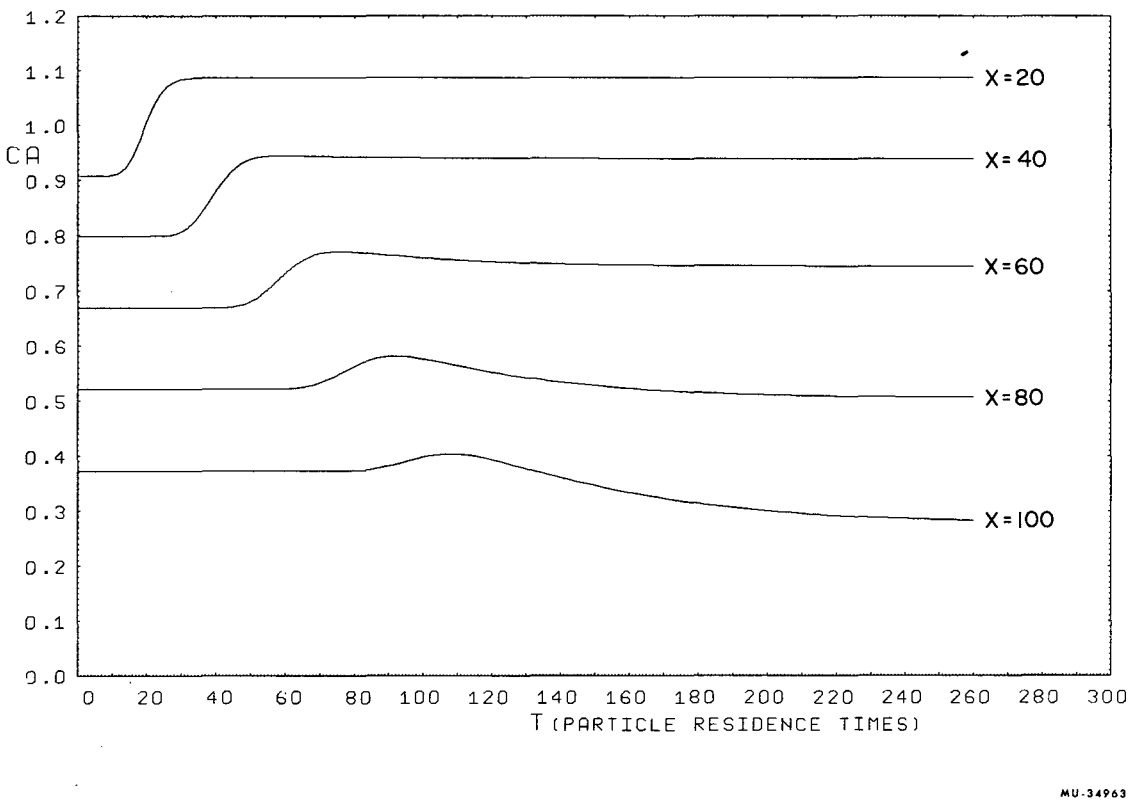

Fig. 55. Response of concentration at selected axial positions to a concentration step (Run 11, FS2D program).

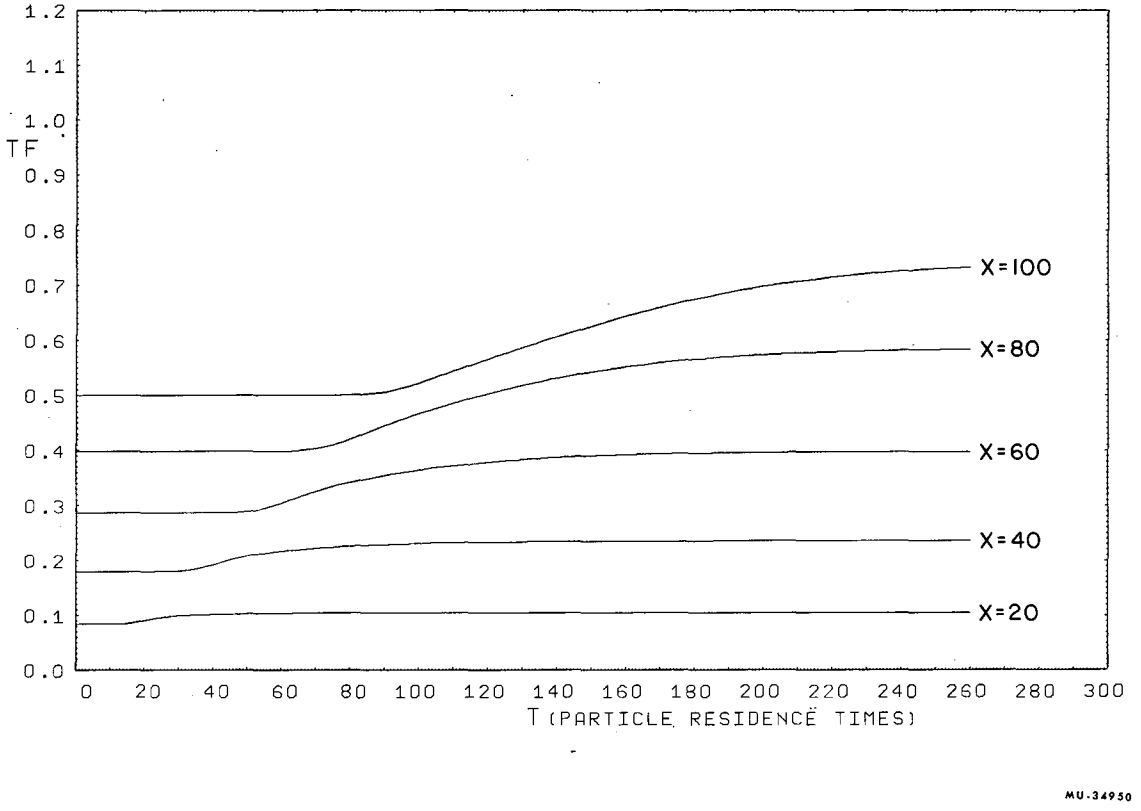

Fig. 56. Response of temperature at selected axial positions to a concentration step (Run 11, FS2D program).

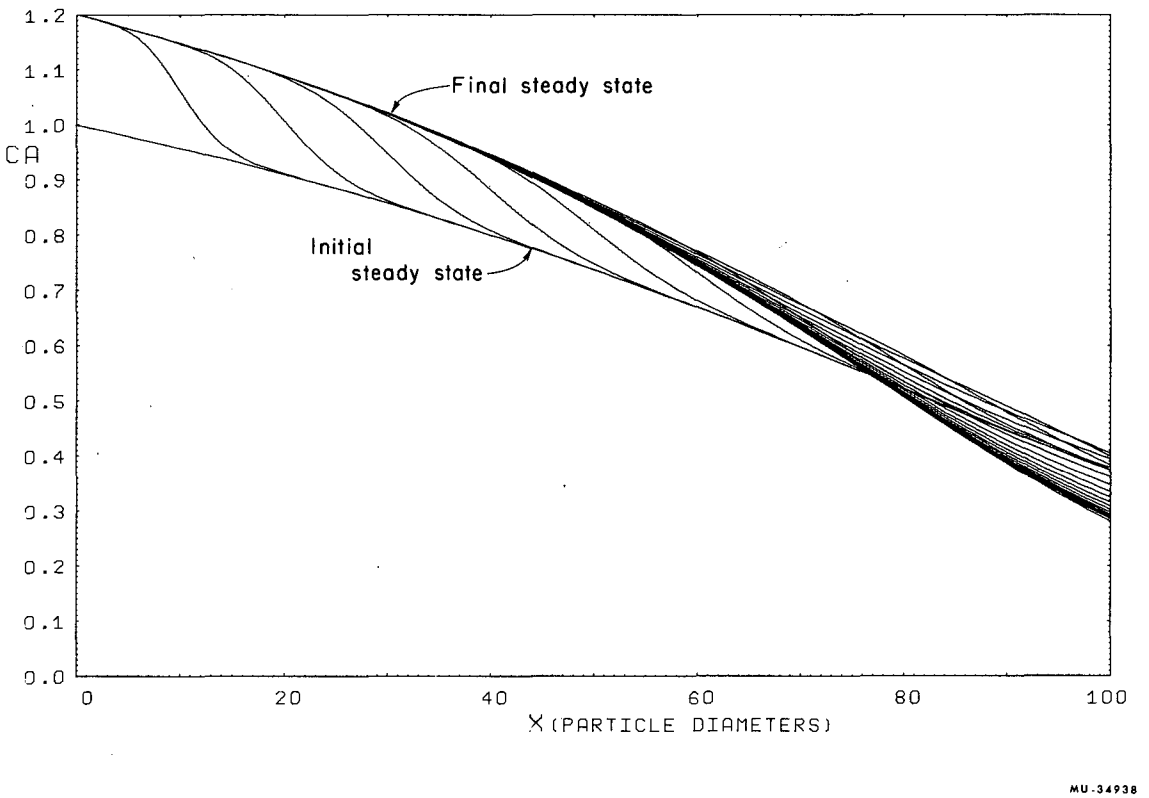

Fig. 57. Transient axial concentration profiles resulting from a concentration step (Run 12, FS1D program). Profiles are shown for times t = 10, 20, 30, 40,....

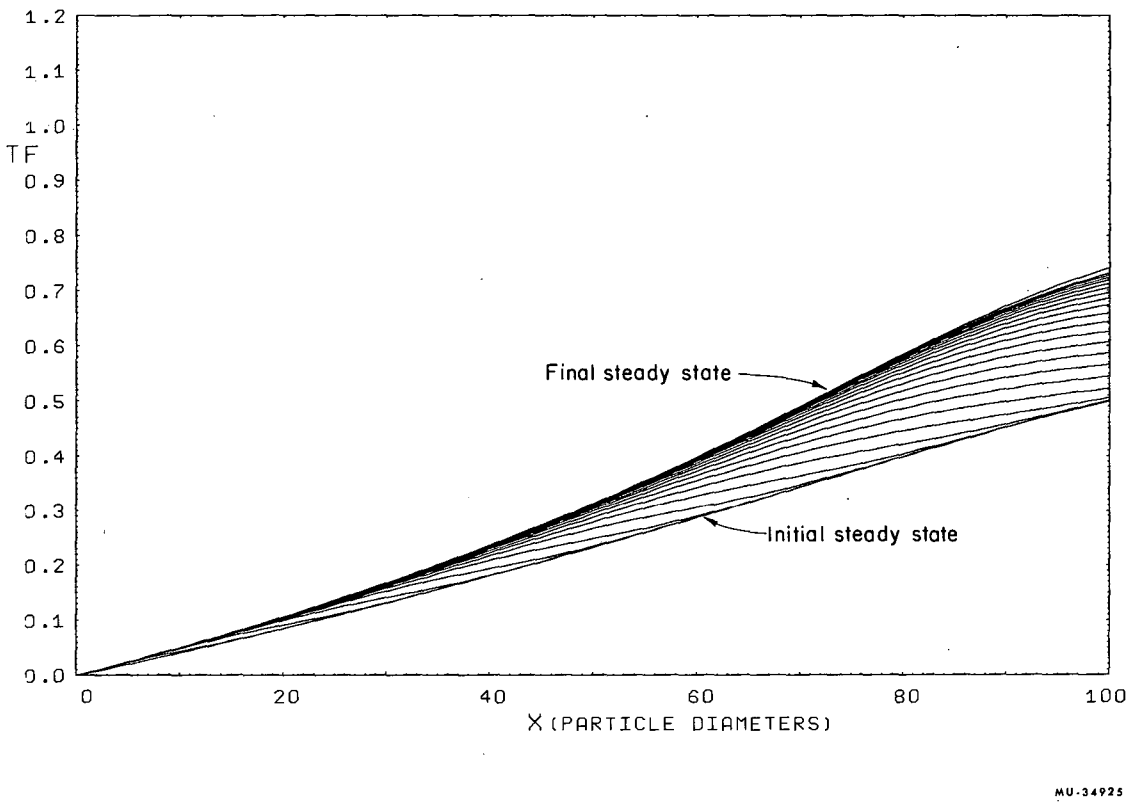

Fig. 58. Transient axial temperature profiles resulting from a concentration step (Run 12, FS1D program). Profiles are shown for times t = 10, 20, 30, 40,....

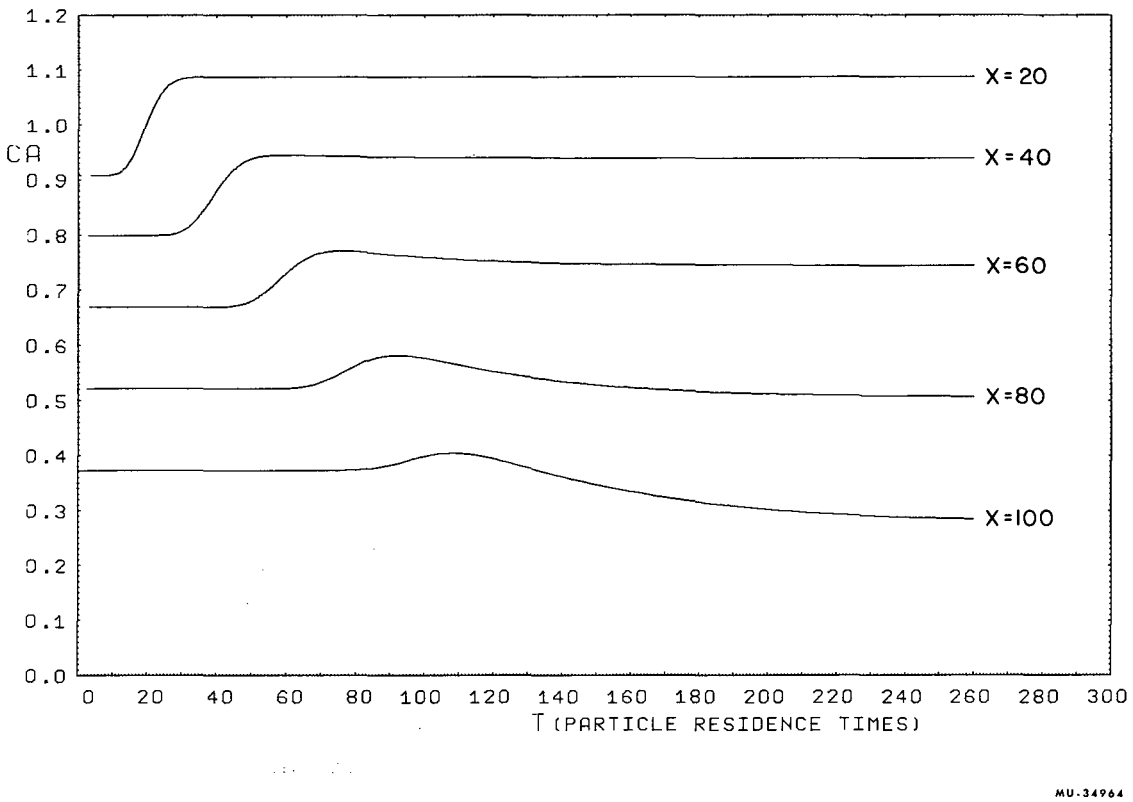

Fig. 59. Response of concentration at selected axial positions to a concentration step (Run 12, FS1D program).

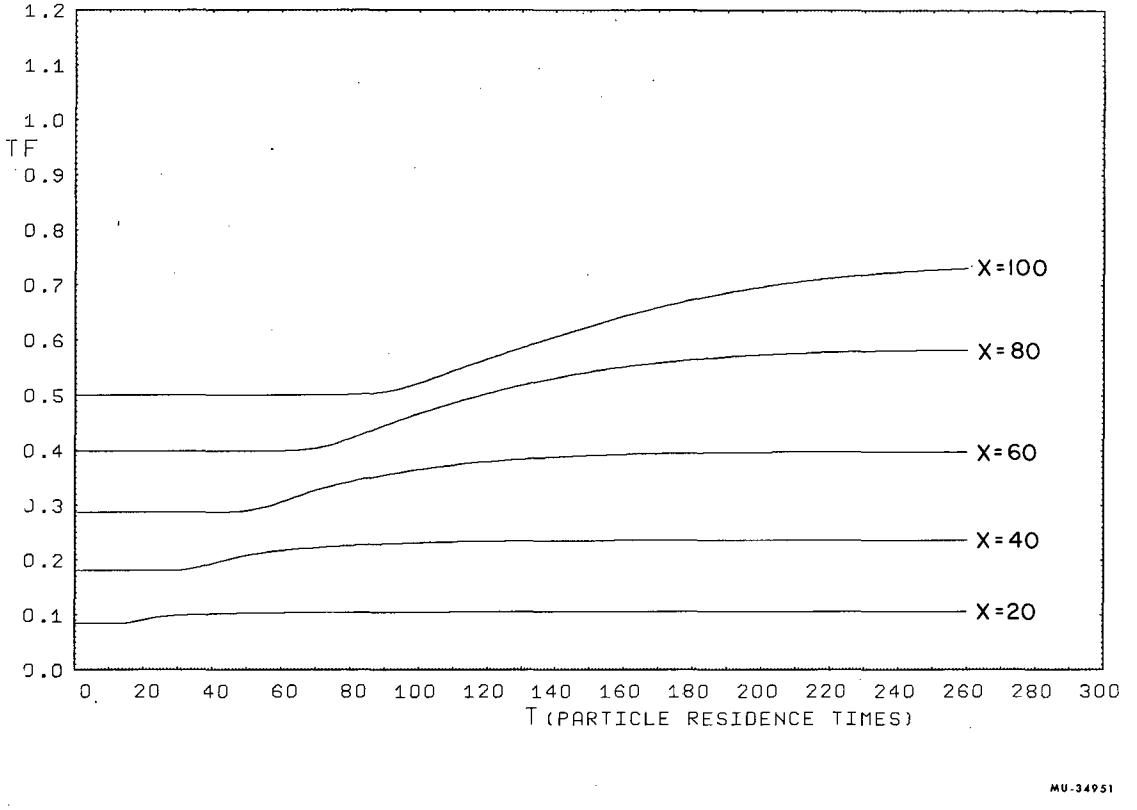

Fig. 60. Response of temperature at selected axial positions to a concentration step (Run 12, FS1D program).

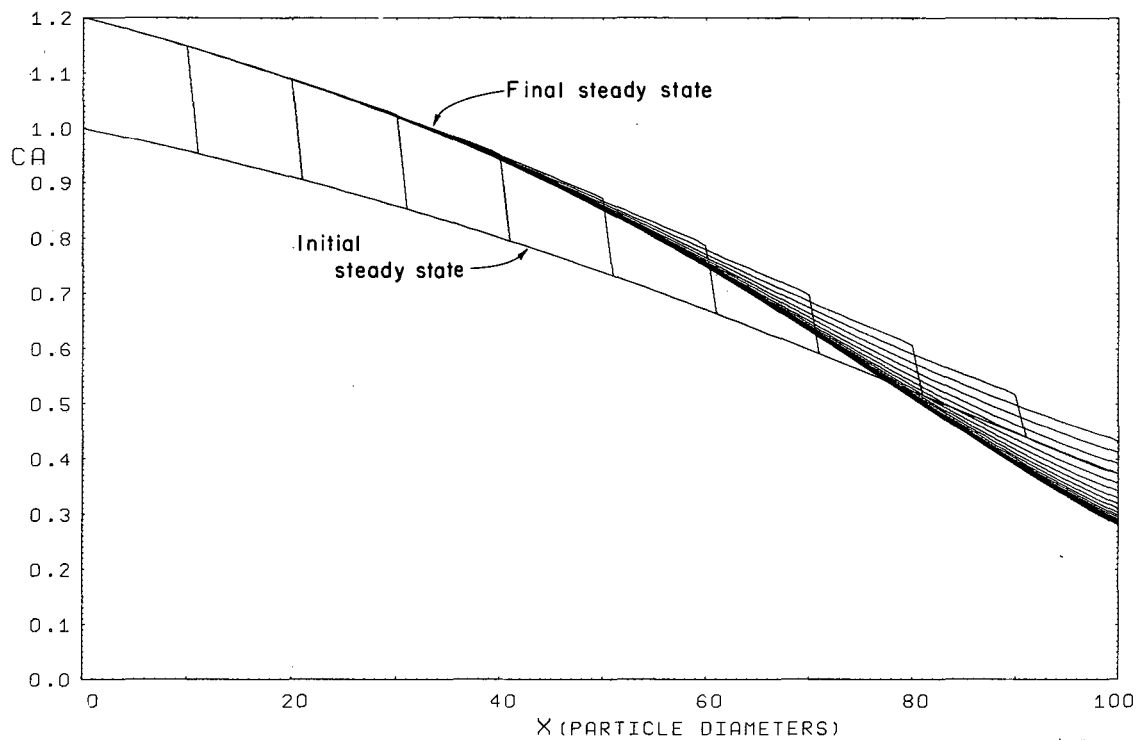

MU-34939

Fig. 61. Transient axial concentration profiles resulting from a concentration step (Run 13, PLGFLO program). Profiles are shown for times t = 10, 20, 30, 40,....

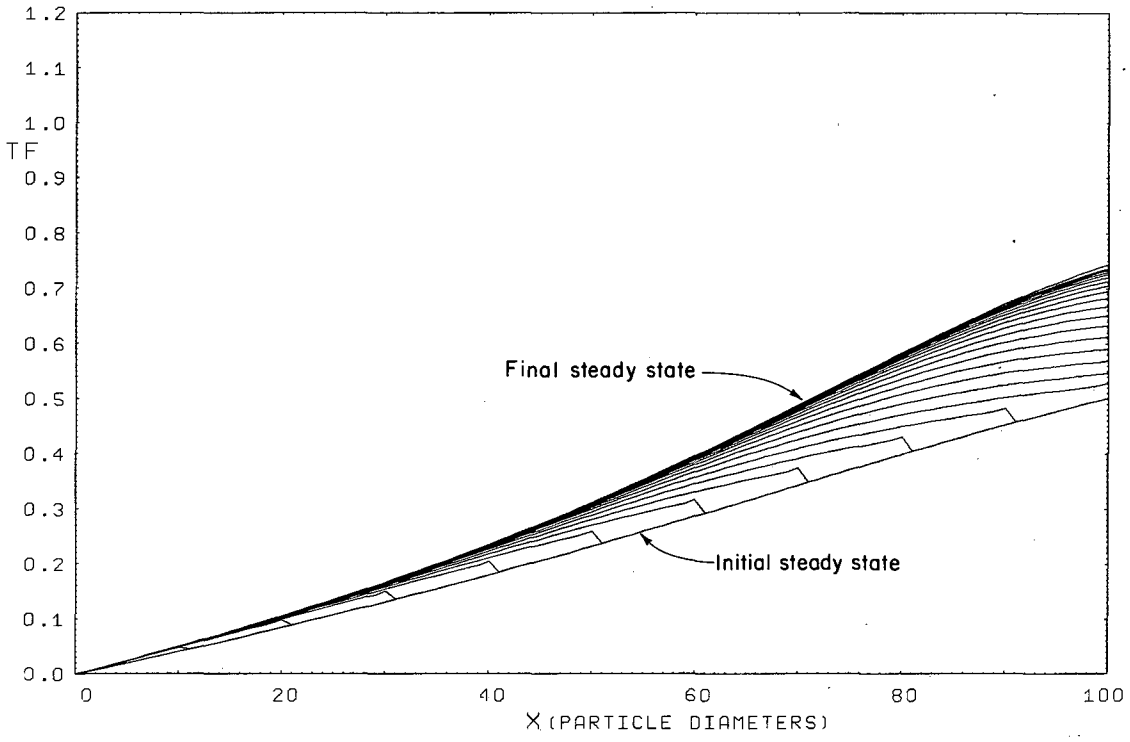

MU-34926

Fig. 62. Transient axial temperature profiles resulting from a concentration step (Run 13, PLGFLO program). Profiles are shown for times t = 10, 20, 30, 40,....

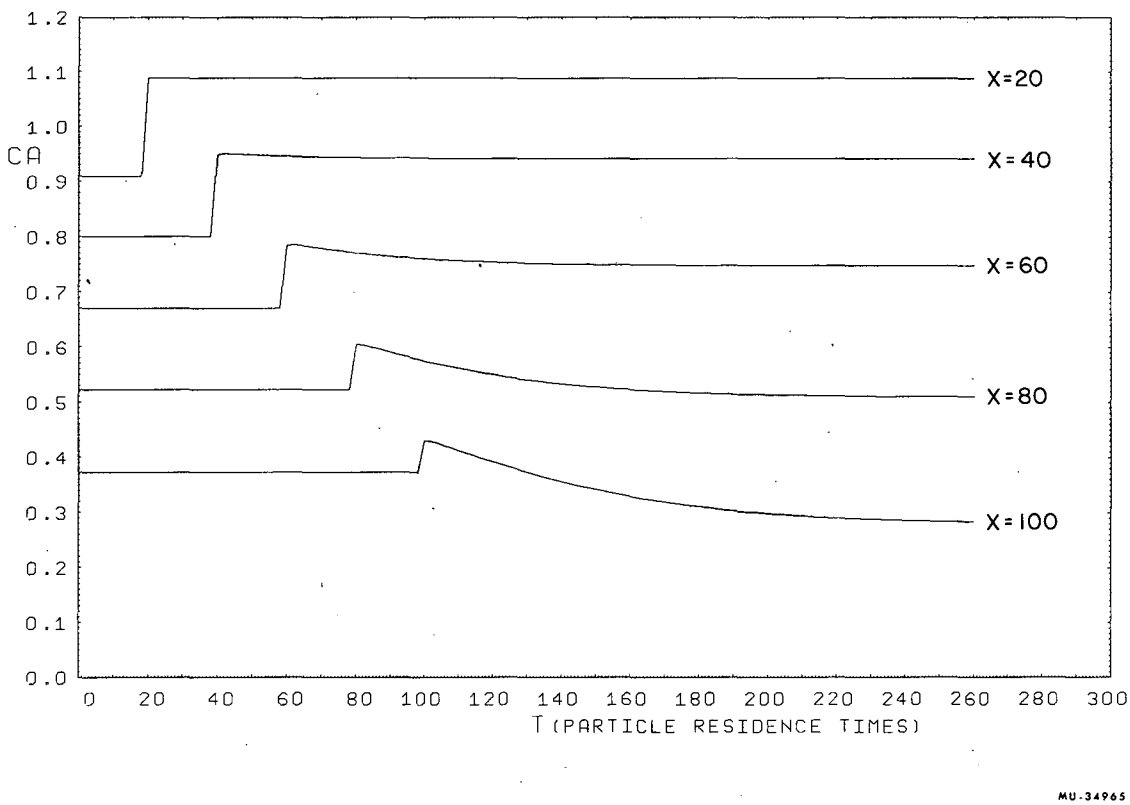

Fig. 63. Response of concentration at selected axial positions to a concentration step (Run 13, PLGFLO program).

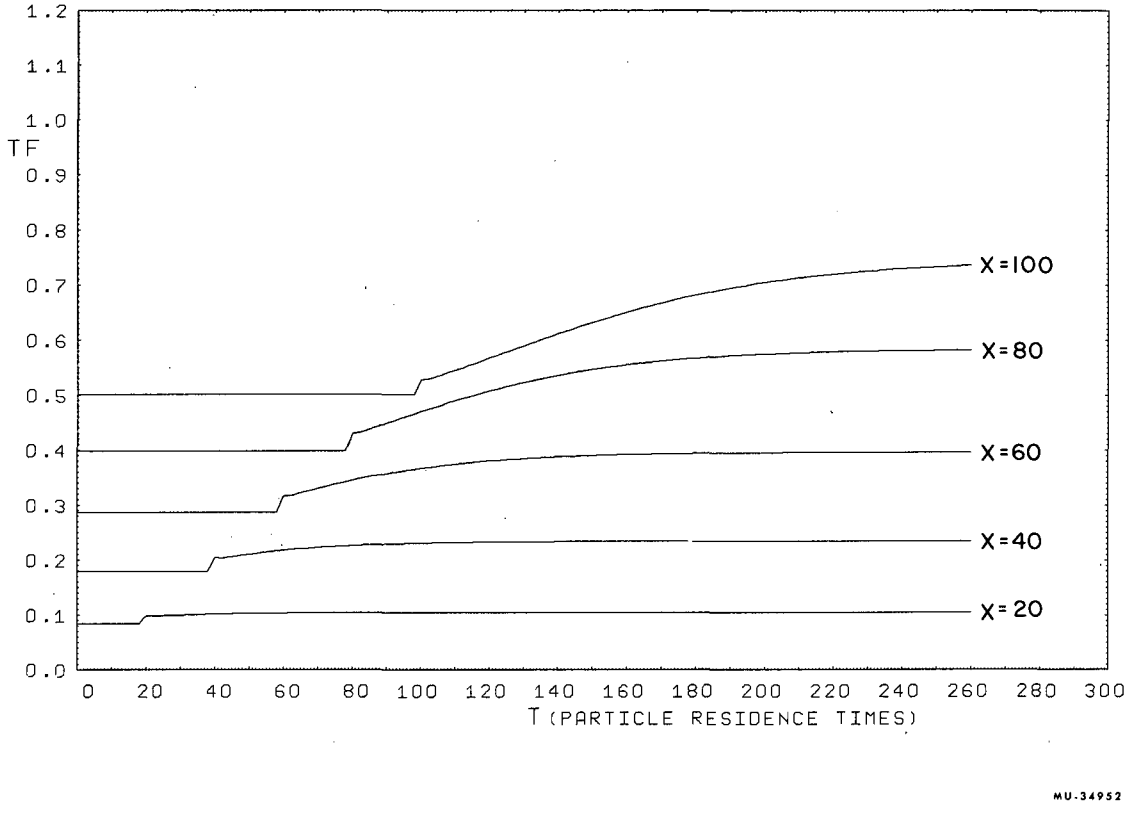

Fig. 64. Response of temperature at selected axial positions to a concentration step (Run 13, PLGFLO program).

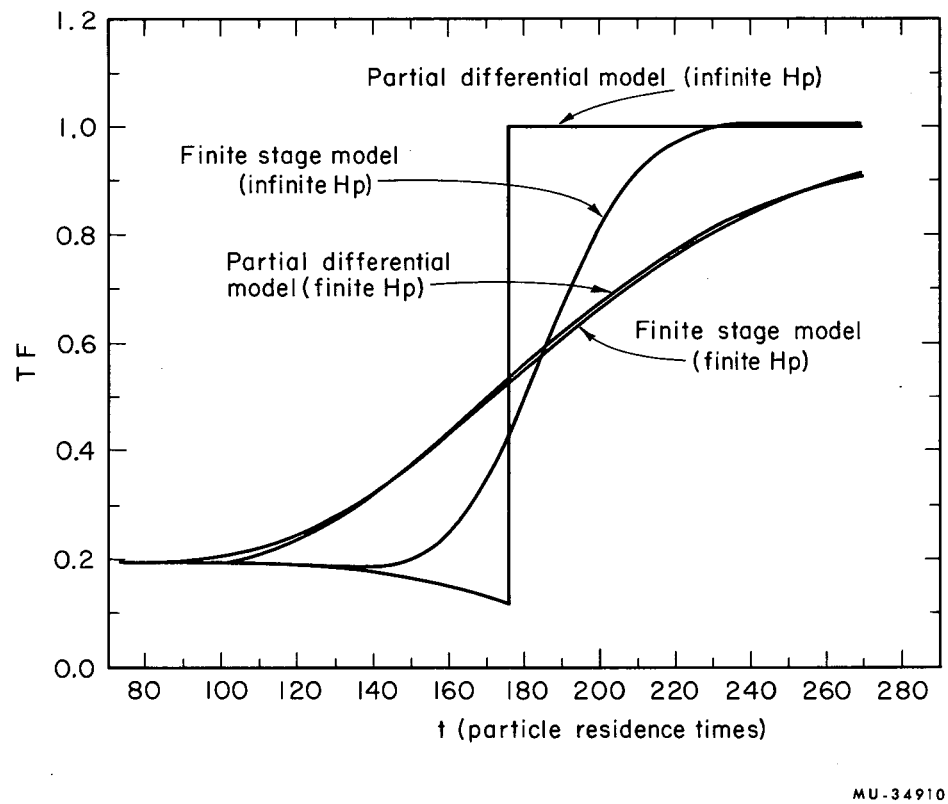

Fig. 65. Response of temperature at exit to a temperature step [Run 0, PLGFLO program (infinite Hp)]. Comparison with Run 7, PLGFLO program (finite Hp); Run 1, FS1D program (infinite Hp); and Run 2, FS1D program (finite Hp).

This plug flow model is described in Chapter 2. It is seen from this description that the heat capacity of the packing determines the velocity at which the temperature disturbance travels through the reactor.

A prototype program of the plug flow model was designed to include the case of infinite Hp. The dynamic behavior of the fluid temperature at the exit (x = 100) as a result of a step in feed temperature, as calculated in this program (Run 0) for the case of infinite Hp, is shown in Figure 65, which also shows the corresponding results from Runs 1, 2, and 7. The parameters for this run are identical to those of Run 1.

An interesting feature of the results of this run, and of the results of run 1, is that the temperature decreases slightly before it increases. The lowest value reached by the temperature in the plug flow model occurs immediately before the temperature wave reaches this position in the reactor. This point, then, lies on one of the characteristic coordinate axes, and this lowest value of the temperature can be calculated by a steady state method, as described in Chapter 2. The temperature in the finite stage model does not reach this lowest value because of the effect of axial dispersion, which is the major difference between the plug flow and the finite stage models.

The temperature decrease can be explained physically to some extent. However, because the plug flow model is a simplified mathematical model, some of its properties are not entirely physically reasonable. For example, it must be accepted that discontinuities in the reactor feed remain discontinuous as they travel through the bed, and that (for the case of infinite Hp) the temperature discontinuity travels at a slower velocity than that of the concentration disturbance and any point in the reactor is at steady state immediately after the passage of the temperature discontinuity.

An increase in temperature causes an increase in the rate of reaction and thus a decrease in the concentration. Thus the steady-state concentration profile reached after an increase in feed temperature is lower than the initial steady-state concentration profile.

This lower final steady-state concentration obtains at any point reached by the temperature discontinuity. Because the speed of this discontinuity is lower than that of the fluid, the fluid carries material of lower concentration into regions in front of (i. e., downstream from) the temperature discontinuity. Thus the concentration at any point in the reactor drops as the temperature discontinuity approaches the point.

However, the fluid does not carry material of higher temperature into regions in front of the temperature discontinuity, because of its complete thermal equilibrium with the packing; it is this mechanism of heat absorption by the packing which causes the temperature discontinuity to travel at a slower speed than that of the fluid. Thus, at any point in the reactor in front of the temperature discontinuity, as the concentration drops, the rate of reaction (proportional to the concentration) drops, and the rate of generation of heat (proportional to the rate of reaction) drops. Thus, the temperature, which is the measure of heat content of the fluid and is originally at the initial steady state, drops in the region in front of the temperature discontinuity. This temperature decrease is small in this case, and is practically negligible in a model which includes axial dispersion, as shown in Figure 65; with systems of different parameters, the decrease may be greater. However, with a finite rate of heat transfer between the particles and the fluid, the effect of this temperature decrease is imperceptible. It is seen that this temperature decrease is a result of the coupling between concentration and temperature; however, it is not a result of the nonlinear nature of the reaction term, because a similar temperature decrease would be seen for the case in which the rate of reaction increases linearly with concentration and with temperature.

Figure 65 shows that a finite rate of heat transfer between the particles and the fluid has a major effect upon the dynamics of an actual packed bed tubular chemical reactor. Because this plug flow model (with infinite Hp) lacks this effect, it cannot be considered an accurate model.

However, for qualitative purposes, the concept of the plug flow reactor with infinite Hp is very useful, because this model exhibits most clearly the effect of the heat capacity of the packing. This model may be considered conceptually as a skeletal model of an actual dynamic packed bed tubular chemical reactor. To this reactor certain other properties may be added for quantitative modelling. The major features of the dynamic behavior of an actual packed tubular reactor can be seen in the behavior of this plug flow model. Thus, a step in the feed (in either concentration or temperature, or both) of an actual packed tubular reactor appears at the exit of the reactor after one residence time. This disturbance affects the temperature in the reactor (either directly or through the coupling term), and the major change in the exit temperature of the reactor appears after approximately β residence times, which is the time at which the temperature discontinuity appears at the exit of the plug flow model (with infinite Hp). Through the coupling of concentration and temperature in the rate of reaction, the concentration in the reactor follows the changing temperature, and simultaneously affects its rate of change.

The Effect of a Finite Rate of Heat Transfer Between the Fluid and the Particles

As Figure 65 shows, and as comparisons of Runs 1 and 2 and Runs 4 and 5 show, a finite rate of heat transfer between the particles and the fluid has the major dispersive effect upon the dynamic behavior of a packed tubular chemical reactor. This heat transfer affects the fluid temperature directly, and the concentration indirectly through the coupling term.

This is the most important effect that can be added to the skeletal model introduced above. The plug flow model with infinite Hp, as presented in Chapter 3, combines these three most important phenomena: the coupling of concentration and temperature, the heat capacity of the packing, and a finite rate of heat transfer between the particles and the fluid.

The dynamic behavior of this plug flow model with finite Hp is seen in the results of computer Runs 6, 7, 10, and 13. With a knowledge of this behavior, and a knowledge of the nature of the model (discussed in Chapter 2), details can be added to the description of the dynamic behavior of an actual packed tubular reactor given in the preceding subsection. Thus, a disturbance in either the feed concentration or the feed temperature produces a disturbance in both the concentration and the temperature at the reactor exit after one residence time. After these disturbances appear at the exit, the exit concentration and the exit temperature monotonically approach their final steady-state values. The rate of approach to the final steady state is determined by the rate of reaction and the rate of heat transfer between the particles and the fluid.

These fluctuations at the exit are themselves discontinuities in the plug flow model (with finite Hp), because of the nature of the plug flow model to propagate discontinuities. Upper bounds of the magnitudes of these fluctuations in an actual packed tubular reactor are those values reached in the plug flow model (with finite Hp). These upper bounds are easily calculated by the quasi-steady state calculation of profiles along the characteristics, as discussed in Chapter 2, in which the particle temperature is taken as its initial steady state value and is used as a parameter in the integration of the steady-state mass balance and fluid heat valance equations. These fluctuations in an actual packed tubular reactor do not reach the bounds calculated in this manner because of the effect of axial dispersion.

Although the discontinuities in the plug flow reactor (with finite Hp) are not negligible, they are generally small, usually of the same order of magnitude, or less, of the discontinuity introduced at the inlet. Except for these small discontinuities, this plug flow reactor, with finite Hp, should in most cases be quite adequate for modelling a dynamic packed chemical reactor.

The Effect of Axial Mixing

Comparison of the results of the appropriate runs (see Table 6.2) shows that turbulent axial mixing also has a dispersive effect upon the reactor dynamics, but this effect is much smaller than that of a finite rate of heat transfer between the particles and the fluid.

With the addition of this effect to the developing model (i. e., the skeletal model introduced previously, with the addition of a finite rate of heat transfer between the particles and the fluid), more detail can be added to the previous descriptions of the dynamics of an actual packed tubular reactor. Because of axial mixing, the initial disturbances, which appear at the exit of the reactor at approximately one residence time, are continuous. Further, these disturbances do not reach the upper bounds predicted by the plug flow model (with finite Hp), because of axial mixing. Finally, the disturbances begin to appear (i. e., the initial steady state is left) slightly before one residence time; that is, the initial part of the disturbance travels slightly faster than the average fluid velocity.

The effect of axial mixing is inherent in the one-dimensional finite stage model and is the major feature which distinguishes this model from the plug flow model (for both models, Hp is finite). Both of these models are simple and yet accurate, and either can be used satisfactorily in most cases to simulate the dynamics of an actual packed tubular reactor. The one-dimensional finite stage model has the additional advantage of representing the small effect of axial mixing.

The Effects of Heat Loss at the Wall and of Radial Mixing

In the one-dimensional models, it is assumed that temperatures and concentrations in an actual reactor can be adequately represented by radially averaged values. The resistance of the packed bed to radial transport of heat, which partially determines the rate of heat loss at the wall, is accounted for somewhat artificially in an overall

heat transfer coefficient. In the one-dimensional models of this study, there is no accounting for bed resistance to radial transport of material; however, because no material is lost at the wall, this detail should not be important.

The only difference between the one-dimensional finite stage model and the two-dimensional finite stage model is that the two-dimensional model accounts for bed resistance to radial flow, or incomplete radial mixing, in a more physically realistic manner.

However, comparison of the results of the appropriate runs (Runs 11 and 12, for example) shows that the dynamic behavior of the two models are practically indistinguishable. This is expected because Hw_2 (the wall heat transfer coefficient) and Hw_1 (the overall heat transfer coefficient) are so close together, indicating that the major resistance to heat transfer is at the wall. The printed output of the variables at each stage in Run 11 indicates that the greatest difference radially between the fluid temperature on the reactor axis and the fluid temperature at the wall was less than 6°C.

But even with this heat transfer coefficient, the steady-state temperature rises were depressed to 60% of the temperature rises at the same axial positions in the adiabatic case. This decrease in temperature is not a measure of the heat loss at the wall in the non-adiabatic case, because a lowering of temperature also lowers the rate of heat generation in the reaction.

With a higher heat transfer coefficient, the bed resistance is more important. However, a higher heat transfer coefficient causes the fluid temperature to approach the wall temperature more closely, in which case the radial gradients are still small (less than 6°C for an infinite wall heat transfer coefficient) and their effect upon the dynamics is still negligible.

The bed resistance to radial heat transport would become more important if the ratio of the reactor diameter to the particle diameter were larger. However, the one-dimensional models would probably still adequately simulate the dynamics of such reactors.

Thus, the effect of incomplete radial mixing upon the dynamics of reactors with liquid reactants is negligible in most cases, and the advantages of the two-dimensional finite stage model in accounting for this effect are much less important than the disadvantages in the practical use of this complex model.

DISCUSSION

In summary, the three phenomena that dominate the dynamic behavior of a packed tubular reactor are: the heat capacity of the packing, which causes the major temperature disturbance to travel through the reactor slower than the fluid velocity; the finite rate of heat transfer between the packing and the fluid, which greatly disperses the temperature disturbance; and the coupling of heat and mass in the reaction, through which concentration disturbances cause temperature disturbances and temperature disturbances cause concentration disturbances. Only the last of these phenomena affects the steady state of the reactor (assuming that multiple steady states do not exist at the operating conditions used).

Axial mixing further disperses the concentration and temperature disturbances and causes part of the disturbances to travel faster than the fluid velocity. These effects are small, but not necessarily negligible.

The effects of the three dominating phenomena are included in the plug flow model (with finite Hp), and the effect of these three phenomena and of axial mixing are included in the one-dimensional finite stage model. Either of these models should suffice in most cases for the simulation of an actual packed tubular reactor with liquid reactants, and yet both are simple and require little computing time.

The effects of incomplete radial mixing appear to be negligible, and an accounting for these effects in a computational model (except for the inclusion of bed resistance in the overall heat transfer coefficient) is usually an unnecessary refinement.

From the descriptions of the effects of these phenomena upon the responses of these models to step forcing, the effects of these phenomena may be roughly described in terms of frequency response, and various models can be suggested for use in studies in various frequency ranges. The low frequencies appear to be influenced only by the heat capacity of the particles, so the skeletal model (the plug flow model with infinite Hp) may be used in this range. The middle frequencies are also influenced by the finite rate of heat transfer between the particles and the fluid. The frequencies at which this effect becomes important may be determined from the characteristic time (dimensionless) of this heat transfer, 1/Hp. The plug flow model, with finite Hp, may be used in this frequency region. Axial mixing apparently affects the middle and high frequencies, where the one-dimensional finite stage model may be useful. Heat transfer at the wall has a steady state attenuation effect, and the effect of incomplete radial mixing (or bed resistance) is too small to be determined in this study.

From the large effect of a finite rate of heat transfer between the particles and the fluid, statements can be made concerning the effect of a finite rate of mass transfer between the particles and the fluid for cases in which the reaction occurs on the solid particles, or in the pores of the particles. Because the capacity for mass in the particles is smaller than the heat capacity, and because the initial concentration fluctuations are not as large as the later concentration changes following the temperature changes, the effect would be a dispersive effect, probably slightly more significant than the dispersive effect of axial mixing.

This study leads to no simplification of the coupling between heat and mass in the reaction. While the temperature is changing significantly, the concentration not only changes with the temperature, but also greatly influences the temperature change. An apparent simplification that the concentration is in an equilibrium with the temperature is not accurate here. (However, in the case of gas

reactors, where the velocity of the major temperature change is several orders of magnitude less than the fluid velocity, this simplification may be useful.) This simplification implies that the time derivative of concentration, $(\partial c_A/\partial t)_x$, is negligible compared with the space derivative, $(\partial c_A/\partial x)_t$. However, calculations of these derivatives from the results of runs with the PLGFLO program indicate that $(\partial c_A/\partial t)_x$ may be up to 25% of $(\partial c_A/\partial x)_t$. Additional calculations show that in many regions of this model in the unsteady state, the rate of heat generation in the reaction is approximately equal to the rate of heat transfer to the particles, which shows that the dynamics are not completely dominated by the heat transfer, but that the heat generation, and thus the coupling of heat and mass, plays an essential part in the dynamics.

A major problem which remains is the determination of the coupling of heat and mass in the reaction, particularly the extent to which these effects are nonlinear. A useful model may be one in which the disturbances are linear deviations from a nonlinear steady state. The models studied here may be useful in determining the adequacy of such linearized models.

Eventually, some kind of transfer function for packed tubular reactors may be devised. The computer programs of this study cannot usefully describe the response of these mathematical models to sinusoidal disturbances or to random disturbances. However, the results and observations of this study and of other studies suggested by this work may be useful in the formulation of such a transfer function.

CHAPTER 7

CONCLUSIONS

In summary, the three phenomena that dominate the dynamic behavior of a packed bed tubular chemical reactor are: the heat capacity of the packing, which causes the major temperature disturbance to travel through the reactor slower than the fluid velocity; the finite rate of heat transfer between the packing and the fluid, which greatly disperses the temperature disturbance; and the coupling of heat and mass in the reaction, through which concentration disturbances and temperature disturbances greatly affect each other. Of minor importance is axial mixing, which further disperses the concentration and temperature disturbances and causes the leading part of the disturbances to travel slightly faster than the fluid velocity.

Effects of these three dominating phenomena are included in the plug flow model (with finite Hp) and the one-dimensional finite stage model. The effects of axial mixing also are included in the latter model. Either model should generally satisfactorily simulate the dynamics of an actual packed tubular reactor.

The equations of the plug flow model can be usefully treated by the method of characteristics, which clearly shows the travelling wave nature of propagating disturbances of a tubular reactor.

The effect of incomplete radial mixing appears to be negligible, thus the necessity of using two-dimensional models is eliminated. A wall heat transfer correlation for the two-dimensional finite stage model is derived, however, through which the effect of incomplete radial mixing, or the resistance of the bed to radial heat transport, can be determined.

A remaining problem is the nonlinear nature of the heat and mass coupling in the reaction term. Study of a model in which the unsteady state is described by linear equations for disturbances from a nonlinear steady state is suggested. The behavior of such a model may be compared with the behavior of the models of the present study to determine the adequacy of such a simplification.

ACKNOWLEDGMENTS

The authors acknowledge with thanks the support of this work by the National Science Foundation, the Computer Center of the University of California, and the Atomic Energy Commission through the Lawrence Radiation Laboratory.

APPENDIX A

A TWO-DIMENSIONAL RUNGE-KUTTA METHOD

In this study, a two-dimensional Runge-Kutta method was developed for the numerical integration of first-order hyperbolic differential equations of the form

$$\left(\frac{\partial c}{\partial y}\right)_z = f(c, u) , \tag{A.1}$$

$$\left(\frac{\partial u}{\partial z}\right)_y = g(c, u) , \tag{A.2}$$

with the boundary conditions

$$\text{at } y = 0 , \quad c = c_0(z) , \tag{A.3}$$

$$\text{at } z = 0 , \quad u = u_0(y) , \tag{A.4}$$

where c, u, f, and g can be either scalar or vector quantities. Such equations may describe unsteady state distributed parameter physical systems, such as the plug flow chemical reactor discussed in Chapter 2, Parts E and F. The other boundary values (e.g., u at y = 0) may be found by integrating the appropriate differential equations [e.g., equation (A.2) for u at y = 0] with standard ordinary differential equation integration methods.[7]

As in Chapter 2, Part F, the region of interest in the y-z plane can be divided into a network or lattice of rectangles, of the form of Figure 10. The sides of the rectangles parallel to the z-axis have length h, and the sides of the rectangles parallel to the y-axis have length k. The location of the lower left corner of a rectangle is y = ik, z = jh. That is, a lattice point at (y, z) can be considered as being located at (i, j) in terms of the increments k and h.

From the boundary conditions, or from previous integrations, c and u at (i, j), (i+1, j), and (i, j+1) are known. In this numerical method, as in the modified Euler method [eqs. (2.108) through (2.111)], the values of c and u at (i+1, j+1) are calculated, based upon the known values at (i, j), (i+1, j), and (i, j+1).

The calculation scheme of Runge-Kutta methods involves the calculation of derivatives at various intermediate points. The combination of derivatives in this method involves parameters which are adjusted so that the value calculated for the next point agrees with a truncated Taylor's series expansion about the previous point.

$c_{i+1,j+1}$ can be expanded in a Taylor's series about point (i, j):

$$c_{i+1,j+1} = c_{i,j} + \left(\frac{\partial c}{\partial y}\right)_{i,j} k + \left(\frac{\partial c}{\partial z}\right)_{i,j} h + \frac{1}{2}\left(\frac{\partial^2 c}{\partial y^2}\right)_{i,j} k^2 + \left(\frac{\partial^2 c}{\partial y \partial z}\right)_{i,j} kh$$

$$+ \frac{1}{2}\left(\frac{\partial^2 c}{dz^2}\right)_{i,j} h^2 + \frac{1}{6}\left(\frac{\partial^3 c}{\partial y^3}\right)_{i,j} k^3 + \frac{1}{2}\left(\frac{\partial^3 c}{\partial y^2 dz}\right)_{i,j} k^2 h$$

$$+ \frac{1}{2}\left(\frac{\partial^3 c}{\partial y \partial z^2}\right)_{i,j} kh^2 + \frac{1}{6}\left(\frac{\partial^3 c}{\partial z^3}\right)_{i,j} h^3 + E_1 \qquad \text{(A.5)}$$

where E_1 is the truncation error, and contains terms of the order k^4, h^3h, k^2h^2, kh^3, and h^4 and of higher orders.

Let $\Delta c_i \equiv c_{i+1,j} - c_{i,j}$, $\Delta c_j \equiv c_{i,j+1} - c_{i,j}$.

An expansion of $c_{i+1,j}$ as a Taylor's series about (i, j) yields:

$$\Delta c_i = \left(\frac{\partial c}{\partial z}\right)_{i,j} h + \frac{1}{2}\left(\frac{\partial^2 c}{\partial z^2}\right)_{i,j} h^2 + \frac{1}{6}\left(\frac{\partial^3 c}{\partial z^3}\right)_{i,j} h^3 + O(h^4) . \qquad \text{(A.6)}$$

Similarly,

$$\Delta c_j \equiv c_{i,j+1} - c_{i,j} = \left(\frac{\partial c}{\partial y}\right)_{i,j} k + \frac{1}{2}\left(\frac{\partial^2 c}{\partial y^2}\right)_{i,j} k^2 + \frac{1}{6}\left(\frac{\partial^3 c}{\partial y^3}\right)_{i,j} k^3 + O(k^4) . \qquad (A.7)$$

With the substitution of (A.6) and (A.7) into (A.5),

$$c_{i+1,j+1} = c_{i,j} + \Delta c_i + \Delta c_j + \left(\frac{\partial^2 c}{\partial y \partial z}\right)_{i,j} kh + \frac{1}{2}\left(\frac{\partial^3 c}{\partial y^2 \partial z}\right)_{i,j} k^2 h + \frac{1}{2}\left(\frac{\partial^3 c}{\partial y \partial z^2}\right)_{i,j} kh^2 + E_2, \qquad (A.8)$$

where E_2 is an error term, similar to E_1.

The notation is now simplified:

$$\text{Let} \quad \left.\begin{aligned} f_{n,m} &\equiv f(c_{n,m}, u_{n,m}) ; \\ g_{n,m} &\equiv g(c_{n,m}, u_{n,m}) ; \end{aligned}\right\} \qquad (A.9)$$

$$f \equiv f_{i,j} ; \quad g \equiv g_{i,j} ; \qquad (A.10)$$

$$f_c = \left(\frac{\partial f}{\partial c}\right)_u , \quad f_u = \left(\frac{\partial f}{\partial u}\right)_c ; \quad g_c = \left(\frac{\partial g}{\partial c}\right)_u , \quad g_u = \left(\frac{\partial g}{\partial u}\right)_c ; \qquad (A.11)$$

$$\left(\frac{\partial c}{\partial z}\right) = \left(\frac{\partial c}{\partial z}\right)_{i,j} ; \quad \left(\frac{\partial u}{\partial y}\right) = \left(\frac{\partial u}{\partial y}\right)_{i,j} . \qquad (A.12)$$

$$\Delta f_i \equiv f_{i+1,j} - f = \left(\frac{\partial f}{\partial z}\right)_{i,j} h + O(h^2) \text{ (Taylor's series)}$$

$$= \left[f_c \left(\frac{\partial c}{\partial z}\right) + f_u g\right] h + O(h^2) , \tag{A.13}$$

and

$$\Delta f_j = f_{i,j+1} - f = \left[f_c f + f_u \left(\frac{\partial u}{\partial y}\right)\right] k + O(k^2) \tag{A.14}$$

The numerical integration step is the calculation of $c_{i+1,j+1}$ from the following formula, which is a linear combination of all information obtainable from c and u at the three known points, with one intermediate derivative calculation:

$$\bar{c}_{i+1,j+1} = c_{i,j} + \Delta c_i + \mu c_j + \beta_1 k\Delta f_i + \beta_2 k\Delta f_j + \beta_3 kf$$

$$+\beta_4 kf(c_{i,j} + \gamma\Delta c,\ u_{i,j} + \delta\Delta u) , \tag{A.15}$$

where

$$\left.\begin{aligned} \gamma\Delta c &\equiv \gamma_1\Delta c_i + \gamma_2\Delta c_j + \gamma_3 k\Delta f_i + \gamma_4 k\Delta f_j + \gamma_5 kf , \\ &\text{and} \\ \delta\Delta u &\equiv \delta_1\Delta u_i + \delta_2\Delta u_j + \delta_3 h\Delta g_i + \delta_4 h\Delta g_j + \delta_5 hg . \end{aligned}\right\} \tag{A.16}$$

The calculated value, $\bar{c}_{i+1,j+1}$, differs from the exact value, $c_{i+1,j+1}$, because of truncation errors.

The parameters ($\beta_1, \beta_2, \beta_3, \beta_4, \gamma_1, \gamma_2, \gamma_3, \gamma_4, \gamma_5, \delta_1, \delta_2, \delta_3, \delta_4$, and δ_5) are chosen so that equation (A.15) agrees with equation (A.8) in all terms except those of functional order of $h^4, h^3k, h^2k^2, hk^3, k^4$, or greater. The terms of equations (A.8) and (A.15) are expanded in terms of f, f_c, f_u, f_{cc}, f_{cu}, and f_{uu}. For example, in equation (A.15),

$$\begin{aligned} f(c_{i,j}+\gamma\Delta c,\ u_{i,j} + \delta\Delta u) = f &+ f_c\gamma\Delta c + f_u\delta\Delta u \\ &+ \frac{1}{2} f_{cc}(\gamma\Delta c)^2 + f_{cu}(\gamma\Delta c)(\delta\Delta u) \\ &+ \frac{1}{2} f_{uu}(\delta\Delta u)^2 + E_3 \end{aligned} \tag{A.17}$$

as expanded in a Taylor's series. [Note that γ and δ are not constant parameters in this particular case; $\gamma\Delta c$ and $\delta\Delta u$ are symbolic notations for the expressions on the right-hand side of equations (A.16)].

The detailed solution for the parameters is given in Appendix B. The results are:

$$\left.\begin{aligned} &\beta_1 = \frac{1}{2}, \quad \beta_2 = -\frac{1}{2}, \ \beta_3 = -\frac{1}{2}, \ \beta_4 = \frac{1}{2}, \\ &\gamma_1 = 1, \quad \gamma_2 = 1 - a, \ \gamma_3 = 1, \ \gamma_4 = \frac{1}{2}a, \ \gamma_5 = a \\ &\delta_1 = 1 - b, \ \delta_2 = 1, \ \delta_3 = \frac{1}{2}b, \ \delta_4 = 1, \ \delta_5 = b \end{aligned}\right\} \tag{A.18}$$

where a and b are arbitrarily chosen constants between 0 and 1. For symmetry, a = b.

Equation (A.15) becomes

$$\begin{aligned} \bar{c}_{i+1,j+1} = {} & (c_{i+1,j} + c_{i,j+1} - c_{i,j}) + \frac{1}{2} k [f_{i+1,j} - f_{i,j+1} - f_{i,j} \\ & + f(c_{i+1,j} + (1-a)c_{i,j+1} - (1-a)c_{i,j} + kf_{i+1,j} + \frac{1}{2} akf_{i,j+1} \\ & - (1 - \frac{1}{2}a)kf_{i,j}, \ (1-b)u_{i+1,j} + u_{i,j+1} - (1-b)u_{i,j} + \frac{1}{2} bhg_{i+1,j} \\ & + hg_{i,j+1} - (1 - \frac{1}{2}b)h_{g_{i,j}}] . \end{aligned} \tag{A.19}$$

A similar equation can be written for $\bar{u}_{i+1,j+1}$ because of the symmetry. With the introduction of intermediate values c^* and u^*, the equations can be rewritten

$$\begin{aligned} c^* &= c_{i+1,j} + kf_{i+1,j} + [(1-a)(c_{i,j+1} - c_{i,j}) + \frac{1}{2} ak(f_{i,j+1} + f_{i,j})] - kf_{i,j}, \\ u^* &= u_{i,j+1} + hg_{i,j+1} + [(1-b)(u_{i+1,j} - u_{i,k}) + \frac{1}{2} bh(g_{i+1,j} + g_{i,j})] - hg_{i,j}; \end{aligned} \tag{A.20}$$

$$\bar{c}_{i+1,j+1} = c_{i+1,j} + \frac{1}{2} k \left[f_{i+1,j} + f(c^*, u^*) \right] + \left[(c_{i,j+1} - c_{i,j}) = \frac{1}{2} k (f_{i,j+1} + f_{i,j}) \right],$$

$$\bar{u}_{i+1,j+1} = u_{i,j+1} + \frac{1}{2} h \left[g_{i,j+1}\ g(c^*, u^*) \right] + \left[(u_{i+1,j} - u_{i,j}) - \frac{1}{2} h (g_{i+1,j} + g_{i,j}) \right].$$

(A.21)

Equations (A.20) and (A.21) are the algorithm of this two-dimensional Runge-Kutta method.

To determine the position in the y-z plane at which c^* and u^* are calculated, let $c = y$ and $u = z$; then $c_{i,j} = k_j$ and $u_{i,j} = h_i$, and $f = 1$ and $g = 1$. From the equations for c^* and u^*,

$$\left.\begin{aligned} y^* &= jk + \left\{ (1 - a)\, k + ak \right\} = (j+1)k, \\ z^* &= ih + \left\{ (1 - b)\, h + bh \right\} = (i+1)h\ . \end{aligned}\right\} \qquad \text{(A.22)}$$

Thus c^* and u^* are initial estimates of $c_{i+1,j+1}$ and $u_{i+1,j+1}$, although they are not necessarily the best initial estimates, because in Runge-Kutta methods intermediate calculations do not necessarily give best values of the variables being calculated.

Equations (A.21) may conceivably be iterated, with the replacement of c^* and u^* with the value of $\bar{c}_{i+1,j+1}$ and $\bar{u}_{i+1,j+1}$ calculated in the previous iteration step. The limit of this iteration is

$$(\bar{c}_{i+1,j+1} - c_{i+1,j}) - \frac{1}{2} k (\bar{f}_{i+1,j+1} + f_{i+1,j}) = (c_{i,j+1} - c_{i,j}) - \frac{1}{2} k (f_{i,j+1} + f_{i,j}) \qquad \text{(A.23)}$$

and thus this difference is independent of i:

$$(\bar{c}_{i+1,j+1} - c_{i+1,j}) - \frac{1}{2} k (\bar{f}_{i+1,j+1} + f_{i+1,j}) = -\frac{1}{12} k^3 \left(\frac{\partial^3 c}{\partial y^3} \right)_{0,j+\xi}$$

(A.24)

Thus in this iterative scheme, the third-order correction terms along the boundaries are used throughout the unsteady state region. The non-iterative scheme should be superior because in it these third-order correction terms are recalculated approximately at each step, as $f(c^*, u^*)$ is not assumed to be $f_{i+1,j+1}$.

To compare the two methods with each other, a sample problem was chosen which has a known analytic solution. The problem is

$$\frac{\partial c}{\partial y} = u - c \,, \qquad \frac{\partial u}{\partial z} = c - u \tag{A.25}$$

with the boundary conditions

$$c(0, x) = 1 \,, \qquad t(y, 0) = 0 \,. \tag{A.26}$$

The solution is

$$c(y, z) = 1 - \int_0^y e^{-z-\xi} I_0(2\sqrt{z\xi})\, d\xi$$

$$u(y, z) = \int_0^z e^{-y-\xi} I_0(2\sqrt{y\xi})\, d\xi \,. \tag{A.27}$$

This problem was chosen because the solution was known, the problem has no complicating parameters, and the equations describe an unsteady-state distributed parameter system (in dimensionless form), such as a fixed bed absorber or a fixed bed heat exchanger, similar to the plug flow reactor model of this study.[20]

From the solution, it is seen that

$$c - u = e^{-y-z} I_0(2\sqrt{yz}) \,. \tag{A.28}$$

Along the line $y = z$, $c + u = 1$; then along this line,

$$c(y, y) = \frac{1}{2} + \frac{1}{2} e^{-2y} I_0(2y)$$
$$u(y, y) = \frac{1}{2} - \frac{1}{2} e^{-2y} I_0(2y) \tag{A.29}$$

The two programs were coded in FORTRAN, with the double precision feature to eliminate machine round-off errors, and calculations were performed on the IBM 7090. The calculations were performed for several values of h (here, $h = k$), and the values of c at various points on the line $y = z$ as calculated by the two numerical methods were compared with the known values. For $c(1, 1)$, the errors for some choices of h became significant. When $y = 1$,

$$e^{-2y} = e^{-2} = 0.13533\ 52832\ , \tag{A.30}$$ [21]

and

$$I_0(2y) = I_0(2) = 2.27958\ 530\ . \tag{A.31}$$ [22]

Therefore

$$c(1, 1) = 0.65425\ 416 \tag{A.32}$$

Figure 66 shows the magnitudes of the error in the values of $c(1, 1)$, calculated with the two methods, as a function of h. For the Runge-Kutta method, curves are shown for values of a of 0, $\frac{1}{2}$, and 1 (here $a = b$); for the modified Euler method, curves are shown for one, two, three and infinite iterations. Of course, an infinite number of iterations were not made, but rather the iterations were continued until there was no significant difference in two consecutive iterated values of c. In general, the errors of the two methods are of opposite sign.

Figure 66 shows that the errors of both methods are proportional to h^2. Clearly, for this case the Modified Euler method is superior to the Runge-Kutta method in all respects. Evidently, the theoretical advantage of the Runge-Kutta method, which lies in the estimation of third partial derivatives, disappears rapidly as the points of calculation move away from the boundaries.

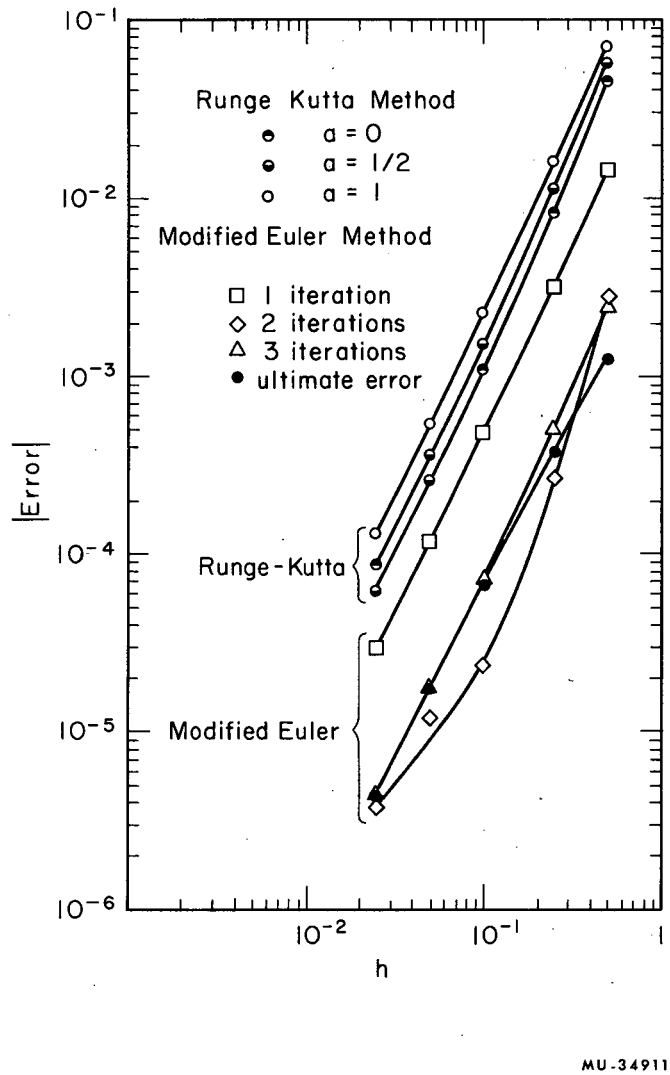

Fig. 66. Comparison of errors of two-dimensional numerical integration methods as functions of interval size.

This unusual two-dimensional Runge-Kutta method warrants more study, to determine the reason its theoretical superiority is not realized and to extend to other similar problems the concepts used in its derivation.

APPENDIX B

DERIVATION OF THE TWO-DIMENSIONAL RUNGE-KUTTA METHOD

The first three terms on the right-hand side of equation (A.8) are identical with those of equation (A.15) so the problem becomes that of finding the parameters so that

$$\beta_1 \Delta f_i + \beta_2 \Delta f_j + \beta_3 f + \beta_4 f(c_{i,j} + \gamma \Delta c,\ u_{i,j} + \delta \Delta u)$$

$$= \left(\frac{\partial^2 c}{\partial y \partial z}\right) h + \frac{1}{2}\left(\frac{\partial^3 c}{\partial y^2 \partial z}\right) kh + \frac{1}{2}\left(\frac{\partial^3 c}{\partial y \partial z^2}\right) h^2 + E. \qquad \text{(B.1)}$$

The symbol E in equation (B.1) and other equations in this appendix represents additional terms which are of the order h^3, h^2k, hk^2, k^3, and of higher order. E does not necessarily have the same value in different equations.

The following derivative identities of f and g will be of use in the development:

$$\frac{\partial f}{\partial y} = f_c f + f_u \left(\frac{\partial u}{\partial y}\right), \qquad \text{(B.2)}$$

$$\frac{\partial f}{\partial z} = f_c \left(\frac{\partial c}{\partial z}\right) + f_u g, \qquad \text{(B.3)}$$

$$\frac{\partial^2 f}{\partial f^2} = (f_c)^2 f + f_c f_u \left(\frac{\partial u}{\partial y}\right) + f_u \left(\frac{\partial^2 u}{\partial y^2}\right) + f_{cc} f^2 + 2 f_{cu} f \left(\frac{\partial u}{\partial y}\right) + f_{uu} \left(\frac{\partial u}{\partial y}\right)^2, \qquad \text{(B.4)}$$

$$\frac{\partial^2 f}{\partial y \partial z} = (f_c)^2 \left(\frac{\partial c}{\partial z}\right) + f_c f_u g + f_u f g_c + f_u g_u \left(\frac{\partial u}{\partial y}\right) + f_{cc} f \left(\frac{\partial c}{\partial z}\right) + f_{cu} f g + f_{cu} \left(\frac{\partial c}{\partial z}\right)\left(\frac{\partial u}{\partial y}\right) + f_{uu} g \left(\frac{\partial u}{\partial y}\right), \qquad \text{(B.5)}$$

$$\frac{\partial^2 f}{\partial z^2} = f_c \left(\frac{\partial^2 c}{\partial z^2}\right) + f_u g_c \left(\frac{\partial c}{\partial z}\right) + f_u g_u g + f_{cc}\left(\frac{\partial c}{\partial z}\right)^2 + 2f_{cu} g \left(\frac{\partial c}{\partial z}\right) + f_{uu} g^2, \tag{B.6}$$

$$\frac{\partial g}{\partial y} = g_c f + g_u \left(\frac{\partial u}{\partial y}\right), \text{ and} \tag{B.7}$$

$$\frac{\partial g}{\partial z} = g_c \left(\frac{\partial c}{\partial z}\right) + g_u g \ . \tag{B.8}$$

The right-hand side of equation (B.1) becomes

$$\begin{aligned}
\frac{\partial^2 c}{\partial y \partial z} h + \frac{1}{2}\left(\frac{\partial^3 c}{\partial y^2 \partial z}\right) hk + \frac{1}{2}\left(\frac{\partial^3 c}{\partial y \partial z^2}\right) h^2 &= \frac{\partial f}{\partial z} h + \frac{1}{2}\left(\frac{\partial^2 f}{\partial y \partial z}\right) hk \\
&\quad + \frac{1}{2}\left(\frac{\partial^2 f}{\partial z^2}\right) h^2 \\
&= hf_c\left[\left(\frac{\partial c}{\partial z}\right) + \frac{1}{2} f_c \left(\frac{\partial c}{\partial z}\right) k + \frac{1}{2}\left(\frac{\partial^2 c}{\partial z^2}\right) h\right] + \frac{1}{2} f_c f_u ghk \\
&\quad + hf_u\left[g + \frac{1}{2} fg_c k + \frac{1}{2} g_u \left(\frac{\partial u}{\partial y}\right) k + \frac{1}{2} g_c \left(\frac{\partial c}{\partial z}\right) h + \frac{1}{2} g_u gh\right] \\
&\quad + hf_{cc}\left[\frac{1}{2} f \left(\frac{\partial c}{\partial z}\right) k + \frac{1}{2}\left(\frac{\partial c}{\partial z}\right)^2 h\right] \\
&\quad + hf_{cu}\left[\frac{1}{2} fgk + \frac{1}{2}\left(\frac{\partial c}{\partial z}\right)\left(\frac{\partial u}{\partial y}\right) k + g\left(\frac{\partial c}{\partial z}\right)\right] h \\
&\quad + hf_{uu}\left[\frac{1}{2} f \left(\frac{\partial u}{\partial y}\right) k + \frac{1}{2} g^2 h\right] + E \ .
\end{aligned} \tag{B.9}$$

The Δf terms of the left-hand side of equation (B.1) can be developed as:

$$\begin{aligned}
\Delta f_i = f_{i+1,j} - f &= \left(\frac{\partial f}{\partial z}\right) h + \frac{1}{2}\left(\frac{\partial^2 f}{\partial z^2}\right) h^2 + E \\
&= hf_c\left[\left(\frac{\partial c}{\partial z}\right) + \frac{1}{2}\left(\frac{\partial^2 c}{\partial z^2}\right) h\right] + hf_u\left[g + \frac{1}{2} g_c \left(\frac{\partial c}{\partial z}\right) h + \frac{1}{2} g_u gh\right] \\
&\quad + \frac{1}{2} f_{cc}\left(\frac{\partial c}{\partial z}\right)^2 h + f_{cu} g \left(\frac{\partial c}{\partial z}\right) h^2 + \frac{1}{2} f_{uu} g^2 h^2 + E
\end{aligned} \tag{B.10}$$

and

$$\Delta f_j = f_{i,j+1} - f = \left(\frac{\partial f}{\partial y}\right) k + \frac{1}{2}\left(\frac{\partial^2 f}{\partial y^2}\right) k^2 + E$$

$$= kf_c\left[f + \frac{1}{2} f_c f k\right] + \frac{1}{2} f_c f_u \left(\frac{\partial u}{\partial y}\right) k^2$$

$$+ k f_u \left[\left(\frac{\partial u}{\partial y}\right) + \frac{1}{2}\left(\frac{\partial^2 u}{\partial y^2}\right) k\right]$$

$$+ \frac{1}{2} f_{cc} f^2 k^2 + f_{cu} f \left(\frac{\partial u}{\partial y}\right) k^2 + \frac{1}{2} f_{uu} \left(\frac{\partial u}{\partial y}\right)^2 k^2 + E. \tag{B.11}$$

The term $f(c_{i,j} + \gamma\Delta c,\ u_{i,j} + \delta\Delta u)$ can be expanded in a Taylor's series:

$$f(c_{i,j} + \gamma\Delta c,\ u_{i,j} + \delta\Delta u) = f_c(\gamma\Delta c) + f_u(\delta\Delta u)$$

$$+ \frac{1}{2} f_{cc}(\gamma\Delta c)^2 + f_{cu}(\gamma\Delta c)(\delta\Delta u) + \frac{1}{2} f_{uu}(\delta\Delta u)^2$$

$$+ E. \tag{B.12}$$

From equations (A.6), (A.7), (A.1), and (B.2),

$$\left.\begin{aligned} \Delta c_i &= \left(\frac{\partial c}{\partial z}\right) h + \frac{1}{2}\left(\frac{\partial^2 c}{\partial z^2}\right) h^2 + O(h^3) \\ \text{and} \quad \Delta c_j &= fk + \frac{1}{2} f_c f k^2 + \frac{1}{2} f_u \left(\frac{\partial u}{\partial y}\right) k^2 + O(k^3)\ . \end{aligned}\right\} \tag{B.13}$$

Similarly,

$$\left.\begin{aligned} \Delta u_i &= gh + \frac{1}{2} g_c \left(\frac{\partial c}{\partial z}\right) h^2 + \frac{1}{2} g_u g h^2 + O(h^3) \\ \text{and} \quad \Delta u_j &= \left(\frac{\partial u}{\partial y}\right) k + \frac{1}{2}\left(\frac{\partial^2 u}{\partial y^2}\right) k^2 + O(k^3) \end{aligned}\right\} \tag{B.14}$$

Therefore

$$\gamma\Delta c = \gamma_1\Delta c_i + \gamma_2\Delta c_j + \gamma_3 k\Delta f_i + \gamma_4 k\Delta f_j + \gamma_5 kf$$

$$= \gamma_1 h\left[\left(\frac{\partial c}{\partial z}\right) + \frac{1}{2}\left(\frac{\partial^2 h}{\partial z^2}\right)h\right] + \gamma_2 k\left[f + \frac{1}{2}f_c f_k + \frac{1}{2}f_u\left(\frac{\partial u}{\partial y}\right)k\right]$$

$$+ \gamma_3 hk\left[f_c\left(\frac{\partial c}{\partial z}\right) + f_u g\right] + \gamma_4 k^2\left[f_c f + f_u\left(\frac{\partial u}{\partial y}\right)\right] + \gamma_5 hf + E$$

(B.15)

and

$$\delta\Delta u = \delta_1\Delta u_i + \delta_2\Delta u_j + \delta_3 h\Delta g_i + \delta_4 h\Delta g_i + \delta_5 hg$$

$$= \delta_1 h\left[g + \frac{1}{2}g_c\left(\frac{\partial c}{\partial z}\right)h + \frac{1}{2}g_u gh\right] + \delta_2 k\left[\left(\frac{\partial u}{\partial y}\right) + \frac{1}{2}\left(\frac{\partial^2 u}{\partial y^2}\right)\right]k$$

$$+ \delta_3 h^2\left[g_c\left(\frac{\partial c}{\partial z}\right) + g_u g\right] + \delta_4 hk\left[g_c f + g_u\left(\frac{\partial u}{\partial y}\right)\right]$$

$$+ \delta_5 hg + E\,. \quad \text{(B.16)}$$

Use was made in equation (B.16) of the equations

$$\Delta g_i = g_{i+1,j} - g = \left(\frac{\partial g}{\partial z}\right)h + O(h^2) = g_c\left(\frac{\partial c}{\partial z}\right)h + g_u gh + O(h^2)\,,$$

$$\Delta g_j = g_{i,j+1} - g = \left(\frac{\partial g}{\partial y}\right)k + O(k^2) = g_c fk + g_u\left(\frac{\partial u}{\partial y}\right)k + O(k^2)\,.$$

(B.17)

With the substitution of equations (B.15) and (B.16) into (B.12), the left-hand side of equation (B.1) becomes

$$\beta_1\Delta f_i + \beta_2\Delta f_j + \beta_3 f + \beta_4 f(c_{i,j} + \gamma\Delta c,\ u_{i,j} + \delta\Delta u) = f\left[\beta_3 + \beta_4\right]$$

$$+ f_c\left[\beta_1\left(\frac{\partial c}{\partial z}\right)h + \frac{1}{2}\beta_1\left(\frac{\partial^2 c}{\partial z^2}\right)h^2 + \beta_2 fk + \frac{1}{2}\beta_2 f_c fk^2 + \beta_4\gamma_1\left(\frac{\partial c}{\partial z}\right)h\right.$$

$$+ \frac{1}{2}\beta_4\gamma_1\left(\frac{\partial^2 c}{\partial z^2}\right)h^2$$

(B.18 continued)

$$+ \beta_4\gamma_2 fk + \frac{1}{2}\beta_4\gamma_2 f_c fk^2 + \beta_4\gamma_3 f_c \left(\frac{\partial c}{\partial z}\right) hk + \beta_4\gamma_4 f_c fk^2 + \beta_4\gamma_5 fk\Big]$$

$$+ f_c f_u \left[\frac{1}{2}\beta_2\left(\frac{\partial u}{\partial y}\right)k^2 + \frac{1}{2}\beta_4\gamma_2\left(\frac{\partial u}{\partial y}\right)k^2 + \beta_4\gamma_3 ghk + \beta_4\gamma_4\left(\frac{\partial u}{\partial y}\right)k^2\right]$$

$$+ f_u\Big[\beta_1 gh + \frac{1}{2}\beta_1 g_c\left(\frac{\partial c}{\partial z}\right)h^2 + \frac{1}{2}\beta_1 g_u gh^2 + \beta_2\left(\frac{\partial u}{\partial y}\right)k + \frac{1}{2}\beta_2\left(\frac{\partial^2 u}{\partial y^2}\right)\Big]k^2$$

$$+ \beta_4\delta_1 gh + \frac{1}{2}\beta_4\delta_1 g_c\left(\frac{\partial c}{\partial z}\right)h^2 + \frac{1}{4}\beta_4\delta_1 g_u gh^2 + \beta_4\delta_2\left(\frac{\partial u}{\partial y}\right)k\ \frac{1}{2}\beta_4\delta_2\left(\frac{\partial^2 u}{\partial y^2}\right)k^2$$

$$+ \beta_4\delta_3 g_c\left(\frac{\partial c}{\partial z}\right)h^2 + \beta_4\delta_3 g_u gh^2 + \beta_4\delta_4 g_c fhk + \beta_4\delta_4 g_u\left(\frac{\partial u}{\partial y}\right)hk + \beta_4\delta_5 gh\Big]$$

$$+ f_{cc}\Big[\frac{1}{2}\beta\left(\frac{\partial c}{\partial z}\right)^2 h^2 + \frac{1}{2}\beta_2 f^2k^2 + \frac{1}{2}\beta_4\gamma_1{}^2\left(\frac{\partial c}{\partial z}\right)^2 h^2 + \beta_4\gamma_1(\gamma_2+\gamma_5)\, f\left(\frac{\partial c}{\partial z}\right)hk$$
$$+ \frac{1}{2}\beta_4(\gamma_2+\gamma_5)^2 f^2k^2\Big]$$

$$+ f_{cu}\Big[\beta_1 g\left(\frac{\partial c}{\partial z}\right)h^2 + \beta_2 f\left(\frac{\partial u}{\partial y}\right)k^2 + \beta_4\gamma_1(\delta_1+\delta_5)\, g\left(\frac{\partial c}{\partial z}\right)h^2$$

$$+ \beta_4\gamma_1\delta_2\left(\frac{\partial c}{\partial z}\right)\left(\frac{\partial u}{\partial y}\right)hk + \beta_4(\gamma_2+\gamma_5)(\delta_1+\delta_5)\, gfhk + \beta_4(\gamma_2+\gamma_5)\,\delta_2 f\left(\frac{\partial u}{\partial y}\right)k^2\Big]$$

$$+ f_{uu}\Big[\frac{1}{2}\beta_1 g^2h^2 + \frac{1}{2}\beta_2\left(\frac{\partial u}{\partial y}\right)^2 k^2 + \frac{1}{2}\beta_4\delta_1{}^2 g^2h^2 + \beta_4\delta_1\delta_2\left(\frac{\partial u}{\partial y}\right)hk$$

$$+ \frac{1}{2}\beta_4\delta_2{}^2\left(\frac{\partial u}{\partial y}\right)^2 k^2 + \beta_4\delta_1\delta_5 g^2h^2 + \frac{1}{2}\beta_4\delta_5{}^2 g^2h^2 + \beta_4\delta_2\delta_5\, g\left(\frac{\partial u}{\partial y}\right)hk\Big] + E. \tag{B. 18}$$

Equating the coefficients of like terms on the right-hand sides of equation (B. 4) and (B. 18) gives the equations for the parameters:

terms compared	parameter equations		
f	$\beta_3 + \beta_4$	$= 0$	(B. 19)
$f_c\left(\frac{\partial c}{\partial z}\right)h$ and $\frac{1}{2}f_c\left(\frac{\partial^2 c}{\partial z^2}\right)h^2$	$\beta_1 + \beta_4\gamma_1$	$= 1$	(B. 20)
$(f_c)^2\left(\frac{\partial c}{\partial z}\right)hk$ and $f_c f_u ghk$	$\beta_4\gamma_3$	$= \frac{1}{2}$	(B. 21)
$f_c f_k$	$\beta_2 + \beta_4\gamma_2 + \beta_4\gamma_5$	$= 0$	(B. 22)
$\frac{1}{2}(f_c)^2 fk^2$ and $\frac{1}{2}f_c f_u\left(\frac{\partial u}{\partial y}\right)k^2$	$\beta_2 + \beta_4\gamma_2 + 2\beta_4\gamma_4$	$= 0$	(B. 23)
$f_u gh$	$\beta_1 + \beta_4\delta_1 + \beta_4\delta_5$	$= 1$	(B. 24)
$f_u fghk$ and $f_u g_u\left(\frac{\partial u}{\partial y}\right)hk$	$\beta_4\delta_4$		(B. 25)
$\frac{1}{2}f_u g_c\left(\frac{\partial c}{\partial z}\right)h^2$ and $\frac{1}{2}f_u g_u gh^2$	$\beta_1 + \beta_4\delta_1 + 2\beta_4\delta_3$	$= 1$	(B. 26)
$f_u\left(\frac{\partial u}{\partial y}\right)k$ and $\frac{1}{2}f_u\left(\frac{\partial^2 u}{\partial y^2}\right)k^2$	$\beta_2 + \beta_4\delta_2$	$= 0$	(B. 27)
$f_{cc} f\left(\frac{\partial c}{\partial z}\right)hk$	$\beta_4\gamma_1(\gamma_2 + \gamma_5)$	$= \frac{1}{2}$	(B. 28)
$\frac{1}{2}f_{cc}\left(\frac{\partial c}{\partial z}\right)^2 h^2$	$\beta_1 + \beta_4\gamma_1^2$	$= 1$	(B. 29)
$\frac{1}{2}f_{cc}\, f^2k^2$	$\beta_2 + \beta_4(\gamma_2 + \gamma_5)^2$	$= 0$	(B. 30)
$f_{cu} fghk$	$\beta_4(\gamma_2 + \gamma_5)(\delta_1 + \delta_5)$	$= \frac{1}{2}$	(B. 31)
$f_{cu}\left(\frac{\partial c}{\partial z}\right)\left(\frac{\partial u}{\partial y}\right)hk$	$\beta_4\gamma_1\delta_2$	$= \frac{1}{2}$	(B. 32)
$f_{cu} g\left(\frac{\partial c}{\partial z}\right)h^2$	$\beta_1 + \beta_4\gamma_1(\delta_1 + \delta_5)$	$= 1$	(B. 33)
$f_{cu} f\left(\frac{\partial u}{\partial y}\right)k^2$	$\beta_2 + \beta_4(\gamma_2 + \gamma_5)\delta_2$	$= 0$	(B. 34)
$f_{uu} g\left(\frac{\partial u}{\partial y}\right)hk$	$\beta_4(\delta_1 + \delta_5)\delta_2$	$= \frac{1}{2}$	(B. 35)

$$\frac{1}{2}f_{uu}g^2h^2 \qquad \beta_1 + \beta_4(\delta_1 + \delta_5)^2 = 1 \qquad \text{(B. 36)}$$

$$\frac{1}{2}f_{uu}\left(\frac{\partial u}{\partial y}\right)^2 k^2 \qquad \beta_2 + \beta_4\delta_2^2 = 0 \qquad \text{(B. 37)}$$

These equations are solved in the following tabulation; each statement is justified by the equations cited:

$\beta_4 \neq 0$	(B. 21); (B. 25); (B. 28); (B. 31); (B. 32); (B. 35)	(B. 38)
$\gamma_1 = \delta_1 + \delta_5$	(B. 20); (B. 24); (B. 29); (B. 33); (B. 36)	(B. 39)
$\delta_2 = \gamma_2 + \gamma_5$	(B. 22); (B. 27); (B. 30); (B. 34); (B. 37)	(B. 40)
$\gamma_1 \neq 0$	(B. 32)	(B. 41)
$\delta_2 \neq 0$	(B. 32)	(B. 42)
$\gamma_1 = \gamma_1^2 = 1$	(B. 20); (B. 29); (B. 38); (B. 41)	(B. 43)
$\delta_2 = \delta_2^2 = 1$	(B. 27); (B. 37); (B. 38); (B. 42)	(B. 44)
$\beta_4 = \frac{1}{2}$	(B. 32); (B. 43); (B. 44)	(B. 45)
$\beta_1 = \frac{1}{2}$	(B. 20);)B. 43); (B. 45)	(B. 46)
$\beta_2 = -\frac{1}{2}$	(B. 27); (B. 44); (B. 45)	(B. 47)
$\gamma_3 = 1$	(B. 21); (B. 45)	(B. 48)
$\delta_4 = 1$	(B. 25); (B. 45)	(B. 49)
$\beta_3 = -\frac{1}{2}$	(B. 19); (B. 45)	(B. 50)
$\gamma_4 = \frac{1}{2}\gamma_5$	(B. 22); (B. 23); (B. 45)	(B. 51)
$\delta_3 = \frac{1}{2}\delta_5$	(B. 24); (B. 26); (B. 45)	(B. 52)

Let $a = \gamma_5$ and $b = \delta_5$. Therefore, in summary,

$$\beta_1 = \frac{1}{2},\quad \beta_2 = -\frac{1}{2},\quad \beta_3 = \frac{1}{2},\quad \beta_4 = \frac{1}{2};$$

$$\gamma_1 = 1,\quad \gamma_2 = 1 - a,\quad \gamma_3 = 1,\quad \gamma_4 = \frac{1}{2}a,\quad \gamma_5 = a; \qquad \text{(B. 53)}$$

$$\delta_1 = 1 - b,\quad \delta_2 = 1,\quad \delta_3 = \frac{1}{2}b,\quad \delta_4 = 1,\quad \delta_5 = b\ .$$

Equation (A. 15) becomes

$$\bar{c}_{i+1,j+1} = c_{i,j} + (c_{i+1,j} - c_{i,j}) + (c_{i,j+1} - c_{i,j}) + \frac{1}{2}k(f_{i+1,j} - f_{i,j}) - \frac{1}{2}k(f_{i,j+1} - f_{i,j}) - \frac{1}{2}kf_{i,j} + \frac{1}{2}kf(c_{i,j} + \gamma\Delta c,\ u_{i,j} + \delta\Delta u)\ , \tag{B. 54}$$

where $\gamma\Delta c = (c_{i+1,j} - c_{i,j}) + (1-a)(c_{i,j+1} - c_{i,j}) + k(f_{i+1,j} - f_{i,j}) + \frac{1}{2}ak(f_{i,j+1} - f_{i,j}) + akf_{i,j}$ (B. 55)

and

$$\delta\Delta u = (1-b)(u_{i+1,j} - u_{i,j}) + (u_{i,j+1} - u_{i,j}) + \frac{1}{2}bh(g_{i+1,j} - g_{i,j}) + h(g_{i,j+1} - g_{i,j}) + bhg_{i,j}\ . \tag{B. 56}$$

Combining terms, the equation becomes

$$\bar{c}_{i+1,j+1} = (c_{i+1,j} + c_{i,j+1} - c_{i,j}) + \frac{1}{2}k\Big[f_{i+1,j} - f_{i,j+1} - f_{i,j} + f(c_{i+1,j} + (1-a)c_{i,j+1} - (1-a)c_{i,j} + kf_{i+1,j} + \frac{1}{2}akf_{i,j+1} - (1 - \frac{1}{2}a)kf_{i,j},\ (1-b)u_{i+1,j} + u_{i,j+1} - (1-b)u_{i,j} + \frac{1}{2}bhg_{i+1,j} + hg_{i,j+1} - (1 - \frac{1}{2}b)hg_{i,j})\Big]. \tag{B. 57}$$

The error involved in using equation (B. 57) to calculate $c_{i+1,j+1}$ is of the functional order h^4, h^3k, h^2k^2, hk^3, and k^4. There is probably no choice of values for a and b such that this error can be minimized in general. The calculations to show this, however, are too lengthy to be carried out at this time.

TABLE OF NOTATION

(Numbers in parenthesis indicate equations in which the relevant symbol is defined).

A = in chemical equations, the primary reactant (1.5), (1.7); in mathematical equations, the dimensionless activation energy (1.20).

A_j, $A_{j,j+1}$, = areas important to a stage in the two-dimensional finite stage model. See Chapter 2, Part A.

a = an adjustable parameter in the two dimensional Runge-Kutta method of integration: $0 \leq a \leq 1$.

a_p = the specific surface area of the packing particles. For spheres, $a_p = 6/d_p$.

B = in chemical equations, the secondary reactant.

Bi = the Biot number for the reactor bed (3.8).

b = an adjustable parameter in the two dimensional Runge-Kutta method of integration: $0 \leq b \leq 1$.

c = a vector of general dependent variables. Particular forms of c include c_i, $c_{i,j}$, c^*.

c_A = the dimensionless concentration of the primary reactant A. The dimensional concentration of A is c_A^*. The initial value of c_A at the feed is $c_{A_{if}}$; the final value of c_A at feed is $c_{A_{ff}}$. Particular forms of c_A include $c_{A_{i,j}}$ and c_{A_i}. CA is the representation of c_A on machine-plotted graphs. (1.9).

c_B = the dimensionless concentration of the secondary reactant B. The dimensional concentration of B is c_B^* (1.10).

c_f = the heat capacity of the fluid per unit mass.

c_p = the heat capacity of the packing particles per unit mass.

c_r = the reference concentration used to define dimensionless concentrations.

D = a factor in the Newton-Raphson method applied to simultaneous equations (2.62).

D_r = the effective turbulent diffusivity in the radial direction (1.26).

D_x = the effective turbulent diffusivity in the axial direction (1.25).

d_p = the average diameter of the packing particles, used as a fundamental unit of length in this study.

E = the activation energy of the reaction.

f = a general fector function.

g = a general function, sometimes a vector function.

Hp = the dimensionless heat transfer coefficient between the particles and the fluid (1.23).

Hw = the dimensionless wall heat transfer coefficient (1.24). Hw_2 is for the two-dimensional finite stage model, Hw_1 is for the one-dimensional finite stage model, and Hw_p is for the plug flow model. $Hw_{1\infty}$ is the value of Hw_1 when the corresponding Hw_2 is infinite. (See Chapter 3.)

h = an interval size used in two-dimensional numerical integration methods.

h_p = the heat transfer coefficient between the particles and the fluid.

h_w = the wall heat transfer coefficient.

i, j = general subscripts.

J_0, j_1 = Bessel functions of the first kind and of zero and first order, respectively.

k = the dimensionless pre-exponential coefficient in chemical rate equations (1.17). The corresponding dimensional value is k^*. Also, k is an interval size used in two-dimensional numerical integration methods.

k_i = variables in the Runge-Kutta-Gill method (2.67).

k_r = the effective thermal conductivity of the bed in the radial direction.

k_x = the effective thermal conductivity of the bed in the axial direction.

M = the dimensionless diameter of the reactor (1.2). The corresponding dimensional diameter is M^*.

m = a superscript which indicates the number of iterations in iterative numerical methods.

N = the dimensionless length of the reactor (1.1). The corresponding dimensional length is N^*.

P_{e_r} = the radial Peclet number (1.27).

P_{e_x} = the axial Peclet number (1.28).

$p_{c_i}, p_{c_{i,j}}$ = concentration feed streams to a stage (2.36), (2.37), (2.38), (2.73).

$p_n(\lambda)$ = auxiliary determinants used in the heat transfer coefficient calculation (3.48).

$p_{T_{i,j}}, p_{T_i}$ = temperature feed streams to a stage (2.41), (2.42), (2.43), (2.74).

Q = the volumetric flow rate of fluid through the reactor: $Q = 1/4\pi M^2 d_p^2 \epsilon v$. Flow rates through stages of the finite stage models are Q_{im}, Q_i, and Q_j (2.2), (2.7).

q_i = variables in the Runge-Kutta-Gill method (2.67).

R = the dimensionless rate of reaction (1.21). The corresponding dimensional form is R^* (1.6), (1.7). Other particular forms are R_i and $R_{i,j}$.

R_g = the gas constant.

r = the dimensionless radial variable (3.1).

r_i = variables in the Runge-Kutta-Gill method (2.67).

S = the fluid mixing and heat transfer matrix of the two-dimensional finite stage model (3.31).

T = the dimensionless temperature of the fluid (1.12). The corresponding dimensional form is T^*. The initial value of T at the feed is T_{if}; the final value of T at the feed is T_{ff}. Particular forms of T include $T_{i,j}$, T_i, and $\overline{T}_i$. TF is the representation of T on machine plotted graphs.

T_0 = the ratio of the reference temperature to the total adiabatic temperature rise (1.15).

T_p = the dimensionless temperature of the particles (1.13). The corresponding dimensional form is T_p^*. Particular forms of T_p include $T_{p_{i,j}}$ and T_{p_i}.

T_r = a dimensional temperature used for reference in defining dimensionless temperatures.

t = dimensionless time, $t^* v/d_p$. Dimensional time is t^*.

u = a vector of general dependent variables.

V = the finite stage averaging vector (3.34).

V_j = the volume of the stages of finite stage models (2.1).

v = the actual average velocity of the fluid through the bed.

x = the dimensionless axial variable (1.3). The corresponding dimensional variable is x^*.

y, z = the characteristic coordinate variables (2.85), (2.92).

Greek Symbols

β = the dimensionless heat capacity parameter (1.22).

β_1 = the smallest positive root of equation (3.7). β_n is the nth root of equation (3.7). $\beta_{1\infty}$ is the smallest positive root of $J_0(\beta) = 0$.

γ = the stoichiometric coefficient (1.7).

γ_n = coefficients in the recursive relations for $p_n(\lambda)$ (3.48).

$(-\Delta H)$ = the heat of reaction.

ΔT_a = the total adiabatic temperature rise for the reaction (1.11).

δ = the stoichiometric concentration difference (1.30). δ_0 is the value of δ at the inlet of the reactor.

ϵ = the void fraction of the packed bed.

θ = a generalized wall heat transfer term for the finite stage models (2.44), (2.45), (2.46), (2.75).

λ = the variable of the characteristic polynomial $\psi(\lambda)$ of S. The largest root of $\psi(\lambda) = 0$ is λ_1; a general root is λ_r.

μ_1 = a parameter related to λ_1 (3.49).

ρ_f = the density of the fluid.

ρ_p = the density of the packing particles.

$\psi(\lambda)$ = the characteristic polynomial of S (3.46).

REFERENCES

1. K. W. McHenry and R. H. Wilhelm, Axial Mixing of Binary Gas Mixtures Flowing in a Random Bed of Spheres, A. I. Ch. E. Journal 3, 83 (1957).
2. John Beck, Design of Packed Catalytic Reactors, Advances in Chemical Engineering, Volume 3 (Academic Press, New York, 1962). pp. 203-271.
3. Harry A. Deans, A Computational Model for Prediction and Evaluation of the Dynamic Behavior of Fixed Bed Processes (Ph. D. Thesis) (Department of Chemical Engineering, Princeton University, 1960).
4. H. A. Deans and Leon Lapidus, A Computational Model for Predicting and Correlating the Behavior of Fixed Bed Reactors: I. Derivation of Model for Nonreactive Systems, A. I. Ch. E., Journal 6, 656 (1960).
5. H. A. Deans and Leon Lapidus, A Computational Model for Predicting and Correlating the Behavior of Fixed Bed Reactors: II. Extension to Chemically Reactive Systems, A. I. Ch. E. Journal 6, 663 (1960).
6. Jose Sinai, Experimental Frequency Response Study of a Packed Tabular Chemical Reactor (Ph. D. Thesis) (Department of Chemical Engineering, University of California; in preparation).
7. F. B. Hildebrand, Introduction to Numerical Analysis (McGraw-Hill Book Company, Inc., New York, 1956).
8. Leon Lapidus, Digital Computation for Chemical Engineers (McGraw Hill Book Company, Inc., New York, 1962). p. 292.
9. S. Gill, A Process for the Step-by-Step Integration for Differential Equations in an Automatic Digital Computing Machine, Proc. Camb. Phil. Soc. 47, 96 (1951).
10. John Olmstead Cowles, Mathematical Simulation of a Fixed Bed Tubular Reactor During Periods of Transient Operation (Ph. D. Thesis) (Department of Chemical Engineering, University of Michigan, 1963).

11. Andreas Acrivos, Method of Characteristics Technique Applied to Heat and Mass Transfer Problems, Ind. Eng. Chem. 48, 703 (1956).

12. A. Jeffrey and T. Taniuti, Non-Linear Wave Propagation (Academic Press, New York, 1964).

13. L. O. Gonzales and E. H. Spencer, Studies on the Numerical Solution of a Model Simulating Fixed Bed Regeneration, Chem. Eng. Sci. 18, 753 (1963).

14. J. F. Wehner and R. H. Wilhelm, Boundary Conditions of Flow Reactor, Chem. Eng. Sci. 6, 89 (1956).

15. H. S. Carslaw and J. C. Jaeger, The Conduction of Heat in Solids, Second Edition (Oxford at the Clarendon Press, 1959). pp. 201-202.

16. R. A. Frazier, W. J. Duncan, and A. R. Collar, Elementary Matrices (Cambridge: At the University Press, 1952). pp. 78-79.

17. J. L. Spencer, The Effect of Axial Mixing on a Tubular Chemical Reactor (Ph.D. Thesis) (Department of Chemical Engineering, University of Pennsylvania, 1961). Chapter 5.

18. Charles D. Hodgman, ed., Handbook of Chemistry and Physics, 38th Edition (Chemical Rubber Publishing Company, Cleveland, 1956).

19. John H. Perry, ed., Chemical Engineer's Handbook, Third Edition (McGraw-Hill Book Company, Inc., New York, 1950). p. 1548.

20. R. B. Bird, W. E. Stewart, and E. N. Lightfoot, Transport Phenomena (John Wiley and Sons, Inc., New York, 1960). pp. 702-705.

21. National Bureau of Standards, Tables of the Exponential Function e^x (United States Government Printing Office, Washington, 1951).

22. British Association for the Advancement of Science, Mathematical Tables, Volume X, Bessel Functions, Part II (Cambridge University Press, Cambridge, 1952). p. 198.

This report was prepared as an account of Government sponsored work. Neither the United States, nor the Commission, nor any person acting on behalf of the Commission:

A. Makes any warranty or representation, expressed or implied, with respect to the accuracy, completeness, or usefulness of the information contained in this report, or that the use of any information, apparatus, method, or process disclosed in this report may not infringe privately owned rights; or

B. Assumes any liabilities with respect to the use of, or for damages resulting from the use of any information, apparatus, method, or process disclosed in this report.

As used in the above, "person acting on behalf of the Commission" includes any employee or contractor of the Commission, or employee of such contractor, to the extent that such employee or contractor of the Commission, or employee of such contractor prepares, disseminates, or provides access to, any information pursuant to his employment or contract with the Commission, or his employment with such contractor.